ABSTRACT

Title of dissertation: SYNCHRONIZATION IN NETWORKS OF COUPLED OSCILLATORS

Juan Gabriel Restrepo, Doctor of Philosophy, 2005

Dissertation directed by: Professors Edward Ott and Brian Hunt
Departments of Physics and Mathematics, respectively.

We study different aspects of synchronization in networks of coupled oscillators:

- We adapt a previous model and analysis method (the *master stability function*), extensively used for studying the stability of the synchronous state of networks of identical chaotic oscillators, to the case of oscillators that are similar but not exactly identical. We find that bubbling induced desynchronization bursts occur for some parameter values. These bursts have spatial patterns, which can be predicted from the network connectivity matrix and the unstable periodic orbits embedded in the attractor. We test the analysis of bursts by comparison with numerical experiments. In the case that no bursting occurs, we discuss the deviations from the exactly synchronous state caused by the mismatch between oscillators.

- We present a method to determine the relative parameter mismatch in a collection of nearly identical chaotic oscillators by measuring large deviations from the synchronized state. We demonstrate our method with an ensemble of slightly different circle maps. We discuss how to apply our method when there is noise, and show an example where the noise intensity is comparable to the mismatch.

- We consider a ring of identical or near identical coupled periodic oscillators in which the connections have randomly heterogeneous strength. We use the master stability function method to determine the possible patterns at the desynchronization transition that occurs as the coupling strengths are increased. We demonstrate Anderson localization of the modes of instability, and show that such localized instability generates waves of desynchronization that spread to the whole array. Similar results should apply to other networks with regular topology and heterogeneous connection strengths.

- We study the transition from incoherence to coherence in large networks of coupled phase oscillators. We present various approximations that describe the behavior of an appropriately defined order parameter past the transition, and generalize recent results for the critical coupling strength. We find that, under appropriate conditions, the coupling strength at which the transition occurs is determined by the largest eigenvalue of the adjacency matrix. We show how, with an additional assumption, a mean field approximation recently proposed is recovered from our results. We test our theory with numerical simulations, and find that it describes the transition when our assumptions are satisfied. We find that our theory describes the transition well in situations in which the mean field approximation fails. We study the finite size effects caused by nodes with small degree and find that they cause the critical coupling strength to increase.

Dissertation prospectus: Dynamics on networks of coupled oscillators

by

Juan G. Restrepo

Dissertation submitted to the Faculty of the Graduate School of the
University of Maryland, College Park in partial fulfillment
of the requirements for the degree of
Doctor of Philosophy
2005

Advisory Committee:

Professor Edward Ott, Chair/Advisor
Professor Brian R. Hunt, Co-Advisor
Professor James A. Yorke
Professor Thomas M. Antonsen, Jr.
Professor Rajarshi Roy

ACKNOWLEDGMENTS

I would like to thank Professor Ed Ott for all that he has taught me. He made possible this work by constantly providing ideas, advice and encouragement. It has been a pleasure to work with and to learn from him. I also want to thank Professor Brian Hunt. His insights were always illuminating our discussions and many times he showed me different ways of looking at a problem. I was very fortunate to have these two men as my advisors.

I also want to thank my parents and my family for all their support and encouragement. The hardest part of the Ph. D. was having to be away from them.

My wife, Ana Maria, deserves a very special thank you. Without her support, love and patience this work would not have been possible.

I benefited from help and discussions from the always friendly students of the chaos group at Maryland. I want to mention Yue-Kin Tsang, Jonathan Ozik, Seung-Jong Baek, Xing Zheng, Doug Armstead, and Michael Ocskowski.

I also would like to thank my friends here for all the non academic help and for everything else.

TABLE OF CONTENTS

LIST OF TABLES

LIST OF FIGURES

Chapter 1

Introduction

In recent years, it has been recognized that many real world systems can be represented by large complex networks, and therefore the study of these networks has become a rapidly growing interdisciplinary field. Some examples of systems that have been studied under this perspective are the Internet [1] the World Wide Web [2], the electric power grid [3], protein networks [4], and social networks [5]. Remarkably, some common features have been found in all these networks. It has been found, for example, that for many different networks the distribution of the degrees (the degree of a node in the network is the number of other nodes connected to it) follows a power law [6]. Much research has been done lately in order to explain how networks evolve and acquire their particular structure. For a review of recent and ongoing research on complex networks, see for example [7, 8, 9].

In this dissertation we consider the problem of synchronization in complex networks. In this scenario, the nodes of the network are dynamical systems and the links between nodes correspond to dynamical coupling. Many systems can be thought of as examples of this situation; for example, coupled arrays of lasers [10]-[12], electrical circuits [13], chemical reactions [14], interacting cells [15]-[18], and even flashing fireflies that interact by observing each other [19]. See [18], [20], and [21] for more examples. Under some circumstances, the coupled systems synchronize. In some cases, the synchronization of the elements is desirable (e.g., cells in the heart); in other cases, the synchronization can be harmful (e.g., simultaneous firing of neurons in the brain is sometimes associated with epileptic seizures). In any case, one would like to be able to determine if synchronization is going to occur in a given system, and whether or not the synchronized state is stable.

In Chapter 2 we study the stability of the synchronous state in networks of nearly identical coupled chaotic oscillators. It is known that in some cases, when there is noise or parameter mismatch, the synchronized state can be interrupted by periods of large desynchronization, called desynchronization bursts [22]-[24]. We studied the effect of the network structure on this phenomenon, and found that the desynchro-

nization bursts present spatial patterns (i.e., some nodes in the network deviate more than others from the average state). These patterns depend on the eigenvectors of the matrix describing the network connections, and on the dynamics of the individual oscillators.

In Chapter 3 we apply the results of Chapter 2 to estimate the parameter mismatch in a collection of nearly identical chaotic oscillators. When synchronizing nearly identical oscillators, the small parameter mismatch degrades the quality of synchronization. Knowledge of the mismatch characteristics can be useful in order to minimize its effect by judiciously arranging the configuration of the oscillators.

Usually, studies of coupled oscillators assume a regular distribution of coupling strengths between different oscillators (e.g., constant coupling strength, or a function of their distance on a lattice). In Chapter 4 we study the effect of random heterogeneous coupling strenghts in an array of nearly identical coupled periodic oscillators. It is found that, under some circumstances, as the coupling strength is increased, the system desynchronizes in a localized region. From this region waves of desynchronization propagate, eventually producing a highly ordered final state.

In Chapter 5 we consider the case of synchronization in a network of heterogeneous oscillators. A simple model for interacting heterogeneous oscillators was introduced by Kuramoto [25], who showed that, in the case of all-to-all coupling, a transition to coherence exists for a critical coupling strength that depends on the distribution of the natural frequencies of the individual oscillators. His model has been studied extensively in the last decades and provides a guide as to how the characteristics of the individual oscillators (i.e., their frequencies) determine the transition to synchronization. Some generalizations and further studies of this model include external noise [26], finite-size effects [27, 28], general coupling functions [29], and delays [30]. For a review of the model and a more comprehensive account of its generalizations and improvements see [31], Chapter 12 of [20], Chapter 6 of [32], and references therein. As discussed above, a network in which every node is connected to every other node does not realistically represent many real world networks. In Chapter 5, we consider the Kuramoto model adapted to a general network. The problem of studying the Kuramoto model on a general network has recently started to attract attention [33]-[35], and a mean field approach to study this problem was proposed [36, 37]. We developed a more general approach and found, among other things, that there is still a transition to coherent behavior

for a critical coupling strength, and this coupling strength is determined by the largest eigenvalue of the adjacency matrix determining the connections of the network.

This dissertation is based on the following publications:

- Chapter 2:

  Juan G. Restrepo, Brian R. Hunt, and Edward Ott, *Spatial patterns of desynchronization bursts in networks of coupled oscillators.* Phys. Rev. E **69** 066215 (2004).

- Chapter 3:

  Jupiter Bagaipo and Juan G. Restrepo, *Parameter mismatch estimation using large deviations from synchronization.* nlin.CD/0412049, submitted to Phys. Rev. E.

- Chapter 4:

  Juan G. Restrepo, Brian R. Hunt, and Edward Ott, *Desynchronization waves and localized instabilities in oscillator arrays.* Phys. Rev. Lett. **93** 114101 (2004).

- Chapter 5:

  Juan G. Restrepo, Brian R. Hunt, and Edward Ott, *The onset of synchronization in large networks of coupled oscillators.* cond-mat/0411202, to appear in Phys. Rev. E.

Chapter 2

Spatial patterns of desynchronization bursts in networks of nearly identical coupled oscillators

In this Chapter we study the synchronization of networks of coupled chaotic units that are nearly, but not exactly, identical. In particular, we will be concerned with the spatial patterns of desynchronization bursts that appear when this synchronization is present but intermittent.

When two or more identical dynamical systems are coupled, they can synchronize under appropriate circumstances. The synchronization of chaotic units has been studied extensively [20, 38] and is of significance in biology [15]-[18], laser physics [10]-[12], and other areas [14, 39]. At the same time, the importance of complex networks has been recently appreciated, and progress has been made towards their understanding, including characteristics that might help distinguish qualitatively different networks [7]-[40]. The dynamics of a network of coupled oscillators, and, in particular, its synchronization, has therefore emerged as a subject of great interest.

There are different notions of synchronization, among them *phase synchronization* [41], *generalized synchronization* [42], *lag synchronization* [43], and *identical synchronization* [13]. The concept of identical synchronization is useful when dealing with identical coupled oscillators. Here we will consider oscillators that are nearly the same, although not identical. Thus we will be concerned with *near identical* synchronization, in which the states of the different units remain close to each other as a function of time.

Pecora and Carroll [44] have proposed a model and analysis method (the *master stability function*) for the study of the stability of the synchronous state of networks of *identical* coupled chaotic units, and this technique has recently been extensively applied [45, 46] to study the synchronization properties of different kinds of networks of identical noiseless chaotic units. These networks include small world [47] and scale-free networks [6].

The analysis of network synchronization by use of the master stability function technique has so far assumed all the units to be identical and noise-free, so that an exact synchronized state is possible. In

practice, however, even if one strives to make the oscillators the same, they are still expected to have a small amount of parameter mismatch, and a small amount of noise is also expected to be present. Under such circumstances, it is known that the synchronization can be interrupted by sporadic periods of desynchronization (bursts). The bursts are typically caused by a periodic orbit that is embedded in the synchronized chaotic attractor and is unstable in a direction transverse to the synchronization manifold. This phenomenon is commonly referred to as *bubbling* [22]-[24], and has been studied extensively for two coupled oscillators [48, 49].

Our purpose in this Chapter is to study desynchronization bursts in networks of coupled chaotic nonidentical units. (Noise has a similar effect but will not be treated in this Chapter.) We will use the master stability function approach and, in order to account for the possibility of bubbling, we will also extend this approach to include the stability of embedded periodic orbits. In this case, the bursts have the added feature of having spatial patterns on the network, and we find that these patterns can be predicted from the network connectivity matrix. We will show how these bursts affect different parts of the network in different ways. In particular, we will see how adding connections in a ring can destabilize precisely those nodes that are the most connected, leaving other parts of the network substantially synchronized. (This a somewhat counterintuitive effect related to the fact that, in some cases, increasing the coupling strength destabilizes the synchronous state [44, 50].)

Arbitrarily small amounts of mismatch will eventually, through the bubbling mechanism, induce desynchronization bursts. We will show that some of the spatial patterns of this possibly microscopic mismatch might get amplified to a macroscopic size in the bursts. We will discuss how one can use knowledge of the parameter mismatch of the dynamical units in the network to decrease the effective size of the mismatch driving the bursts, thereby improving the robustness of the synchronization.

If synchronization is desired, the network and the parameters should be constructed so that the synchronous state for the identical oscillator system is robustly stable (this implies the absence of noise or mismatch induced desynchronization bursts). Even then, the synchronization will not be perfect if the oscillators have parameter mismatch. We will describe the characteristics of the deviations from exact synchronization in terms of the mismatch and the master stability function.

This Chapter is organized as follows. In Section 2.1 we review the master stability function approach and apply it to the case of coupled Rössler units. We also discuss the bubbling mechanism by including the embedded periodic orbits in the master stability function analysis. In Section 2.2 we numerically consider particular networks as examples and show the resulting bursts and their spatial patterns. The patterns we obtain are long and short wavelength modes in a ring and localized bursts produced by strengthening of a single connection in a ring. In Section 2.3 we study the effects of the spatial patterns of the mismatch in the development of the bursts. In Section 2.4 we study the deviations from the synchronous state caused by the mismatch when the synchronous state of the identical oscillator system is stable. In Section 2.5 we discuss our results.

2.1 Master stability function and bubbling

We now briefly review the master stability function approach introduced in [44]. Consider a system of N dynamical units, each one of which, when isolated, satisfies $\dot{X}_i = F(X_i, \mu_i)$, where $i = 1, 2, \ldots N$, and X_i is the d-dimensional state vector for unit i. In [44] the parameter vectors μ_i are taken to be the same, $\mu_i = \mu$. Here, however, the parameter vectors μ_i are in general different for each unit, but we assume the difference, or *mismatch*, between them to be small. Generalizing the situation treated in Ref. [44] to the case where the individual units are not identical (i.e., the μ_i are not all equal), the system of coupled dynamical units is taken to be of the form

$$\dot{X}_i = F(X_i, \mu_i) - g \sum_{j=1}^{N} G_{ij} H(X_j), \tag{2.1}$$

where the coupling function H is independent of i and j, and the matrix G is a Laplacian matrix ($\sum_j G_{ij} = 0$) describing the topology of network connections. For $i \neq j$, the entry G_{ij} is zero if oscillator i is not connected to oscillator j and nonzero otherwise. The nondiagonal entries of G are determined by the connections, and the diagonal elements are the negative of the sum of the nondiagonal matrix elements in their row. The coupling constant g determines the global strength of the coupling.

Assume first that all the dynamical units are identical, that is, $\mu_i = \mu$. We will refer to this situation as the *idealized* case. In this case there is an exactly synchronized solution $X_1 = X_2 = \cdots = X_N = s(t)$

whose time evolution is the same as the uncoupled dynamics of a single unit, $\dot{s} = F(s, \mu)$. This convenient result arises because the Pecora-Carroll model uses the particular choice of coupling in (2.1) that ensures that the summation is identically zero when all of the X_j are equal. We will denote this synchronization manifold, $X_1 = X_2 = \cdots = X_N$, by M. This manifold is a d - dimensional surface within the Nd - dimensional phase space of Eq. (2.1).

The stability of the synchronized state can be determined from the variational equations obtained by considering an infinitesimal perturbation ϵ_i from the synchronous state, $X_i(t) = s(t) + \epsilon_i(t)$,

$$\dot{\epsilon}_i = DF(s)\epsilon_i - g\sum_{j=1}^{N} G_{ij} DH(s)\epsilon_j. \tag{2.2}$$

Let $\epsilon = [\epsilon_1, \epsilon_2, \ldots, \epsilon_N]$ be the $d \times N$ matrix representing the deviation of the entire network from the synchronized state. In matrix notation, Eq. (2.2) becomes

$$\dot{\epsilon} = DF(s)\epsilon - gDH(s)\epsilon G^T. \tag{2.3}$$

While (2.3) allows for nonsymmetric coupling, we henceforth assume the coupling matrix G to be symmetric, $G = G^T$. We write the symmetric matrix G as $G = L\Lambda L^T$, where Λ is the diagonal matrix of real eigenvalues $\lambda_1, \lambda_2, \ldots, \lambda_N$ of G and L is the orthogonal matrix whose columns are the corresponding real orthonormal eigenvectors of G ($L^T L = I$). Define the $d \times N$ matrix $\eta = [\eta_1, \eta_2, \ldots, \eta_N]$ by $\epsilon = \eta L^T$. Then Eq. (2.3) is equivalent to

$$\dot{\eta} = DF(s)\eta - gDH(s)\eta\Lambda. \tag{2.4}$$

Componentwise,

$$\dot{\eta}_k = \left(DF(s) - g\lambda_k DH(s)\right)\eta_k. \tag{2.5}$$

The quantity η_k is the weight of the k^{th} eigenvector of G in the perturbation ϵ. The linear stability of each 'spatial' mode k is determined by the stability of Eq. (2.5). As a consequence of the condition $\sum_j G_{ij} = 0$, there is a special eigenvalue, $\lambda = 0$, whose eigenvector is $\epsilon_N = [1, 1, 1, \ldots, 1]$, corresponding to perturba-

tions *in* the synchronization manifold M. Since these are not perturbations from the synchronous state, the analysis is focused on the perturbations corresponding to nonzero eigenvalues.

By introducing a scalar variable $\alpha = g\lambda_k$, the set of equations given by (2.5) can be encapsulated in the single equation,

$$\dot{\eta} = (DF(s) - \alpha DH(s))\,\eta. \tag{2.6}$$

The *master stability function* $\Psi(\alpha)$ [44] is the largest Lyapunov exponent for this equation for a typical trajectory in the attractor. This function depends only on the coupling function H and the chaotic dynamics of an individual uncoupled element, but not on the network connectivity. The network connectivity determines the eigenvalues λ_k (independent of details of the dynamics of the chaotic units). In the sense of typical Lyapunov exponents, the stability of the synchronized state of the network is determined by $\Psi_* = \sup_k \Psi(g\lambda_k)$, where $\Psi_* > 0$ indicates instability. Thus the Pecora-Carroll model cleanly breaks the stability problem into two components, one from the dynamics [obtaining $\Psi(\alpha)$] and one from the network (determining the eigenvalues λ_k).

In contrast to previous work using the master stability function technique, in this Chapter we are interested in the dynamics of systems in which a small parameter mismatch is present. (Even though in this Chapter our examples are restricted to the case of mismatch, we emphasize that the same type of bursting phenomenon is expected for identical oscillators if noise is present [22]-[24].) Although the synchronization manifold M present in the dynamics of the idealized system is, in general, not invariant for the system with mismatch, it still may provide a useful approximation to the dynamics in systems with small mismatch. If M is stable for the idealized system, and the mismatch is small enough, then trajectories near M will tend to stay near M, and we regard the vicinity of M to be the "synchronized" state. However, stability of M in the idealized case of identical oscillators is not sufficient to guarantee robust synchronization in a real system where the oscillators are not identical[22]-[24]. While in the vicinity of the synchronization manifold M, a typical trajectory will eventually follow very closely a periodic orbit embedded in the attractor of the idealized system. Some of these periodic orbits may be unstable in a direction transverse to M. When in the vicinity of a transversally unstable periodic orbit, mismatch (or noise) will cause the trajectory to

have a component in the direction transverse to M and hence to leave the vicinity of the synchronization manifold M. If there are no other attractors, the trajectory will eventually return to the vicinity of M, and the process will repeat, the result being bursts of desynchronization sporadically interrupting long intervals of near synchronization. This type of dynamics is called bubbling [22].

Thus, in the presence of mismatch (or noise), to determine the robustness of synchronization, it is necessary to determine the transverse stability of the embedded periodic orbits for the noiseless system of identical oscillators. For coupling as in (2.1), this analysis is independent of the network, and such analyses have been carried out before, e.g., for the analysis of *two* coupled oscillators in Ref. [49]. Equation (2.6) can be used as before to construct the master stability function for each periodic orbit, if the appropriate periodic trajectories are inserted for $s(t)$ in (2.3).

As an example, in this Chapter we work with the Rössler system [51]:

$$\begin{aligned} \dot{x} &= -(y+z), \\ \dot{y} &= x + ay, \\ \dot{z} &= b + z(x-c). \end{aligned} \tag{2.7}$$

In terms of our previous notation, $d = 3$, $\mu = [a, b, c]^T$, and $X = [x, y, z]^T$. We choose the parameters of the idealized system to be $a = b = 0.2$, $c = 7$. For these parameters, the system has a chaotic attractor (see Fig. 2.1). We found the periodic orbits embedded in this attractor up to period five, and performed the analysis described above on them. We found these orbits by looking at the Poincare surface of section $\{y = 0, x < 0\}$. To a good approximation, in this surface of section the dynamics is well described by a one dimensional map $x_{n+1} = f(x_n)$, which we approximated using a polynomial fit. From this approximation to f, we determined periodic orbits of period p by using Newton's method to find the roots of $x = f^p(x)$, where f^p denotes the p times composition of f. We found one period 1 orbit, one period 2 orbit, two period 3 orbits, three period 4 orbits, and four period 5 orbits. Using coupling through the x coordinate,

$$H([x, y, z]^T) = [x, 0, 0]^T, \tag{2.8}$$

we obtained a stability function $\Psi(\alpha)$ for each orbit, the largest of which will determine if the synchro-

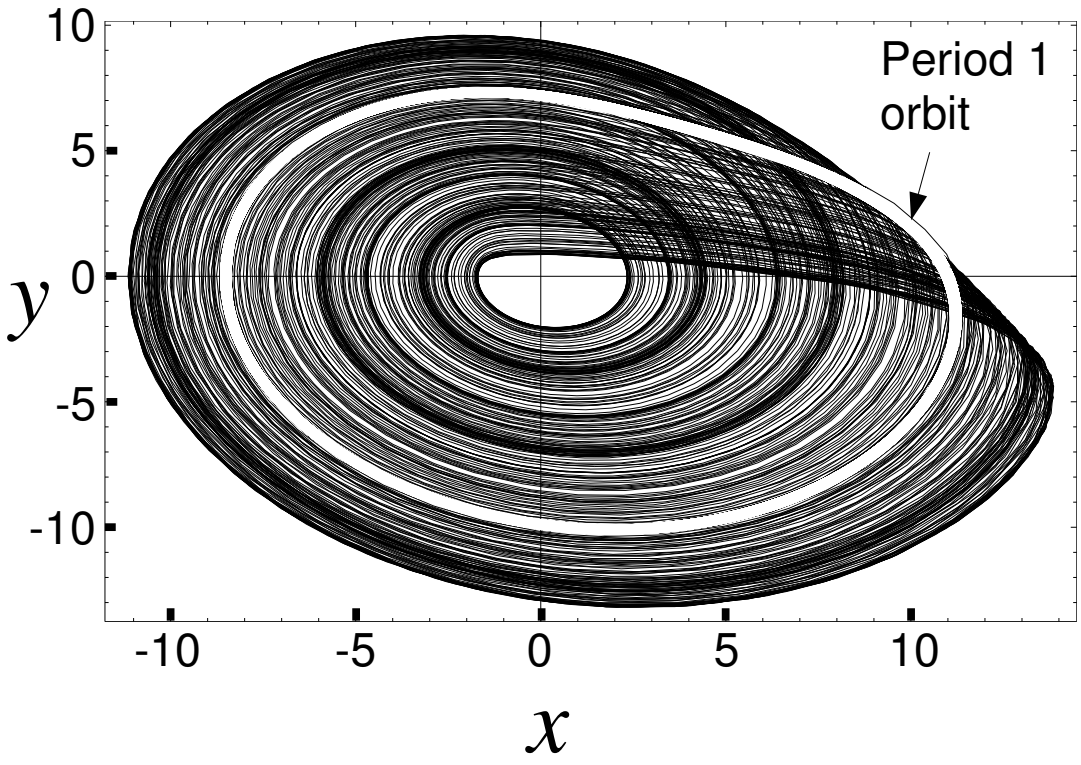

Figure 2.1: Rössler attractor (projection onto $x-y$ plane) and embedded period 1 orbit, displayed as a thick white curve inside the attractor. The parameters are $a = b = 0.2$, $c = 7$.

nization is robust. Results are shown in Fig. 2.2. For all values of α, we found that the master stability function corresponding to the period 1 orbit (thick red dashed curve) is larger than that for a typical chaotic orbit (thick black continuous curve), as well as those for the other periodic orbits we have found (several of which are shown as orange thin curves).

Based on the discussion above, bubbling induced bursting should occur whenever the master stability function for a typical chaotic orbit in the attractor is negative for $\alpha = g\lambda_k$ and all k, while the period one orbit has positive master stability function for $\alpha = g\lambda_k$ for some value of k. Denoting the master stability function for a typical chaotic orbit by $\Psi_0(\alpha)$ (Thick black continuous curve in Fig. 2.2) and for the period one orbit by $\Psi_1(\alpha)$ (Thick red dashed curve in Fig. 2.2), the *bubbling region* of α corresponds to $\Psi_0(\alpha) < 0$, $\Psi_1(\alpha) > 0$. In our example, this region corresponds to $0.16 < \alpha < 0.48$ or $3.8 < \alpha < 4.5$. The range $0.48 < \alpha < 3.8$ will be referred to as the *stable region*, and the remaining zone will be called

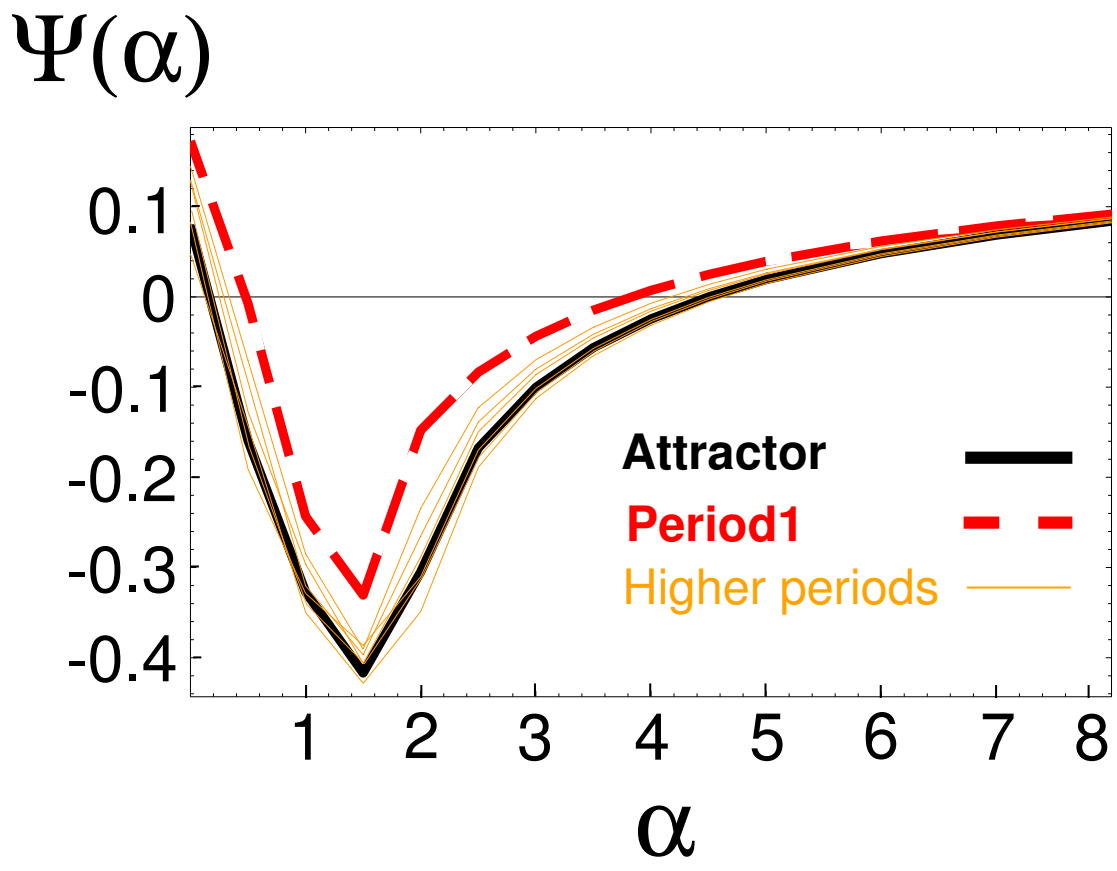

Figure 2.2: Master stability function $\Psi(\alpha)$ for a typical trajectory in the attractor (thick black continuous curve), for the period 1 orbit (thick red dashed curve), and for periodic orbits up to period 4 (thin orange curves). The curves for the four period 5 orbits are similar to the latter and were left out for clarity.

the *unstable region*.

If a network of slightly mismatched chaotic systems coupled according to Eq. (2.1) is to be robustly synchronizable without bursts of desynchronization, $g\lambda_k$ must lie in the stable region for all k, where λ_k is the kth eigenvalue of G. If $g\lambda_k$ lies in the stable region for some k and in the bubbling region for other k, then bubbling will typically occur.

2.2 Examples

In this Section we provide examples of spatially patterned bursting by considering different configurations of the chaotic units. We will first work with the units connected in a ring with each connection of equal strength. The Laplacian matrix G for this arrangement is

$$G = \begin{pmatrix} 2 & -1 & 0 & 0 & \cdots & 0 & -1 \\ -1 & 2 & -1 & 0 & \cdots & 0 & 0 \\ 0 & -1 & 2 & -1 & \cdots & 0 & 0 \\ \vdots & \vdots & \vdots & \vdots & \vdots & \vdots & \vdots \\ -1 & 0 & \cdots & 0 & 0 & -1 & 2 \end{pmatrix}, \tag{2.9}$$

and its eigenvalues are given by $\lambda_k = 4\sin^2(\frac{\pi k}{N})$. Since $\lambda_k = \lambda_{N-k}$, each eigenvalue has multiplicity two, with the exception of $\lambda_N = 0$, and, if N is even, $\lambda_{\frac{N}{2}} = 4$. The matrix G is *shift invariant*, that is, its entries satisfy, modulo N, $G_{i,j} = G_{0,i-j}$. Under these conditions, the diagonalization procedure described above corresponds to a discrete Fourier transform [50]. For the eigenvalue λ_k we choose the eigenvector w_k given by $w_k \propto [\sin(\frac{2\pi jk}{N})]_{j=1}^N$ for $1 \leq k < \frac{N}{2}$, and by $w_k \propto [\cos(\frac{2\pi jk}{N})]_{j=1}^N$ for $\frac{N}{2} \leq k \leq N$. (Due to the degeneracy of the eigenvalues in this case, there is some arbitrariness in choosing the eigenvectors.) Thus, the longest wavelength modes have the smallest eigenvalues, and viceversa.

2.2.1 Long wavelength burst

First we consider a case in which bursting of the longest wavelength mode occurs. We consider $N = 12$ and $g = 0.71$. With these values, the longest wavelength mode corresponds to $\alpha = g\lambda_1 \approx 0.19$. This value is in the bubbling region, and all other modes are in the stable region.

To introduce heterogeneity in the dynamical units, we imagine that we have mismatch predominantly in one of the parameters, say a. We simulate this mismatch by adding random perturbations to the parameter a of each oscillator. These perturbations are uniformly distributed within a $\pm 0.5\%$ range; i.e., a_i is chosen randomly in the interval $[0.995a, 1.005a]$, where a is the parameter value of the unperturbed system ($a = 0.2$). The parameters b and c were taken to be the same for each oscillator, $b_i = b = 0.2$, $c_i = c = 7$. How

a particular choice of the mismatch affects the bubbling process will be discussed in Section IV.

We solved the 12 coupled differential equations [Eq. (2.1)] with the initial conditions chosen near the attractor in the synchronization manifold. In Fig. 2.3 we plot the quantity $x_1 - x_6$ for $1000 \leq t \leq 1600$. Most of the time, this variable is close to zero, as expected if the oscillators are synchronized.

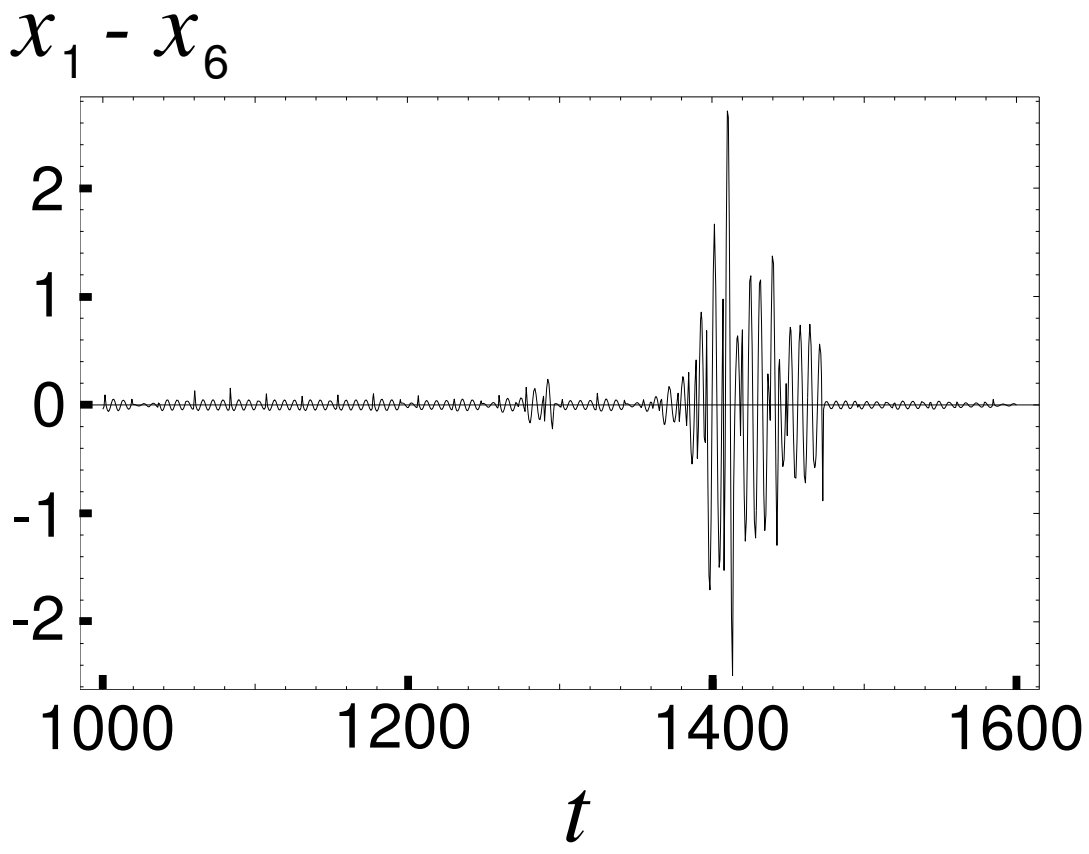

Figure 2.3: $x_1 - x_6$ as a function of time for $N = 12$ Rössler systems connected in a ring with $g = 0.71$. Note the desynchronization burst which starts at $t \approx 1380$.

Approximately at the time $t = 1380$, this difference grows, reaching magnitudes close to 3. By time $t = 1500$, the difference has decreased and is again close to zero.

To confirm the mediating role of the embedded unstable periodic orbits in the development of the desynchronization burst, we show in Fig. 2.4 a plot of x_1 versus y_1 from $t = 1372$ to $t = 1392$, which is near the start of the burst. During this time, the trajectory closely follows the period 1 orbit, which is the

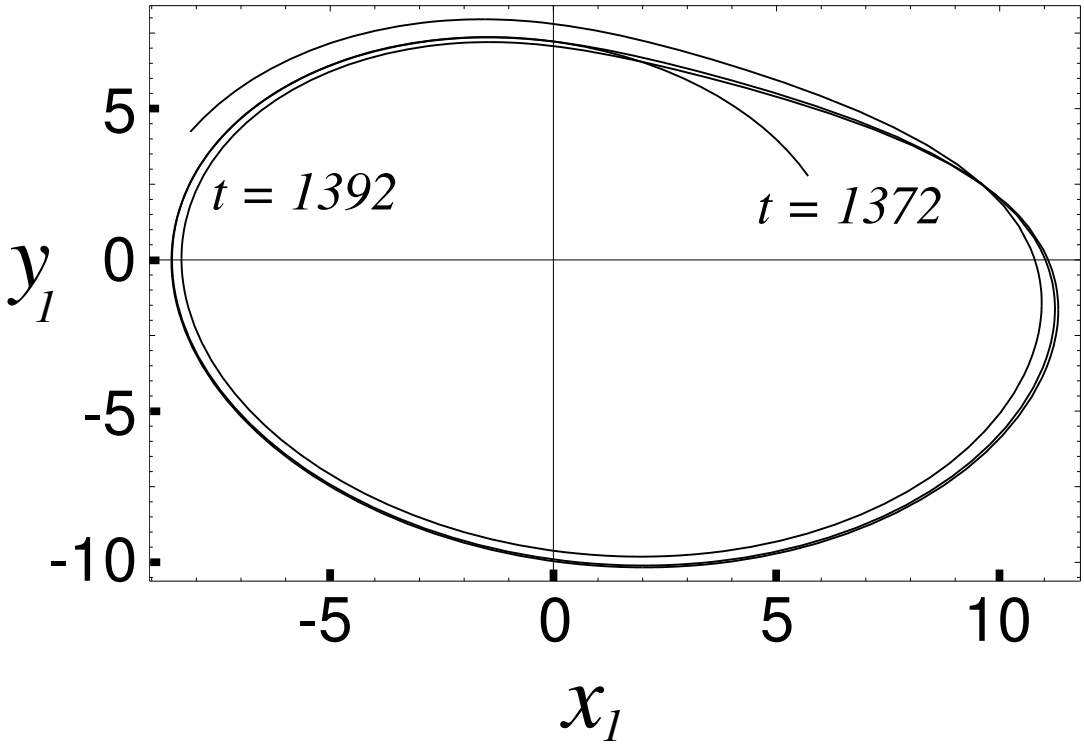

Figure 2.4: x_1 versus y_1 for $1372 \leq t \leq 1392$. During this period, which corresponds approximately to the starting point of the burst in Fig. 2.3, the trajectory follows closely the transversally unstable period 1 orbit embedded in the attractor (See Fig. 2.1).

most transversally unstable of the periodic orbits. Similar observations have been previously reported for *two* coupled chaotic systems [49].

Finally, in Fig. 2.5 we plot $x_j - x_{j-1}$ as a function of j, the oscillator index, for $t = 1360$ (open triangles), $t = 1385$ (open circles), and $t = 1410$ (open squares). The desynchronization burst can be observed developing mainly at the longest possible wavelength.

When subsequent bursts were studied in the same way, it was found that the phase of the long wavelength burst assumed only one value. This is due to the fact that the mismatch is 'frozen', that is, each oscillator has a given set of parameters which differs by a given amount from the mean values. This fixed spatial heterogeneity favors certain spatial patterns over others. We will discuss this in more detail in Section 2.3.

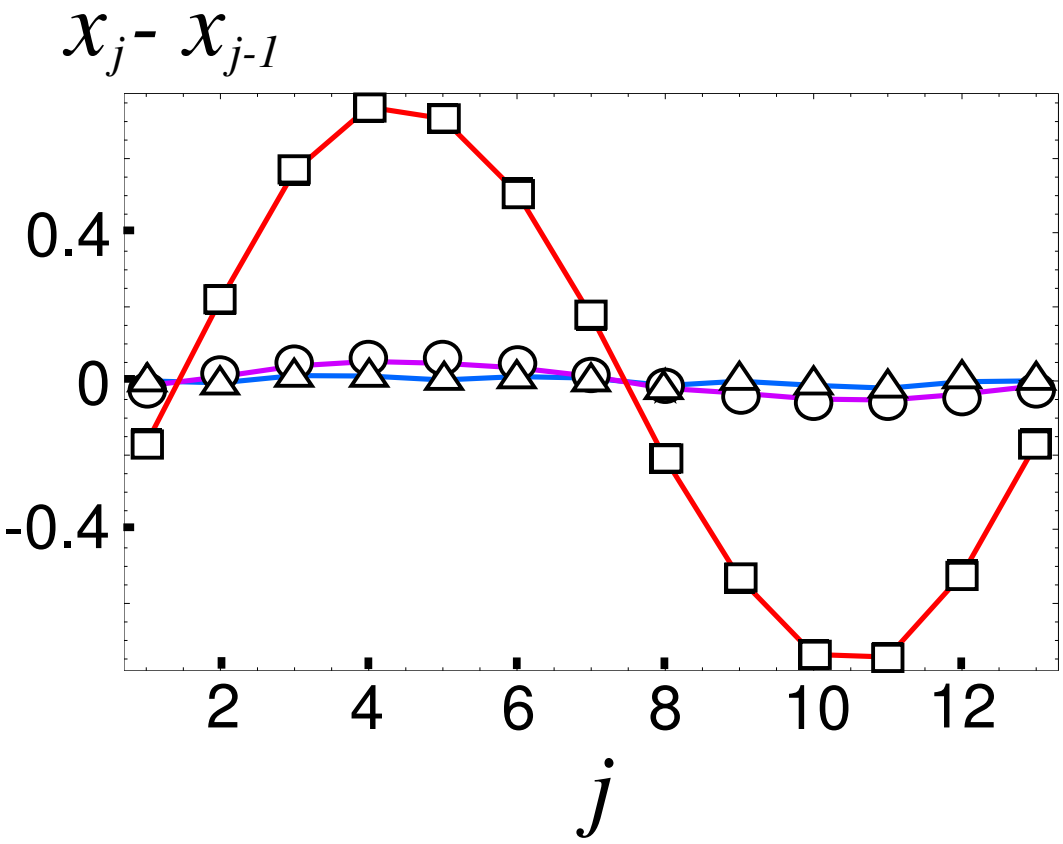

Figure 2.5: $x_j - x_{j-1}$ versus the node index j for $t = 1360$ (open triangles), $t = 1385$ (open circles), and $t = 1410$ (open squares). Note that the burst is absent first and grows with a long wavelength pattern.

2.2.2 Short wavelength burst

Short wavelength bursting can be expected, for example, when $N = 8$ and $g = 1.09$. In this case the value of λ_k corresponding to the shortest wavelength mode yields $g\lambda_k = 4.36$, which is in the bubbling region, while all the other modes are in the stable region. In this case the observation of the bursts is more difficult, as the transversal instability of the orbits and the transversal stability of the attractor are less pronounced [compare $\Psi(4.36)$ for this case vs. $\Psi(0.19)$ for the previous example in Fig. 2.2]. Accordingly, the perturbations of the parameter a were made larger, with perturbations randomly chosen with uniform density within a $\pm 6\%$ range of the ideal values of the parameter ($a = 0.2$). In principle this is not necessary, as a burst will eventually occur after long enough time. In practice, however, it is necessary to reduce the waiting time to a reasonable value. As before, the coupled equations were solved with an initial condition

on the synchronization manifold. In Fig. 2.6 we show $y_1 - y_2$ as a function of time for one choice of initial conditions. The difference $y_1 - y_2$ is usually positive and of magnitude close to 1. This asymmetry is not

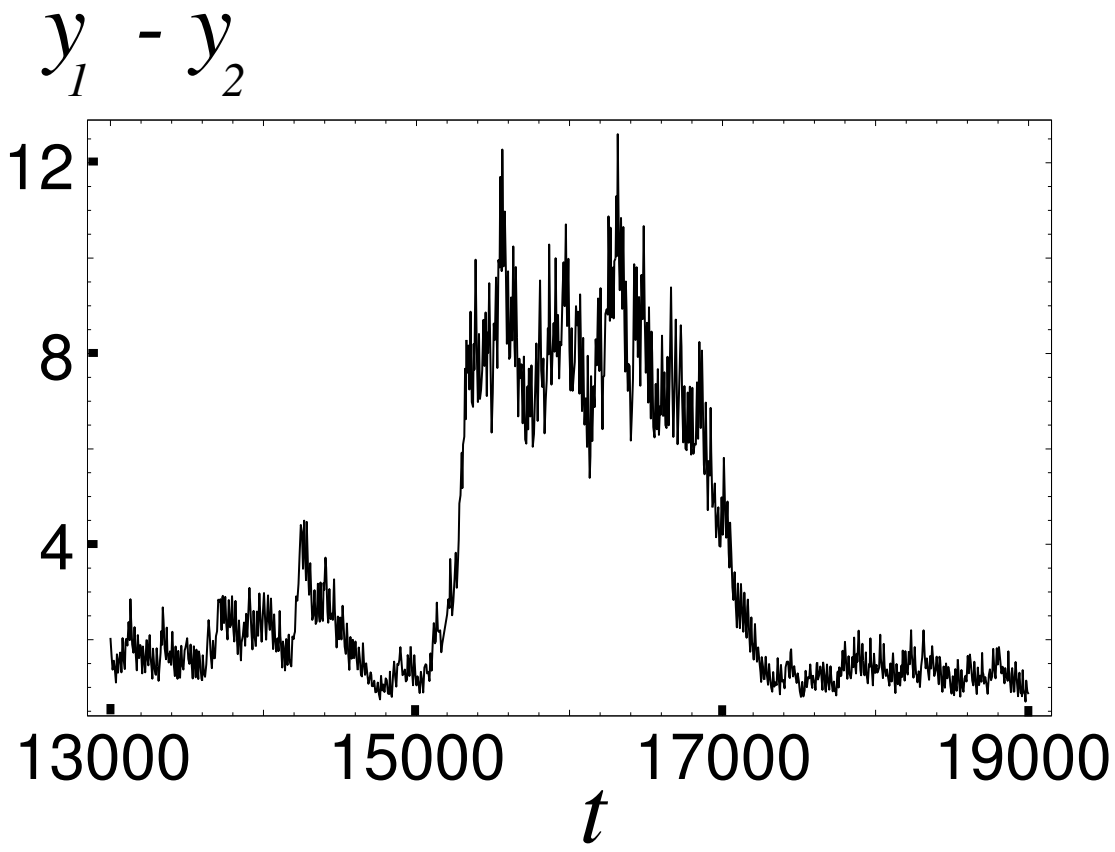

Figure 2.6: $y_1 - y_2$ as a function of time for 8 Rössler systems in a ring. The coupling strength g was 1.09. The desynchronization burst develops at $t \approx 15000$, although it is not as sharp due in part to the smaller magnitude of the transversal Lyapunov exponents ($\Psi(4.36)$ in Fig. 2.2).

a surprise since the oscillators are slightly different. For the relatively large value of the mismatch used, this is the "synchronized state". It is seen in Fig. 2.6 that the difference $y_1 - y_2$ increases rapidly at around $t \approx 15000$, and soon reaches values close to 10. It remains large for a longer time than in the case of the long wavelength burst (see Fig. 2.3) and decays more slowly as well. This is in qualitative agreement with the smaller absolute values of the master stability functions for the short wavelength mode, both for typical orbits on the attractor and for the periodic orbits.

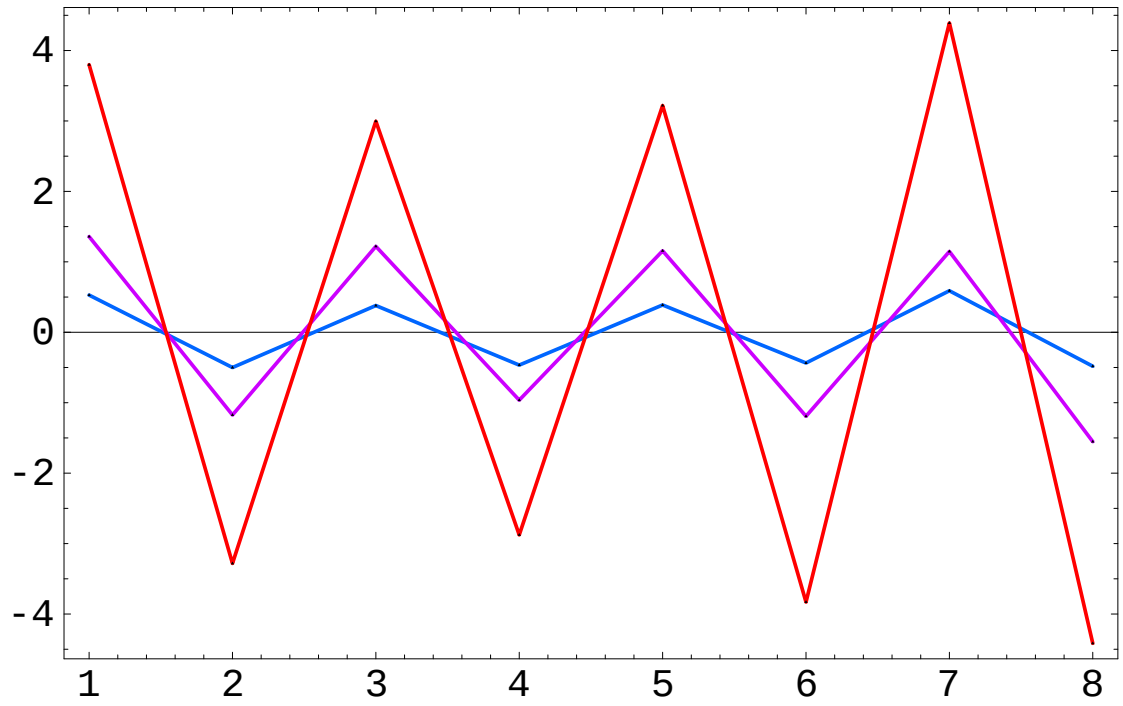

Figure 2.7: $y_j - y_{j-1}$ versus the node index j for $t = 15000$ (open triangles), $t = 15200$ (open circles), and $t = 15400$ (open squares). The desynchronization burst has a short wavelength spatial pattern.

In Fig. 2.7 we plot $y_j - y_{j-1}$ as a function of j, the oscillator index, for $t = 15000$, $t = 15200$ and $t = 15400$. As expected, the burst mainly affects the shortest wavelength mode.

This can be assesed properly by doing a spatial Fourier transform. In this case, the quantities η_k [see (2.5)] correspond to the Fourier coefficients, since the eigenvectors of the matrix (2.9) are sinusoidal. The Fourier coefficients η_k and η_{N-k}, for $1 \leq k < \frac{N}{2}$, correspond to the eigenvectors $w_k \propto [\sin(\frac{2\pi jk}{N})]_{j=1}^{N}$ and $w_k \propto [\cos(\frac{2\pi jk}{N})]_{j=1}^{N}$, and have the same eigenvalue λ_k. At this stage, we are only interested in discriminating between modes with different eigenvalue. For this reason, we will plot as a function of time the quantity ξ_k^2 defined by $\xi_k = \{([\eta_k]_y)^2 + ([\eta_{N-k}]_y)^2\}^{\frac{1}{2}}$ for $1 \leq k < \frac{N}{2}$ and $\xi_{\frac{N}{2}} = \left|[\eta_{\frac{N}{2}}]_y\right|$, where $[\eta_k]_y$ is the y component of the three dimensional vector η_k. Thus, the quantity ξ_k represents the weigth of the modes associated to the eigenvalue λ_k.

In Fig. 2.8, we plot as a function of time the quantities ξ_k^2 for $k = 1, 2, 3, 4$. The short wavelength mode ($k = 4$, upper curve) is dominant during the burst.

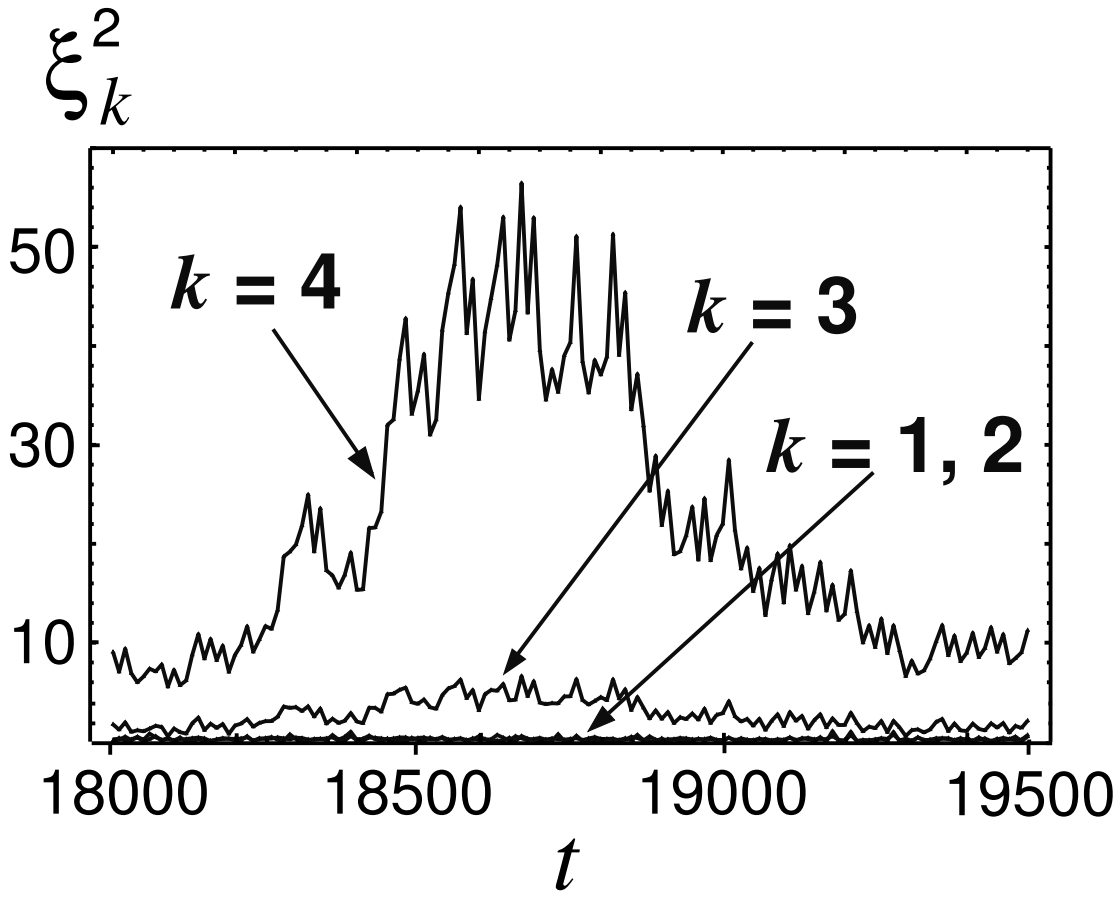

Figure 2.8: ξ_k^2 as a function of time for $k = 1, 2, 3, 4$. The shortest wavelength component corresponds to $k = 4$ (top curve). The curves corresponding to $k = 1, 2, 3$ are close to the horizontal axis.

2.2.3 Localized burst

In the above examples all links had equal weights. As an example of a case with unequal link weights we consider the case where the previous network is modified by doubling the strength of one of the links. Let the link whose strength is doubled be the link that connects nodes p and $p + 1$. For example, for $p = 4$,

$N = 8$, this yields the Laplacian matrix

$$G = \begin{pmatrix} 2 & -1 & 0 & 0 & 0 & 0 & 0 & -1 \\ -1 & 2 & -1 & 0 & 0 & 0 & 0 & 0 \\ 0 & -1 & 2 & -1 & 0 & 0 & 0 & 0 \\ 0 & 0 & -1 & 3 & -2 & 0 & 0 & 0 \\ 0 & 0 & 0 & -2 & 3 & -1 & 0 & 0 \\ 0 & 0 & 0 & 0 & -1 & 2 & -1 & 0 \\ 0 & 0 & 0 & 0 & 0 & -1 & 2 & -1 \\ -1 & 0 & 0 & 0 & 0 & 0 & -1 & 2 \end{pmatrix}, \tag{2.10}$$

Adopting the analysis technique of Ref. [52], we can show that such an enhanced connection has the consequence that the largest eigenvalue of G corresponds to an eigenfunction that is exponentially localized to the region near the strong connection. That is, for large N, the components of this eigenfunction decay exponentially as the distance between the localized region and the node corresponding to a component increases. Using the ideas of Ref. [52], we now provide this analysis. The equations for the eigenvector w and eigenvalue λ are

$$\begin{aligned} -2w_{p+1} - w_{p-1} + 3w_p &= \lambda w_p, \\ -w_{p+2} - 2w_p + 3w_{p+1} &= \lambda w_{p+1}, \\ -w_{j-1} - w_{j+1} + 2w_j &= \lambda w_j, \end{aligned} \tag{2.11}$$

for, respectively, nodes p, $p+1$ and j different from p or $p+1$.

We consider solutions of 2.11 that are (anti-)symmetric, $w_{p+1+k} = \pm w_{p-k}$, and for which $\frac{w_{p+1+j}}{w_{p+j}}$ is constant for $j \geq 1$, i.e., $w_{p+1+k} \propto t^k$ for $k \geq 0$ and some t. This will be a good approximation if the mode is localized (i.e., $|t| < 1$), and the network is big enough that $|t|^{\frac{N}{2}} \ll 1$. In the antisymmetric case, $w_{p+1+k} = -w_{p-k}$, Eqs. (2.11) yield,

$$\begin{aligned} 5 - t &= \lambda, \\ -t - t^{-1} + 2 &= \lambda \end{aligned} \tag{2.12}$$

which gives

$$t = -\frac{1}{3}\,, \quad \lambda = \frac{16}{3}. \tag{2.13}$$

Compare this eigenvalue with the largest eigenvalue for the network in which all links have equal strength, which has a value of 4. The symmetric solution, $w_{p+1+k} = w_{p-k}$, yields $t = 1$ and $\lambda = 0$, corresponding to the eigenvector $[1, 1, \ldots 1]$ of perturbations in the synchronization manifold. The smallest nonzero eigenvalue remains unchanged.

As an example, we show the localized desynchronization bursts produced by one of these strengthened connections for the case $N = 8$, corresponding to G given by (2.10) and the illustration in Fig. 2.9. The parameters of the idealized system are again $a = b = 0.2$, and $c = 7$, with a coupling strength of $g = 0.79$. It is remarkable that despite the small number of nodes, the actual localized eigenvector and

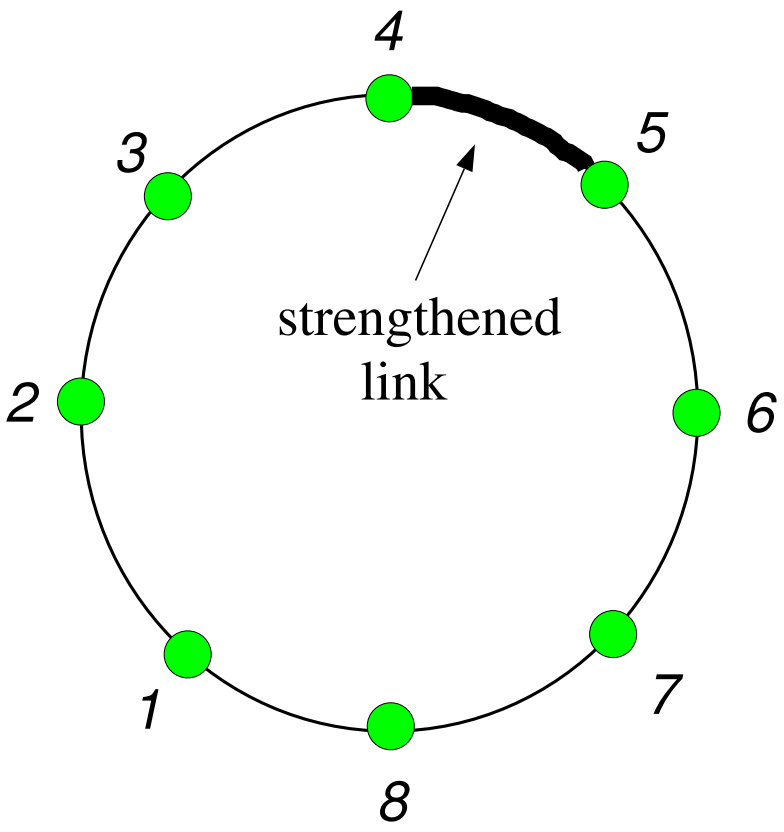

Figure 2.9: Arrangement of the dynamical units in a ring with the strength of the connection between nodes 4 and 5 doubled. The matrix G corresponding to this network is in Eq. (2.10).

eigenvalue agree well with (2.13) ($\lambda = 5.334\ldots$ and $\frac{w_6}{w_5} = -0.334\ldots$).

In Fig. 2.10 we show $x_5 - x_4$ as a function of time. As in the short wavelength case, the burst is not

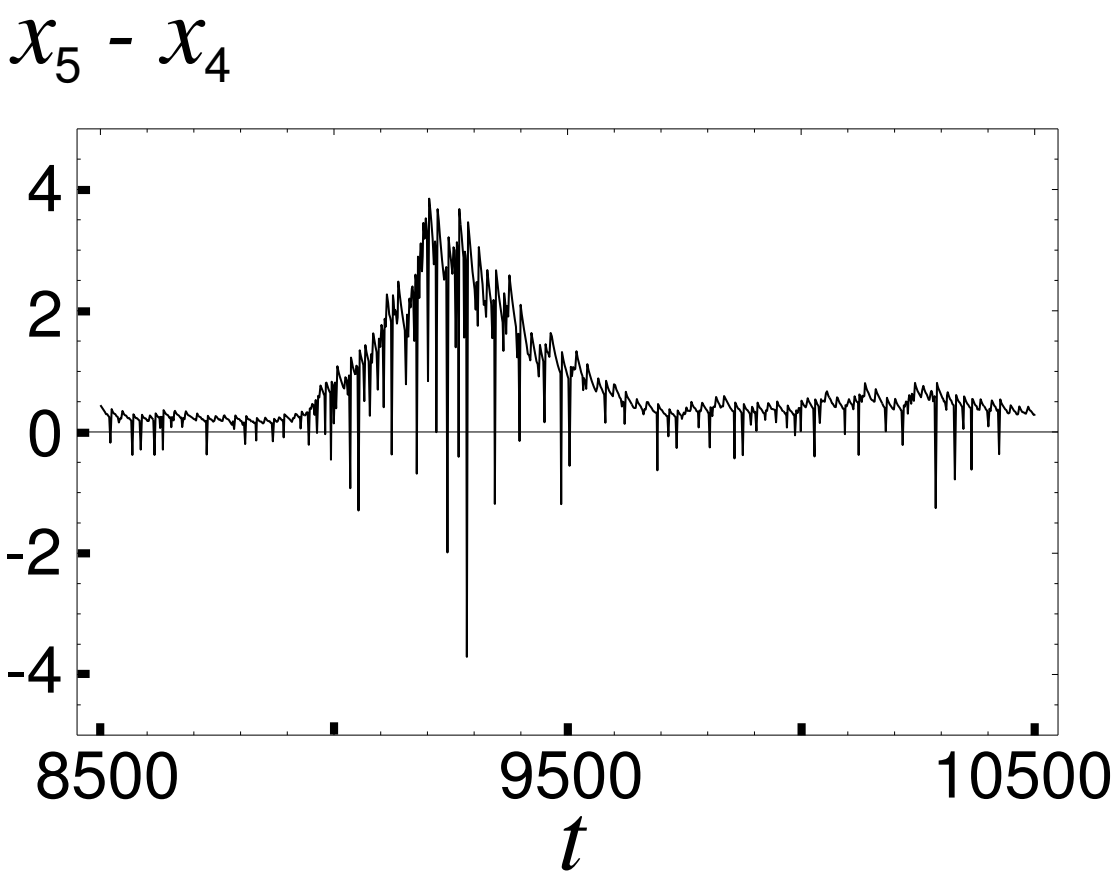

Figure 2.10: $x_5 - x_4$ as a function of time for $N = 8$ Rössler oscillators in a ring with the strength of the connection between nodes 4 and 5 doubled. The coupling strength is $g = 0.79$. A desynchronization burst starts approximately at $t \approx 9000$.

very sharp due to the small magnitude of the transversal Lyapunov exponents. Nevertheless, it can be seen that the difference $x_5 - x_4$ increases approximately at $t = 9000$ and returns to a relatively small value after reaching values considerably above the average.

In Fig. 2.11a we plot the difference between the x coordinate of node j and its mean over all nodes, $x_j - \overline{x}$, where $\overline{x} = \frac{1}{N}\sum_{j=1}^{N} x_j$, as a function of the oscillator index j, for $t = 8750$ (open triangles), $t = 9000$ (open circles), and $t = 9250$ (open squares). In Fig. 2.11b we show the localized eigenvector of

the Laplacian G found numerically. As discussed before, the desynchronization burst affects mainly nodes 4 and 5 (those which share the strengthened connection) and the ones adjacent to them. Nodes 1,2,7 and 8, however, maintain approximate synchronization during the burst.

In Fig. 2.12 we show the mode weights corresponding to the x coordinate as a function of time. The top curve corresponds to $[\eta_4]_x^2$ (for the localized mode), and the curves close to the horizontal axis to $[\eta_k]_x^2$, $k \neq 4$, for the other modes. (The degeneracy of the eigenvalues is broken by the strengthened connection, so we do not combine $[\eta_k]_x$ and $[\eta_{N-k}]_x$ as before.) Confirming the qualitative similarity between the eigenvector and the spatial pattern of the desynchronization burst observed in Fig. 2.11, the weight corresponding to the localized eigenvector is seen to be dominant during the period of time in which the burst occurs.

2.3 Effects of the mismatch spatial patterns

In this section we will discuss the effects that the mismatch spatial patterns have on the development of the desynchronization bursts. For these purposes, it will be convenient to rewrite Eq. (2.1) in the form

$$\dot{X}_i = \overline{F}(X_i) - g\sum_{j=1}^{N} G_{ij} H(X_j) + Q_i(X_i), \tag{2.14}$$

where $\overline{F}(X_i) = F(X_i, \overline{\mu})$ with $\overline{\mu} = \frac{1}{N}\sum_{j=1}^{N} \mu_j$, and $Q_i(X_i) = F(X_i, \mu_i) - \overline{F}(X_i)$. The term Q_i represents the effect of the mismatch and is assumed to be small. As before, we linearize around the synchronous state to get

$$\dot{\epsilon}_i = D\overline{F}(s)\epsilon_i - g\sum_{j=1}^{N} G_{ij} DH(s)\epsilon_j + Q_i(s), \tag{2.15}$$

where we have discarded terms of order $Q\epsilon$. With the previous notation and $Q = [Q_1, Q_2, \ldots Q_N]$, we obtain after the diagonalization

$$\dot{\eta}_k = \left(D\overline{F}(s) - g\lambda_k DH(s)\right)\eta_k + (QL)_k, \tag{2.16}$$

where $(QL)_k$ is the k'th column of the $d \times N$ matrix QL. In the ring with equal coupling along each link, the diagonalization procedure corresponds to a Fourier transform. In this case, we see that the mismatch affects the different modes according to the weigth, $(QL)_k$, of this particular mode in its Fourier expansion.

In other cases, for example in the localized eigenvector, the strength of the mismatch affecting the localized mode is proportional to the weigth of the localized eigenvector in the eigenvector decomposition of the mismatch. We will now discuss two applications of these results.

2.3.1 Amplification of mismatch patterns when modes with the same eigenvalue burst

We have shown that the modes of the mismatch force the corresponding modes of the deviations from the synchronous state. When bubbling induced bursting is expected, the size of the mismatch determines the average time between bursts [24]. Thus, the size of the mismatch component in mode k determines the average interburst time when that mode is in the bubbling regime.

When the spectrum of the matrix G is degenerate, the spatial modes of the mismatch play an extra role. All the modes sharing the same eigenvalue λ have the same stability properties, and thus, when the corresponding value $g\lambda$ is in the bubbling zone, all eigenvectors with this eigenvalue are equally likely to appear. The only difference between these modes is the strength with which they are forced, which is determined by the mismatch component in that mode as shown in Eq. (2.16) (or, if noise is present, by the noise component in that mode).

An example of this situation is the ring with connections of equal strength in the long wavelength bursting scenario. Since the ring is invariant with respect to rotations, the phase of the long wavelength oscillations can not be determined only from the network and dynamics part of the problem. The two modes with the longest wavelength (corresponding to sinusoidal and cosinusoidal oscillations) have the same eigenvalue. It is the mismatch that in this case determines the phase of the long wavelength burst.

We will show how one can determine the phase of the long wavelength desynchronization burst in the case of coupled Rössler systems in a ring with equal coupling along each link. For this system, the mismatch vector $Q_j(X_j)$ is given by

$$Q_j([x_j, y_j, z_j]^T) = \begin{pmatrix} 0 \\ y_j \delta a_j \\ \delta b_j - z_j \delta c_j \end{pmatrix}, \tag{2.17}$$

where $\delta a_j = a_j - \overline{a}$ und similarly for δb_j and δc_j. We define $\mathcal{F}_k(u) = \sum_{j=1}^{N} u_j \hat{w}_j^k$, where $\hat{w}_j^k$ is the

normalized j'th component of the k eigenvector described at the beginning of Section 2.2. With this convention, the term $(QL)_k$ in equation (2.16) is given by

$$(QL)_k = \begin{pmatrix} 0 \\ y\mathcal{F}_k(\delta a) \\ \mathcal{F}_k(\delta b) - z\mathcal{F}_k(\delta c) \end{pmatrix}. \tag{2.18}$$

Here $\delta a = [\delta a_1, \delta_2, \ldots, \delta_N]$ and similarly for δb, δc, and y, z are the trajectories around which the linearization was made.

We consider the case in which mismatch in one parameter is dominant, for example a. The mismatch in the parameters b and c will be assumed negligible compared with that in a, so that δb, $\delta c \ll \delta a$. In this case, only the second component of (2.18) is of relevance. Thus modes η_1 and η_{N-1} are excited with a strength proportional, respectively, to $\mathcal{F}_1(\delta a)$ and $\mathcal{F}_{N-1}(\delta a)$; see (2.16). The magnitude of η_k will be proportional to $\mathcal{F}_k(\delta a)$, and thus the excitation of the long wavelength mode (which is the only one for which perturbations grow) is proportional to

$$\mathcal{F}_1(\delta a)\sin\left(\frac{2\pi j}{N}\right) + \mathcal{F}_{N-1}(\delta a)\cos\left(\frac{2\pi j}{N}\right) \tag{2.19}$$

$$\propto \sin\left(\frac{2\pi j}{N} + \phi\right), \tag{2.20}$$

where $\tan\phi = \mathcal{F}_{N-1}(\delta a)/\mathcal{F}_1(\delta a)$.

We now show results of numerical simulations illustrating the above. The parameters N and g will be as in the long wavelength example in the previous section. We use the same random set of perturbations used in that example. As described above, we obtained the phase ϕ of the long wavelength component of the vector δa_i. In Fig. 2.13 we plot $y_j - y_{j-1}$ for different times during a burst (filled symbols). In the same Figure, we plot a scaled version of $\sin\left(\frac{2\pi j}{12} + \phi\right) - \sin\left(\frac{2\pi(j-1)}{12} + \phi\right)$ (open circles). The phase of the desynchronization burst is in agreement with that of the long wavelength component of the mismatch.

When the mismatch affects predominantly one parameter as in this case, the phase of the bursts can be predicted as described above. When mismatch in different parameters is comparable, the phases of the long wavelength modes of the different parameter mismatches compete and the bursts develop with one of these phases or with a combination of them.

It must be emphasized that this analysis is possible only when there is a degeneracy of the eigenvalues. For example, the location of the localized burst can not be determined in this way, as it is fixed in the position of the strengthened link. In this case, the mismatch component in the localized mode would only affect the average time between bursts.

2.3.2 Artificial supression of unstable modes using knowledge of the mismatch

We will now discuss another consequence of Eq. (2.16). We imagine a situation where we are given a number of nearly identical oscillators that we are to connect in a network which we desire to be in synchronism as much as possible. Furthermore, we imagine that, through measurements made individually on each oscillator, we are aware of the amount of mismatch in each oscillator. The question we address is this: Using our knowledge of the individual mismatches, how should we arrange the oscillators in the network so as to best supress the frequency of desynchronism bursts? To answer this question, we note that, according to the previous discussion, we should reduce the mismatch component in the mode which is in the bubbling region. Since the size of the mismatch affects the average interburst time [24], reducing this component is desirable if one wants to improve the quality of the synchronization. This can be accomplished by judiciously arranging the dynamical units so that the k'th mode of the mismatch is minimized when the corresponding value $g\lambda_k$ is in the bubbling region. For example, to supress long wavelength bursts, one may arrange the units so that the parameter errors alternate above and below the mean. To supress the localized bursting described in the previous section, one could arrange the units so that those with the more similar parameters are the ones in the region of the strengthened connection.

As a concrete example, we test this idea using simulations for the case of short wavelength bursting presented in the previous Section. We again assume for simplicity that mismatch in the parameter a is dominant. We generate random perturbations in the parameter a within a $\pm 6\%$ range of the value $a = 0.2$, as explained in the previous section. With this set of parameters given, we set up the dynamical units in the ring using two different permutations of their positions. One of them (a_s) has a smaller and the other (a_l) a larger short wavelength component $\mathcal{F}_4(a)$ than the original random sequence. The ratio $\mathcal{F}_4(a_l)/\mathcal{F}_4(a_s)$ is approximately 15. In Fig 2.14 we plot $x_1 - x_2$ as a function of time for configuration a_l (top curve) and

for configuration a_s (bottom curve). The difference $x_1 - x_2$ is much smaller in the former case than in the latter, roughly by a factor of 15, as can be expected from the ratio $\mathcal{F}_4(a_l)/\mathcal{F}_4(a_s)$. This qualitative example illustrates how one can use knowledge of the mismatch to supress undesired instabilities.

2.4 Spatial patterns of deviations from the stable synchronous state

So far, we have concentrated in the case in which the value of $g\lambda_k$ is in the bubbling regime for one mode k and in the stable regime for the other modes, so that desynchronization bursts occur sporadically. As we have seen, these bursts present spatial patterns on the network.

If synchronization is desired, one would might try to avoid the bubbling regime by designing the network and adjusting the coupling strength so that all the modes lie in the stable zone. One would also strive to reduce the mismatch, but as mentioned before, there are practical limitations on how much one can make the oscillators exactly the same.

If $\Psi(g\lambda_k)$ is negative for all modes (indicating transversal stability of the synchronous state) one can have, depending on the degree of transversal stability, fair synchronization even with relatively large amounts of mismatch. If one is to operate under such conditions, it is important to know the characteristics of the deviations from the synchronous state.

Thus we ask in this scenario: How large are the spatial patterns of the deviations from the synchronous state, and how does this depend on the mismatch and on the degree of transversal stability?

The spatial modes of these deviations obey Eq. (2.16). In the absence of the term $(QL)_k$, the zero solution is stable, and typical perturbations from it decay, having a negative Lyapunov exponent given by $h_k \equiv \Psi(g\lambda_k)$. The first term in the right hand side of Eq. (2.16) can be thougt of as a damping term with a damping rate given by h_k, and the second term, $(QL)_k$, as a forcing term. Since we are considering the stable case, these two factors, on average, cancel each other. By definition, the Lyapunov exponent for the system without mismatch is given by $h_k = \langle \frac{\eta_k^T (D\overline{F} - g\lambda_k DH)\eta_k}{|\eta_k|^2} \rangle$, where the angle brackets indicate time average. Assuming a solution η_k of the system with mismatch to yield the same value of this time average, we left multiply Eq. (2.16) by $\eta_k^T \, |\eta_k|^{-2}$ and average to obtain

$$|h_k| \approx \langle \frac{\eta_k^T (QL)_k}{|\eta_k|^2} \rangle \sim \langle \frac{|(QL)_k|}{|\eta_k|} \rangle, \tag{2.21}$$

where the angle brackets indicate time average. This leads to the following rough estimate,

$$\langle|\eta_k|\rangle \sim \frac{\langle|(QL)_k|\rangle}{|h_k|}. \tag{2.22}$$

(This is analogous to the result obtained for a linearly damped equation with constant forcing in one dimension, $\dot{\eta} = -h\eta + q$. In this case one has asymptotically $\eta \to \frac{q}{h}$.)

As an example we consider Rössler units in a ring with all connections of equal strength. We choose $N = 8$, $g = 0.6$ [$\Psi(g\lambda_k) < 0$ for all values of k]. Furthermore, we add a random perturbation to the parameter a of each oscillator chosen uniformly from within a $\pm 0.1\%$ range of $a = 0.2$.

In Fig. 2.15 we show, for $k = 1, \ldots, 7$, the quantities $\langle|\eta_k|\rangle$ (squares), $\langle|(QL)_k|\rangle$ (triangles), and $\frac{\langle|(QL)_k|\rangle}{|h_k|}$ (circles). The magnitudes of the forcing term for the different modes ($\langle|(QL)_k|\rangle$) span roughly two orders of magnitude, and the magnitude of the response ($\langle|\eta_k|\rangle$) looks roughly proportional to the latter. When the forcing term is corrected by dividing it by the magnitude of the corresponding Lyapunov vector $|h_k|$, the resulting quantity ($\frac{\langle|(QL)_k|\rangle}{|h_k|}$) matches very well the observed response.

2.5 Discussion

We have studied the stability properties of the synchronized state in a network of coupled chaotic dynamical units when these have a small heterogeneity. We have shown that when the dynamical units that are coupled in a network are sligthly different, the synchronized state can be interrupted by large infrequent desynchronization bursts for some values of the parameters. The range of the parameters for which this phenomenon is expected can be obtained by performing a master stability function analysis of the chaotic attractor and of the periodic orbits embedded in it.

The desynchronization bursts are induced by the bubbling phenomenon, and have spatial patterns on the network. These spatial patterns can be predicted from the eigenvectors of the Laplacian matrix G and the master stability functions mentioned above. We showed examples illustrating the development of bursts with spatial patterns. One of our examples showed that the strengthening of a single connection might destabilize the nodes near this connection, while leaving the rest of the network approximately synchronized.

Direct measurement of the parameter mismatch in the elements of a network might prove useful. We discussed how this knowledge could be used to reduce the frequency of bursts and to predict the relative weights of different spatial patterns in a burst. We also discussed how one could, from knowledge of the mismatch and of the master stability function, describe the spatial patterns and magnitude of the deviations from the synchronized state when the synchronization of the corresponding identical unit system is robust.

We emphasize that although we did not discuss the effects of noise, the phenomenon described in this Chapter also occurs for noisy identical oscillators. Desynchronization bursts with spatial patterns are expected for noisy, identical oscillators if one has them for noiseless, nonidentical oscillators. The difference is that the parameter mismatch is always ‘frozen’, in the sense that the mismatch is always the same for each oscillator, whereas for noise this is not the case.

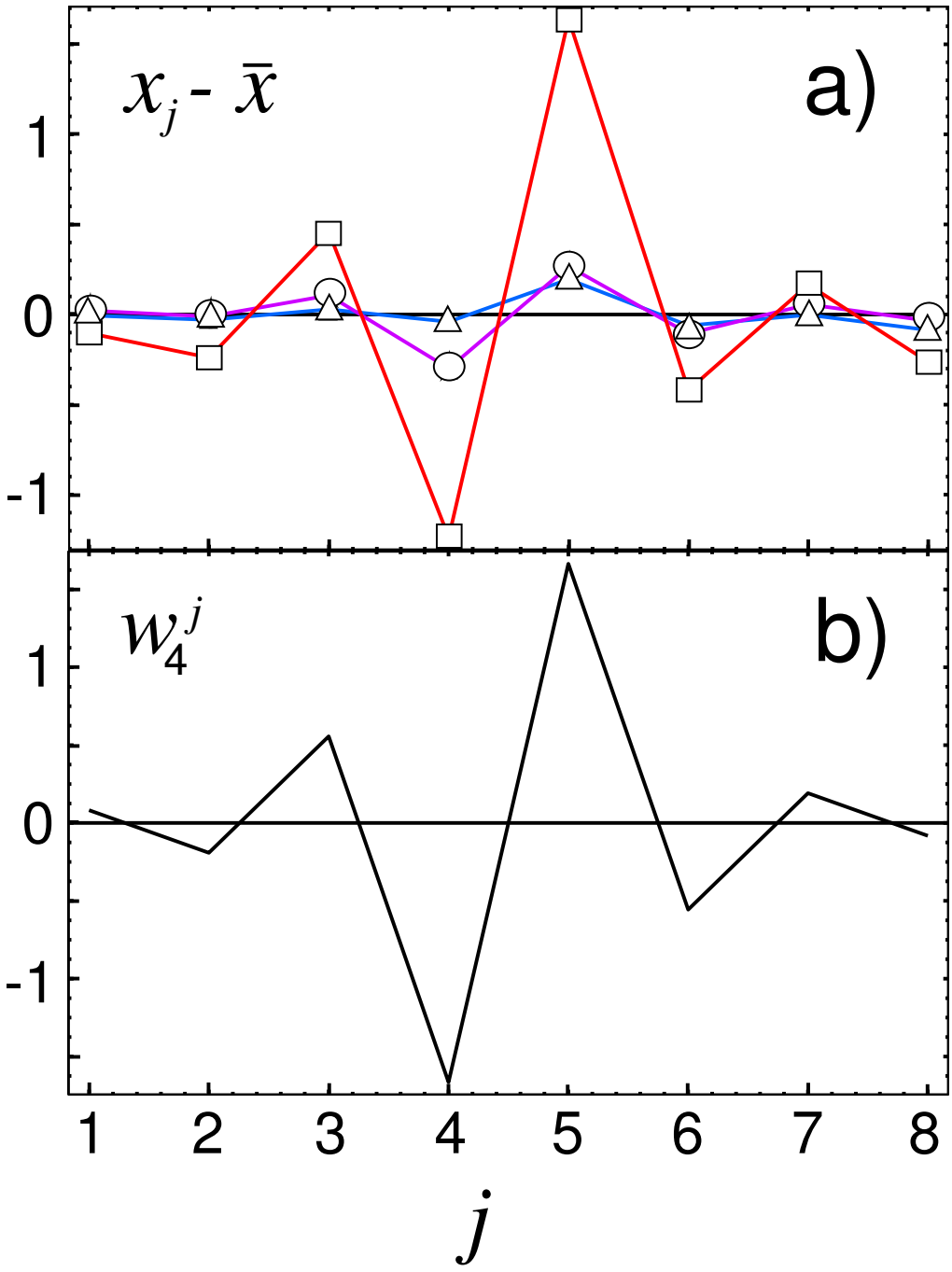

Figure 2.11: a) $x_j - \overline{x}$ for $t = 8750$ (open triangles), $t = 9000$ (open circles), and $t = 9250$ (open squares), for the configuration in Fig. 2.9. The burst develops with the spatial pattern of the localized eigenvector in Fig. 2.11b. b) Localized eigenvector of matrix G in Eq. (2.10).

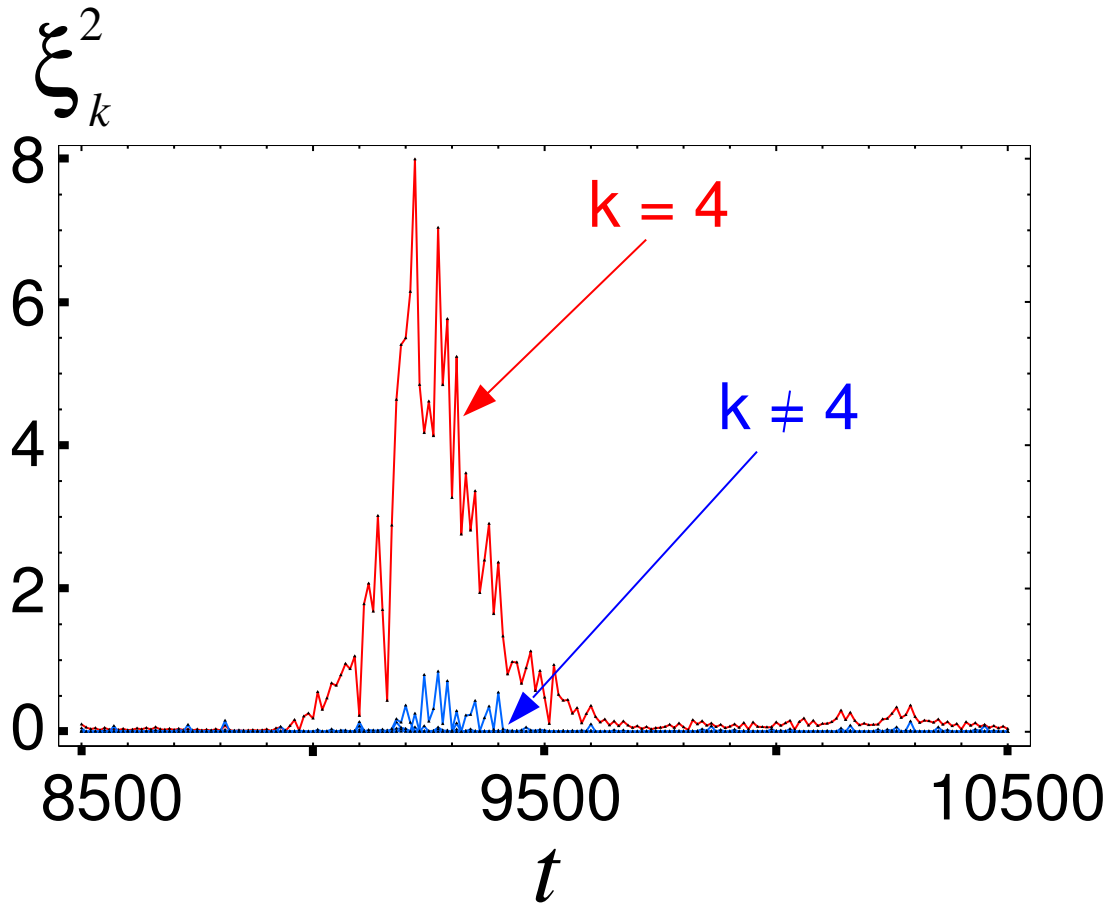

Figure 2.12: $[\eta_k]_x^2$ as a function of time for $k = 4$ (top curve) corresponding to the localized mode, and for $k \neq 4$ (bottom curves, close to zero), corresponding to other modes. In the burst, the localized mode is excited first and only after some time are the other modes also somewhat excited. The localized mode is dominant during the burst.

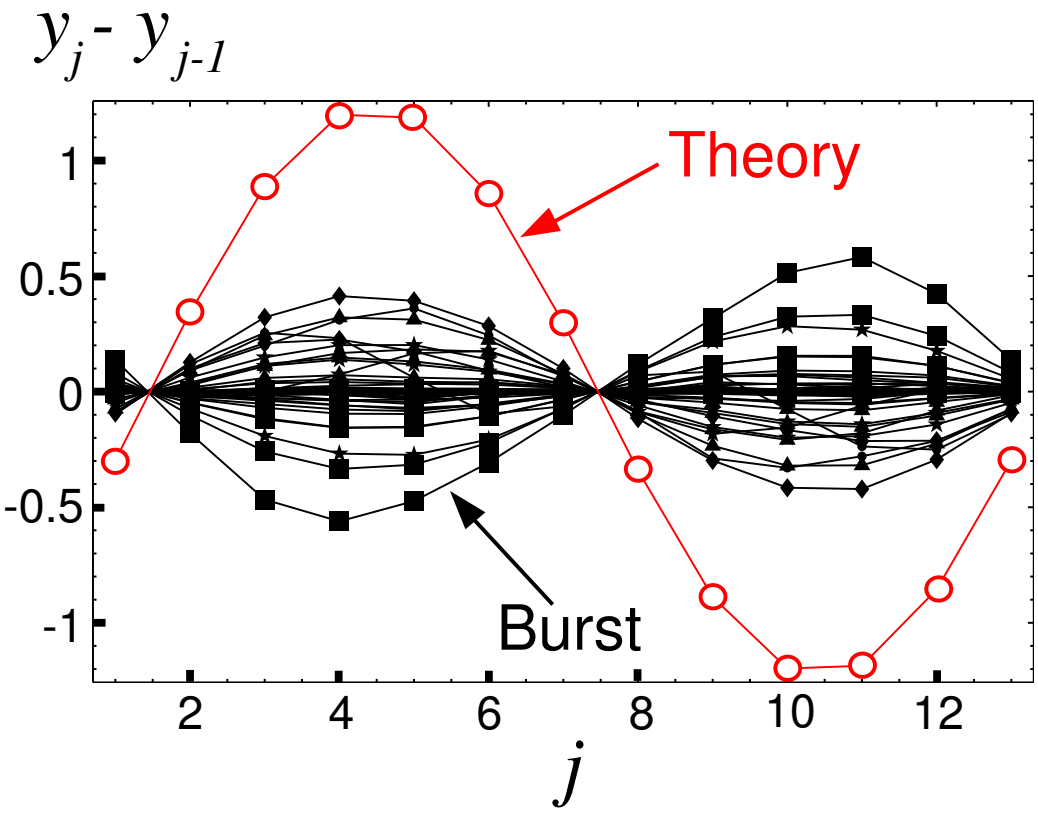

Figure 2.13: $y_j - y_{j-1}$ for different times during a burst (filled symbols), and a scaled version of $\sin\left(\frac{2\pi j}{12} + \phi\right) - \sin\left(\frac{2\pi(j-1)}{12} + \phi\right)$ with ϕ as given in the text (open circles). The phase of the burst spatial pattern coincides with the phase of the long wavelength component of the mismatch.

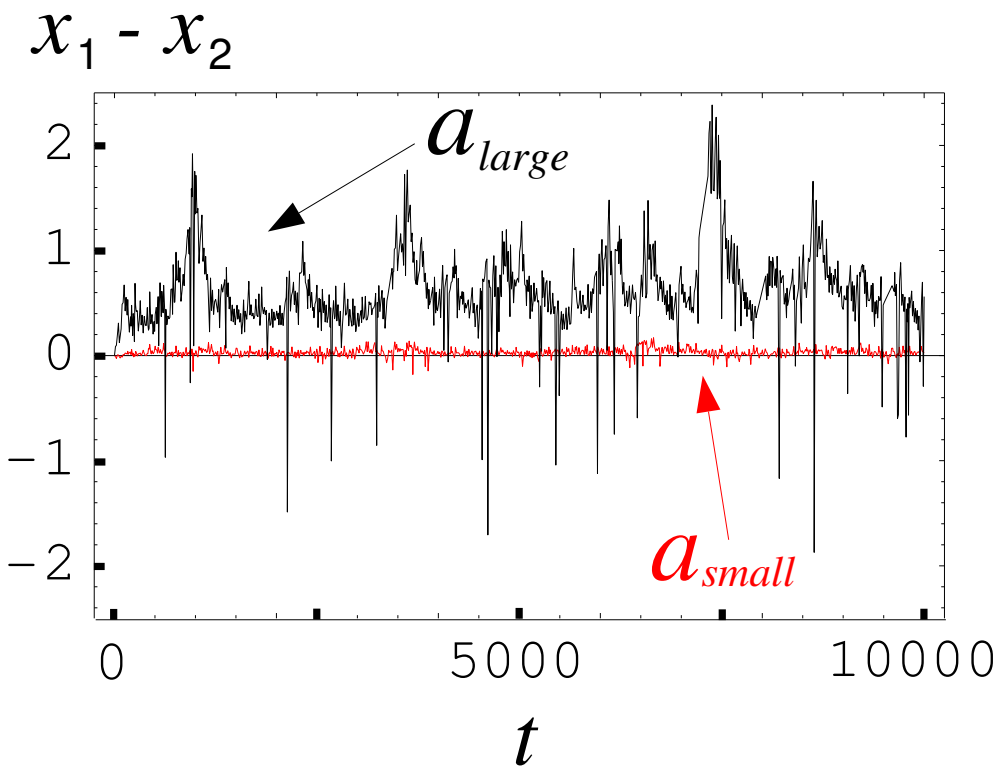

Figure 2.14: $x_1 - x_2$ as a function of time for a configuration of oscillators with a large (top curve) and with a small (curve closer to zero) short wavelength component of the mismatch. The quality of the synchronization is much better in the second case.

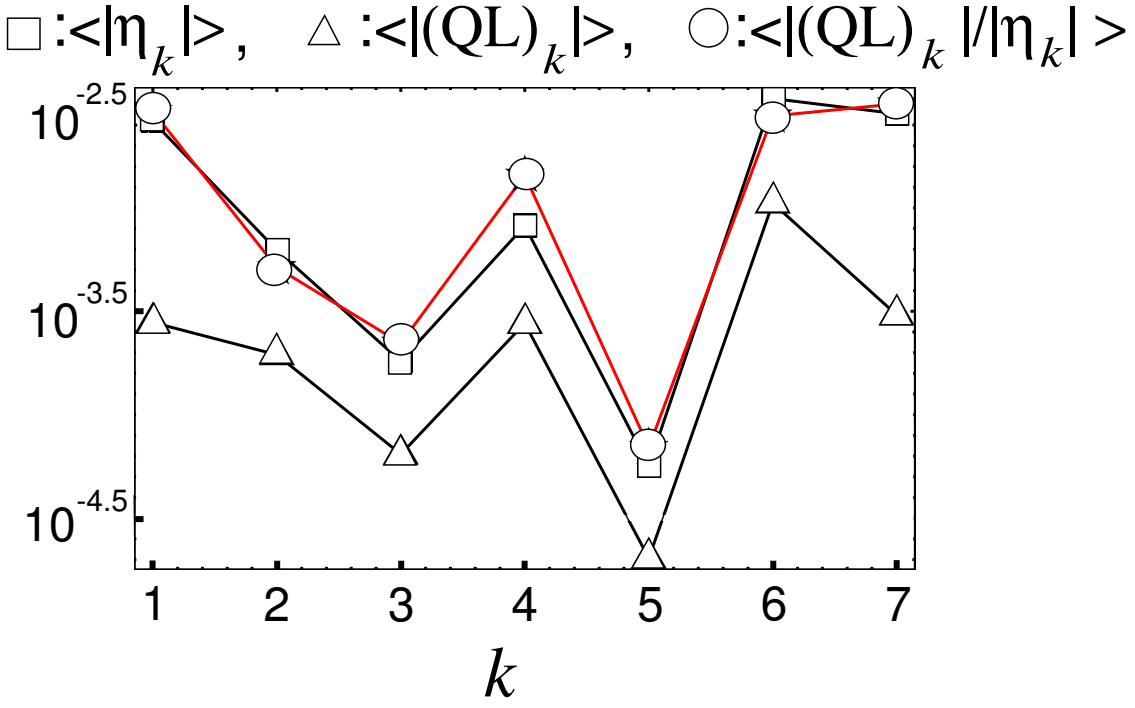

Figure 2.15: $\langle|\eta_k|\rangle$ (open squares), $\langle|(QL)_k|\rangle$ (open triangles), and $\frac{\langle|(QL)_k|\rangle}{h_k}$ (open circles) for $N = 8$, $g = 0.6$, $k = 1, \ldots, 7$. The forcing term (open triangles) roughly determines the response (open squares). The corrected forcing term (open circles) matches well the response (open squares).

Chapter 3

Parameter mismatch estimation using large deviations from synchronization

The study of networks of coupled dynamical systems is an important area of research with applications in diverse fields, ranging from biology to laser physics [10]-[20]. The synchronization of coupled oscillators has been under extensive study in recent years and, in particular, the synchronization of identical oscillators has received considerable interest [18, 20]. Since it is impossible in practice to obtain identical oscillators, the effect of the difference in the parameters of the oscillators, or *parameter mismatch*, might be relevant in some applications. It might be desired to have dynamical units as similar to each other as possible, or to know the characteristics of the parameter mismatch in a collection of nearly identical systems. In this Chapter we propose a method to use deviations from synchronization to extract information on the parameter mismatch of the coupled dynamical units. Existing methods for parameter estimation (see, for example, Refs. [53]-[56]) usually rely on knowledge of the typically small synchronization error. Our method depends on relatively large deviations from the synchronized state, and might be useful in cases in which the small synchronization error can not be measured accurately.

When a number of identical systems are appropriately coupled in a network, a solution exists in which the state of all oscillators at all times is the same. This is referred to as *identical* synchronization [13]. This concept is useful only when the systems are identical. We will deal with systems that are nearly, but not exactly, identical. We will refer to a situation in which the states of the systems are very close to each other as *nearly identical* synchronization. A method to determine the stability of the synchronous state when the systems are identical, the *master stability function*, has been proposed by Pecora and Carroll [44].

In the case of nearly identical chaotic systems, the nearly synchronized state might be interrupted by relatively short periods of desynchronization (*desynchronization bursts*). These bursts develop with spatial patterns on the network. As shown in Chapter 2, these spatial patterns, and the parameters for which they can be expected, can be predicted from the Laplacian matrix describing the network connections, the master stability function of the attractor, and the unstable periodic orbits embedded in it. The spatial patterns of

the bursts depend on the parameter mismatch of the different systems. We use this fact to infer the relative deviation of the parameters of the individual units with respect to their mean from the desynchronization bursts. The proposed method is as follows. The oscillators are connected in such a way that the parameter mismatch determines the spatial patterns of the desynchronization bursts. As we will see later, one such way is all-to-all coupling. The system is set up in a parameter region in which desynchronization bursts are expected. While a burst is developing, measurements are taken of the deviations of the different systems from the synchronous state. From these observations, the relative deviations of the parameters from the mean are deduced. In order to apply our method, it is necessary to connect the oscillators in such a way that all or most of the modes burst at the same time. We therefore assume certain freedom in connecting the oscillators. Our method is not intended to be used in a fixed, preexisting network, but to use one in order to determine the mismatch of the oscillators. After the mismatch is known, the oscillators can be connected in any way, and the obtained knowledge of the mismatch can be used, for example, in order to optimize the configuration of the oscillators in this subsequent network [57].

Some limitations of this method are the following. It is assumed that the dynamics of the systems is known accurately (except for the parameter mismatch), and that measurements can be taken with enough precision such that the deviations from the synchronous state can be measured in the linear regime. Although in some applications the dynamics is unknown, there are important cases in which it is known accurately (e.g., electrical circuits). Also, the presence of noise affects the spatial patterns of the bursts. Although we will describe how to deal with the noise, the effectiveness of the method decreases as the ratio of noise to mismatch increases. It is also assumed that unavoidable small differences in the way in which the systems are connected to each other does not introduce a difference between the systems which is of the same order of magnitude or larger than the parameter mismatch being measured.

In Section 3.1 we briefly describe the master stability function method and its extension to deal with nearly identical systems. In Section 3.2 we present and illustrate our method with an example in the case where the noise is negligible. In Section 3.3 we discuss how to deal with the noise and show an example. In Section 3.4 we present our conclusions to this Chapter.

3.1 Background

For simplicity, we will use one dimensional maps for the chaotic units. The results generalize to other dynamical systems [44, 57]. We consider a model system of N dynamical units, each one of which, when isolated, satisfies $X^i_{n+1} = F(X^i_n, \mu_i)$, where X^i_n is the value of unit i at time n and μ_i is a parameter vector for system i.

The systems, when coupled, are taken to satisfy (e.g., [44])

$$X^i_{n+1} = F(X^i_n, \mu_i) - gZ\left(\sum_{j=1}^{N} G_{ij} H(X^j)\right), \tag{3.1}$$

where Z is a function such that $Z(0) = 0$, G is a symmetric Laplacian matrix ($\sum_j G_{ij} = 0$) describing the network connections, and H is a function independent of i and j. [In our examples, we will take $Z(x) = \sin(2\pi x)$.] The constant g determines the strength of the coupling.

If the systems are identical (i.e., $\mu_i = \mu$ for all i), there is an exactly synchronized solution of Eqs. (3.1), $X^1_n \equiv X^2_n \equiv \cdots \equiv X^N_n = s_n$, whose time evolution is the same as the uncoupled dynamics of a single unit, $s_{n+1} = F(s_n)$, where $F(s) = F(s, \mu)$. The stability of the synchronized state can be determined from the variational equations obtained by considering an infinitesimal perturbation δ^i from the synchronous state, $X^i_n = s_n + \delta^i_n$,

$$\delta^i_{n+1} = DF(s_n)\delta^i_n - gZ'(0)\sum_{j=1}^{N} G_{ij} DH(s_n)\delta^j_n. \tag{3.2}$$

Let $\delta = [\delta^1, \delta^2, \ldots, \delta^N]$, and define the vector $\eta = [\eta^1, \eta^2, \ldots, \eta^N]$ by $\delta = \eta L^T$, where L is the orthogonal matrix whose columns are the corresponding real orthonormal eigenvectors of G; $GL = L\Lambda$, $\Lambda = diag(\lambda_1, \lambda_2, \ldots, \lambda_N)$, where λ_k is the eigenvalue of G for eigenvector k. Then Eqs. (3.2) are equivalent to

$$\eta^k_{n+1} = \left[DF(s_n) - gZ'(0)\lambda_k DH(s_n)\right]\eta^k_n. \tag{3.3}$$

The quantity η^k is the weight of the kth eigenvector of G in the perturbation δ. The linear stability of each 'spatial' mode k is determined by the stability of the solution of Eq. (3.3). By introducing a scalar variable $\alpha = gZ'(0)\lambda_k$, the set of equations given by Eq. (3.3) can be encapsulated in the single equation,

$$\eta_{n+1} = \left[DF(s_n) - \alpha DH(s_n)\right]\eta_n. \tag{3.4}$$

The master stability function $\Psi(\alpha)$ [44] is the largest Lyapunov exponent for this equation. This function depends only on the coupling function H and the dynamics of an individual uncoupled element, but not on the network connectivity. The network connectivity determines the eigenvalues λ_k (independent of details of the dynamics of the chaotic units). The stability of the synchronized state of the network is determined by $\Psi_* = \sup_k \Psi(g\lambda_k)$, where $\Psi_* > 0$ indicates instability.

If the systems are slightly different, one gets instead of Eqs. (3.2) the equations

$$\delta^i_{n+1} = D\overline{F}(s_n)\delta^i_n - gZ'(0)\sum_{j=1}^{N} G_{ij}DH(s)\delta^j_n + Q^i(s_n), \tag{3.5}$$

where $\overline{F}(X^i) \equiv F(X^i, \sum_i^N \mu_i/N)$, and $Q^i(X^i) \equiv F(X^i, \mu_i) - \overline{F}(X^i)$ represents the effect of the mismatch and is assumed to be small. Terms of order $Q\delta$ were neglected. Defining $Q = [Q^1(s_n), Q^2(s_n), \ldots, Q^N(s_n)]$, we obtain an equation analogous to Eq. (3.3),

$$\eta^k_{n+1} = [DF(s_n) - gZ'(0)\lambda_k DH(s_n)]\,\eta^k_n + (QL)^k, \tag{3.6}$$

where $(QL)^k$ is the kth element of the vector QL. The Lyapunov exponent for the solution of Eq. (3.3) is $h_k = \Psi(g\lambda_k)$. Assuming a solution of Eq. (3.6) to have the same average damping as that for Eq. (3.3), then, if h_k is negative for all modes, the amplitude of η_k can be estimated as

$$\langle|\eta^k|\rangle \sim \frac{\langle|(QL)^k|\rangle}{1 - e^{-|h_k|}}. \tag{3.7}$$

(For example, if we model Eq. (3.6) by the simple system $\eta_{n+1} = e^{-h}\eta_n + q$, then η_n satisfies, as $n \to \infty$, $\eta \to \frac{q}{1-e^{-h}}$. See [57].) The largest Lyapunov exponent h_k above corresponds to a typical trajectory in the chaotic attractor. However, the Lyapunov exponent for unstable periodic orbits embedded in the attractor might be larger. Assume that one of these periodic orbits has a positive Lyapunov exponent and the attractor has a negative Lyapunov exponent. In this case, most of the time the amplitude of η_k will be very small and given approximately by Eq. (3.7). Eventually the trajectory s_n will get very close to this transversally unstable periodic orbit. While it is close to this orbit, η in Eq. (3.6) is no longer damped and gets exponentially amplified with the Lyapunov exponent of the unstable periodic orbit. The deviation from the synchronized state becomes large, producing a desynchronization burst. If there are no other attractors, the system returns to the synchronized state and the process repeats. Desynchronization bursts can be

expected when the master stability function for a typical trajectory is negative for all modes, and there is an embedded unstable periodic orbit which has a positive master stability function for at least one mode (i.e., $\overline{\Psi}(g\lambda_k) > 0$ for some k, where $\overline{\Psi}$ is the master stability function of one of the embedded periodic orbits).

We will now use the fact that modes with the same eigenvalue have the same stability. For simplicity, assume that the coupling is all to all, so that all the modes (except the mode in the synchronization manifold, which has zero eigenvalue) have the same eigenvalue, $\lambda_k = N$. Eq. (3.7) implies that the coefficients in the eigenvector decomposition of the deviations from synchrony (η^k) are, on average, proportional to those for the deviations of the mismatch parameters from their mean [$(QL)^k$]. It follows that the mismatch vector Q is proportional to the vector δ_n while these approximations are valid. If the vector δ_n is measured, the deviations of the mismatch from its mean can be determined approximately up to an unknown scaling factor.

For this method to work, the measurements need to be made when the system is still in the linear regime. Since it is assumed that there is a limitation in the measurement accuracy, δ_n needs to be small enough to guarantee linear behavior, but large enough to be measured. One can thus set up the system so that desynchronization bursts are expected and make measurements while a desynchronization burst is developing. If the system allows continuous tuning of the coupling strength, one could also increase it so that the synchronous state becomes unstable and take measurements as the system desynchronizes.

3.2 Parameter mismatch estimation without noise

To illustrate our method, we use the *circle map*, described by the equation

$$\theta_{n+1} = [\theta_n + \omega + \kappa \sin 2\pi\theta_n] \bmod 1. \tag{3.8}$$

We choose the parameters to be $\omega = \frac{\sqrt{5}-1}{2}$ and $\kappa = \frac{1}{\sqrt{3}}$. These parameters produce a chaotic attractor in $\theta \in [0.21, 0.47]$. We found the embedded periodic orbits up to period four. To determine the orbits of period p we used Newton's method to find the roots of $\theta = f^p(\theta)$, where $f(\theta)$ is described by Eq. (3.8) and f^p denotes the p times composition of f. Eliminating all the orbits outside of the attractor, we found one period 1 orbit, two period 2 orbits, and one period 4 orbit. We show in Fig. 3.1 the master stability functions

of the orbits found, and the master stability function of the attractor. Here $\alpha = 2\pi g\lambda_k$, where λ_k is the kth eigenvalue of the coupling matrix and g is the global strength of the coupling.

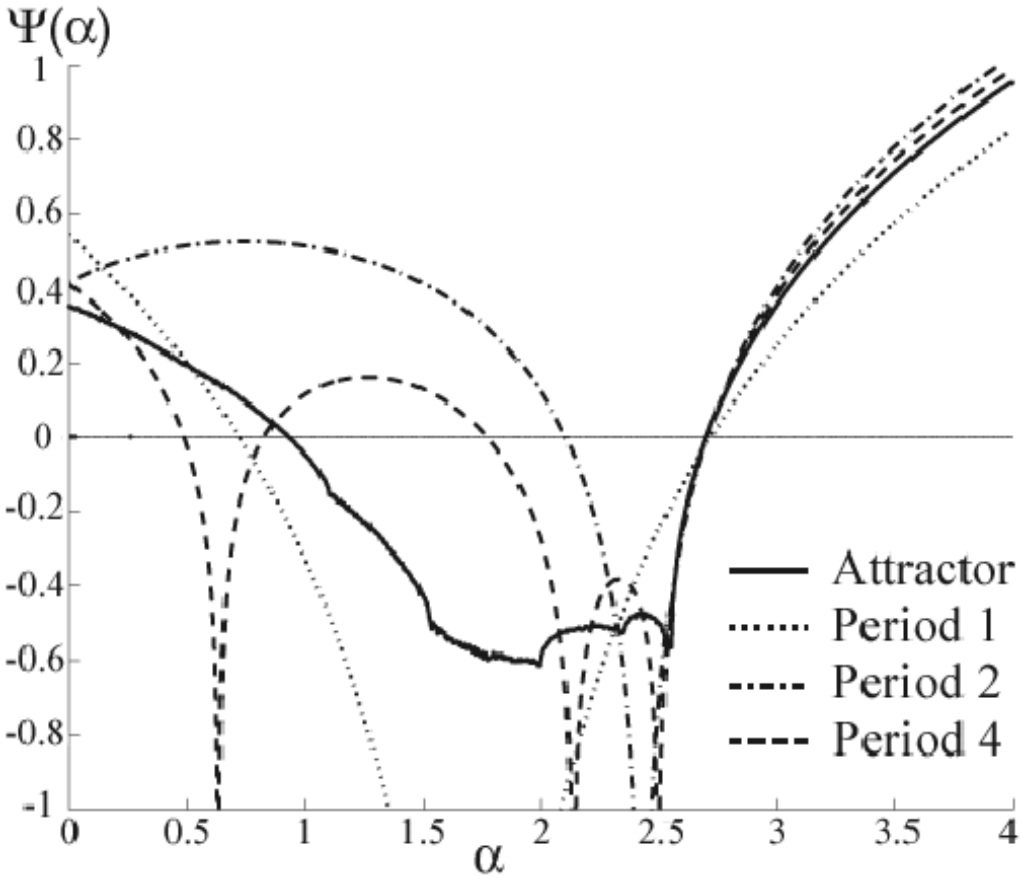

Figure 3.1: Master stability function, $\Psi(\alpha)$, for a typical trajectory in the attractor (continuous curve), for the period 1 orbit (dotted curve), for the period 2 orbit (dashed-dotted curve), and for the period 4 orbit (dashed curve).

For definiteness, we assume a network that is coupled *all to all*. This means that for a network of N systems, an element in the coupling matrix G_{ij} is given by

$$G_{ij} = \begin{cases} N-1 & \text{if } i = j; \\ -1 & \text{if } i \neq j. \end{cases} \tag{3.9}$$

This matrix has two distinct eigenvalues, $\lambda_0 = 0$ and $\lambda_k = N$ for $k = 1, 2, \ldots, N-1$. We ignore the 0 eigenvalue since this corresponds to a perturbation in which all of the systems are displaced by the same amount (thus they remain synchronized). Due to the lack of other distinct eigenvalues, it is easy to pick

an α that produces desynchrozination bursts. For our map the region where bubbling is expected is where $0.9 < 2\pi g\lambda_k < 2.1$ (note that for our example $\lambda_k = N$ is the same for all $k \neq 0$).

We now present an example of the method where noise is negligible. The mismatch is chosen to be in κ since it has a more complicated effect than mismatch in ω. The coupled systems can then be described by the general equation

$$\theta^i_{n+1} = [\theta^i_n + \omega + (\kappa + \delta\kappa^i)\sin 2\pi\theta^i_n - \Phi^i_n] \bmod 1, \tag{3.10}$$

where $\delta\kappa^i$ is the mismatch in system i, $\Phi^i_n = g\sin\left(2\pi\sum_{j=1}^N G_{ij}\theta^j_n\right)$, and $i, j = 1, 2, \ldots, N$ are indices representing the ith and jth system in the network [cf. Eq. (3.1)]. The term Φ^i represents the coupling of oscillator i to other nodes in the network. We chose $N = 5$ systems, $\delta\kappa = [4, -1, 2, -6, -2] \times 10^{-6}$, and g so that $\alpha = 2\pi g/N = 1.5$. It should, however, be noted that this method works for any number of systems (with g being adjusted accordingly) and mismatch of any size, although, if the mismatch becomes small, the waiting time for a desynchronization burst becomes large. The waiting time can be adjusted by changing the values of N, g, and $\delta\kappa$ [24].

We define $\Delta\theta^i_n$, which is a measure of the deviations from the synchronous state, by $\Delta\theta^i_n = \sin 2\pi(\theta^i_n - \bar{\theta}_n)$, with $\bar{\theta}_n = \frac{1}{N}\sum_{i=1}^N \theta^i_n$. We plot $\Delta\theta^i_n$ versus n and look for desynchronization bursts in the network. In Fig. 3.2 we show the time evolution of $\Delta\theta^i_n$ near a desynchronization burst. Our interest is in the vector θ_l where l is the first time that $max_i\{\theta^i_n\}$ is in the *sampling region*, defined as $0.4 < |\Delta\theta^i_n| < 0.6$ (see Fig. 3.2). This region is determined by the limitations on the ability to accurately measure $\Delta\theta^i_n$ and the dynamics of the system considered. The latter exists because the master stability function method relies on the systems being close to synchronization. During the desynchronization burst, the difference in the systems can be so large that the linearization used in the analysis of Sec. I no longer applies. We determined that the upper bound to this region in the circle map is $|\Delta\theta^i_n| \approx 0.6$ or $|\theta^i_n - \bar{\theta}_n| \approx 0.10$. The lower bound was arbitrarily chosen as representing the accuracy of the measurements, which we assume is not enough to measure the mismatch directly. Generally the method becomes more effective the smaller the lower bound is.

According to the previous section, at time l we should have approximately $\theta^i_l - \bar{\theta}_l \propto \delta\kappa^i - \bar{\delta\kappa}$, where $\bar{\delta\kappa} = \frac{1}{N}\sum_{i=1}^N \delta\kappa^i$. We can then obtain the relative deviations of the mismatch parameters, $\delta\kappa^i$,

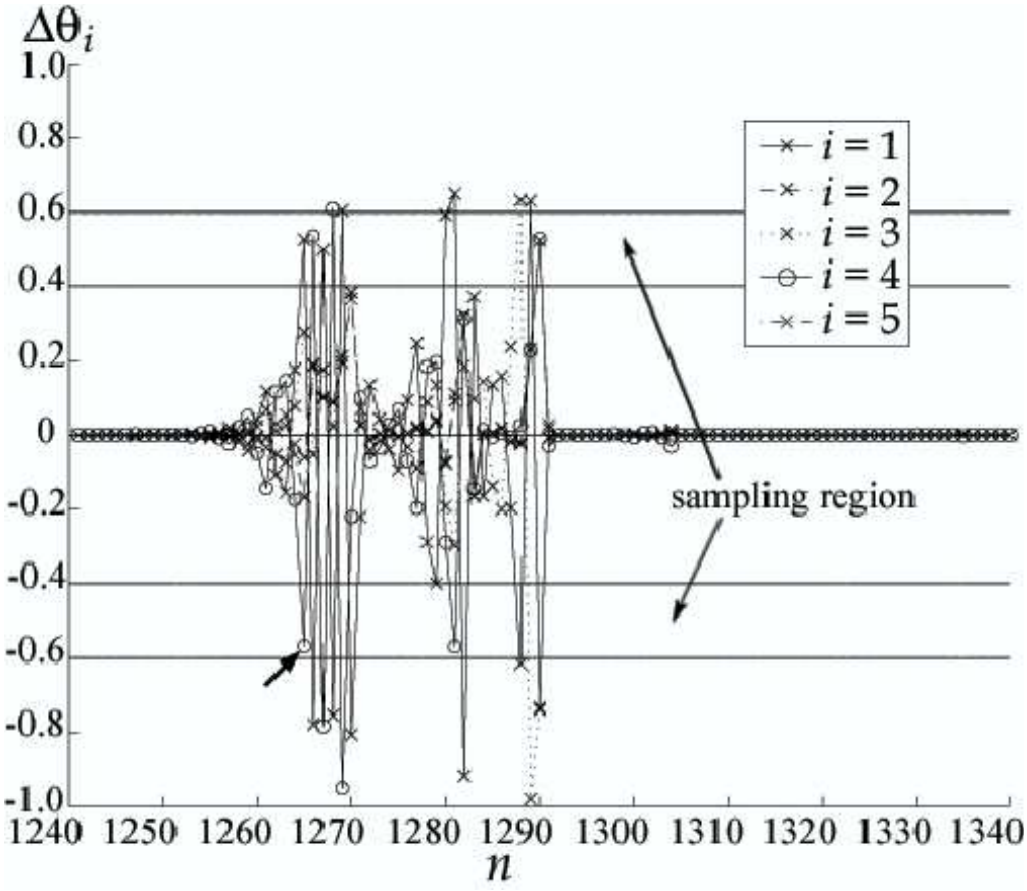

Figure 3.2: Plot of $\Delta\theta_n^i$ vs. n near a region of desynchronization burst. The arrow points to the maximum of $\Delta\theta_n^i$ that is within the sampling region.

by measuring the much larger values of $\theta_l^i - \bar{\theta}_l$. In Fig. 3.3 we show a superimposed plot of $\theta_l^i - \bar{\theta}_l$ and $a(\delta\kappa^i - \bar{\delta\kappa})$ versus i where a, the scaling factor, minimizes $\sum_{i=1}^{N}[(\theta_l^i - \bar{\theta}_l) - a(\delta\kappa^i - \bar{\delta\kappa})]^2$. In Fig. 3.3 we calculated $a \approx 1.5 \times 10^4$ and this corresponds to the amplification of the mismatch. It should be noted that the sign of a is undetermined unless we have knowledge of $\delta\kappa^i$. We see from the figure that $a(\delta\kappa^i - \bar{\delta\kappa}) \approx \theta_l^i - \bar{\theta}_l$.

The definition of the sampling region is somewhat arbitrary, and it may occur that nonlinear effects still play a role in the resulting spatial pattern of the burst. In fact, in Fig. 3.3 we observe that there are still small deviations from the real mismatch pattern. In order to take this into account, we can take the average over various bursts. In the next section, we will discuss how to appropriately take the average, and we will also deal with the effects of noise.

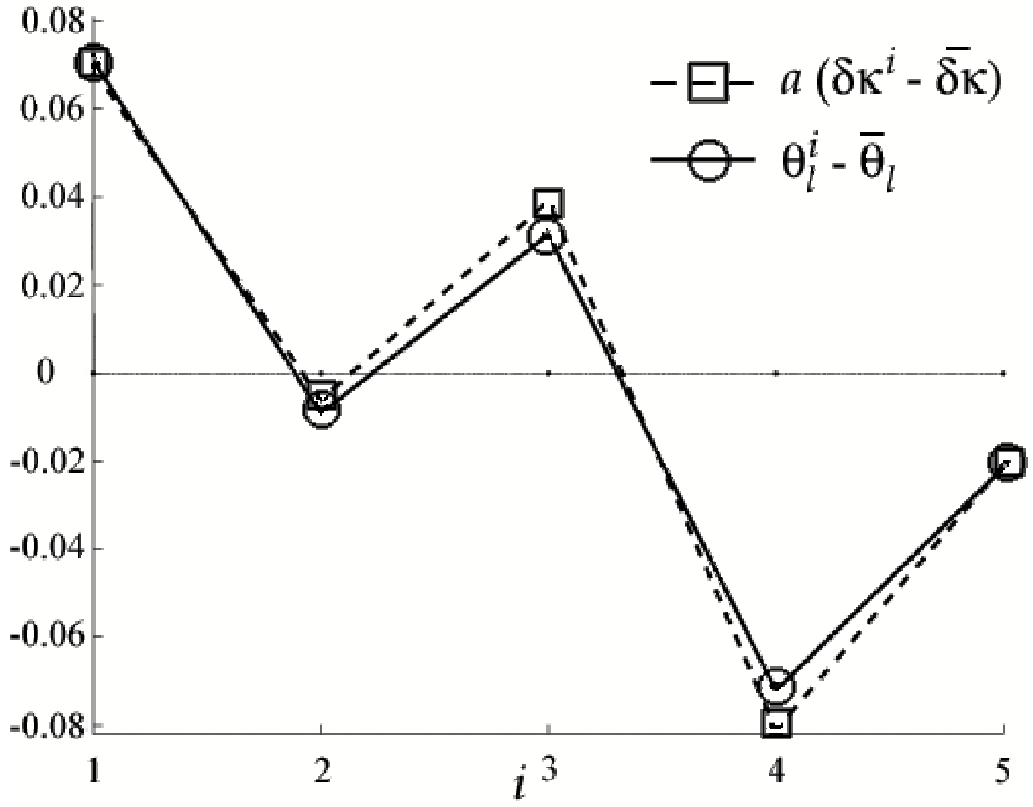

Figure 3.3: Superimposed plot of $a(\delta\kappa^i - \bar{\delta\kappa})$ (dashed line with square markers) and $\theta_l^i - \bar{\theta}_l$ (solid line with circle markers) versus i with $a \approx 1.5 \times 10^4$.

3.3 Parameter mismatch estimation with noise

After learning from the simpler model in Sec. II, we can now analyze a more realistic situation. The method proposed and explained in the previous section applies to a similar network with noise, but there are a few adjustments to be made. We use the same model described by Eq. (3.10), except we modify it to

$$\theta_{n+1}^i = [\theta_n^i + \omega + (\kappa + \delta\kappa^i)\sin 2\pi\theta_n^i - \Phi_n^i + \epsilon_n^i] \bmod 1, \tag{3.11}$$

where $\delta\kappa^i$, Φ_n^i are defined in the same way as before, and ϵ_n^i is a random variable uncorrelated at different i and n simulating the noise. In our example, we choose ϵ_n^i uniformly from the interval $[-10^{-5}, 10^{-5}]$ (note that the noise and mismatch $\delta\kappa$ are of comparable size).

As mentioned in the previous section, nonlinear effects might produce deviations from the simple

relation $\theta_l^i - \bar{\theta}_l = a(\delta\kappa^i - \bar{\delta\kappa})$. We assume that the effects of the nonlinearity and the noise can be represented by a random variable σ^i, such that $\theta_l^i - \bar{\theta}_l = a(\delta\kappa^i - \bar{\delta\kappa}) + \sigma^i$. We furthermore assume that σ^i has zero mean. Under these assumptions, the mismatch is given by

$$\delta\kappa^i - \bar{\delta\kappa} = \left\langle \frac{\theta_l^i - \bar{\theta}_l}{a} \right\rangle - \left\langle \frac{\sigma^i}{a} \right\rangle, \tag{3.12}$$

where the brackets represent an average over realizations of σ. Because of the definition of the sampling region, the scaling factors for different samples will have similar magnitude, but possibly different sign. We thus get approximately, assuming the sign of a is independent of σ^i,

$$\delta\kappa^i - \bar{\delta\kappa} \propto \langle \text{sign}(a)(\theta_l^i - \bar{\theta}_l) \rangle. \tag{3.13}$$

Since the sign of a is unknown, we use a *least-squares optimization* to find the signs which minimize the dispersion from the mean. More precisely, if we have M samples of θ_l's, we can define an average to be $\bar{\Theta} = \frac{1}{M}\sum_{m=1}^{M} \beta_m \theta_m$, where $\{\beta_m\}$ is a sequence of 1's and -1's and θ_m is the vector $[\theta_l^i - \bar{\theta}_l]$ for the mth sample. Note that $\bar{\Theta}$ is an N-dimensional vector and that its ith component is an average of the ith component of the M samples of θ_l's. If we then minimize the error, defined by

$$\text{error} = \frac{1}{M}\sum_{m=1}^{M} \|\beta_m\theta_m - \bar{\Theta}\|^2, \tag{3.14}$$

we can find an optimal sequence of 1's and -1's, which we shall call β^*, that ensures most of the θ_l's are oriented the same way.

To minimize the error we follow an algorithm starting with a randomly generated β as described next. At each iterate, we generate three new β's. The first, β_1, is a new random sequence, β_2 is β altered such that the signs of 1% of the sequence are changed, and β_3 is defined in a similar way but with 5% of the signs changed. We can then compare β_1, β_2, β_3, and β and determine which one has the smaller error determined by Eq. (3.14). The one with the smallest error is then redefined as β and the process is repeated until an approximation to β^*, which we denote as $\bar{\beta}$, is found. We can then define $\Theta_* = \frac{1}{M}\sum_{m=1}^{M} \bar{\beta}_m \theta_m$.

We show in Fig. 3.4 a superimposed plot of $\Theta_*^i - \bar{\Theta}_*$ and $A(\delta\kappa^i - \bar{\delta\kappa})$ versus i where A minimizes $\sum_{i=1}^{N}[(\Theta_*^i - \bar{\Theta}_*) - A(\delta\kappa^i - \bar{\delta\kappa})]^2$. To obtain Θ_* we repeated the process of optimization 10^6 times for $M = 1000$. According to the discussion above, we should have approximately $\Theta_*^i - \bar{\Theta}_* \propto \delta\kappa^i - \bar{\delta\kappa}$ where

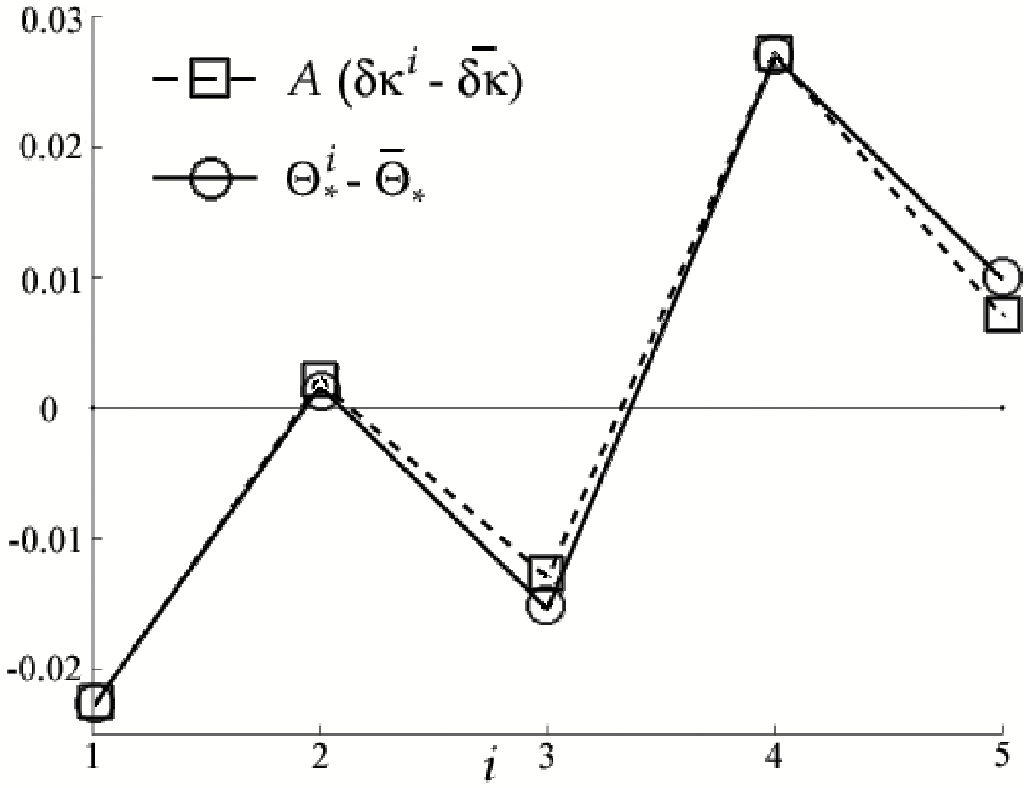

Figure 3.4: Superimposed plot of $A(\delta\kappa^i - \bar{\delta\kappa})$ (dashed line with square markers) and $\Theta_*^i - \bar{\Theta}_*$ (solid line with circle markers) versus i with $A \approx -5 \times 10^3$.

$\bar{\Theta}_* = \frac{1}{N}\sum_{i=1}^{N} \Theta_*^i$. Indeed we see that $A(\delta\kappa^i - \bar{\delta\kappa}) \approx \Theta_*^i - \bar{\Theta}_*$ even when the noise was comparable to the mismatch [$\epsilon \approx \delta\kappa$ in Eq. (3.11)].

3.4 Discussion

We have presented a method to use large deviations from synchronization in order to determine the characteristics of the parameter mismatch in a collection of nearly identical chaotic dynamical systems. It has been noted that knowledge and manipulation of the mismatch patterns can be advantageous in order to improve the quality of the synchronization [57]. The main advantage of our method is that it only requires direct knowledge of the synchronization error when it is large enough to be measured. Furthermore, in principle, there are no limitations on the number of systems it can handle. On the other hand, the method

only provides the relative deviations from the mean and has yet to be extended to systems with comparable mismatch in different parameters. However, there is at least one important application in which our method can yield important information, even if there are different parameters with comparable mismatch size. For example, if it is desired to synchronize the dynamical systems, the relevant mismatch is not that of each individual parameter, but the effective mismatch represented by $(QL)^k$ [see Eqs. (3.6) and (3.7)], and that is the quantity whose size we determine by our method. Systems with the less effective mismatch will yield the synchronization with the best quality.

We have demonstrated our method by determining the relative parameter mismatch in an ensemble of 5 circle maps. By measuring the large deviations from the synchronized state that occur during a desynchronization burst, we were able to determine the very small relative differences in parameters (see Fig. 3.3). We considered the presence of noise, and dealt with it by suitably averaging the measurements taken for various desynchronization bursts. For a noise comparable to the mismatch we were able to determine the relative parameter mismatch by averaging 1000 realizations (see Fig. 3.4). For both situations, we were able to determine the relative parameter mismatch from measurable values even when the mismatch itself was assumed to be immeasurable.

Chapter 4

Localized instabilities and desyncronization waves in arrays of coupled periodic oscillators

In this Chapter we discuss the synchronization of a large number of near-identical oscillators that are locally coupled with connections of random strength. Synchronization in networks of coupled oscillators has recently received considerable interest [18, 20], and has relevance in fields like biology [15]-[18], chemistry [14], lasers [10]-[12], and communications [39]. Usually, the networks studied have been assumed to have connections of equal strength. In practice, the connections between different oscillators may have different strengths, and in some cases this strength could have a large spread (e.g., in biological systems). A model and analysis method has been proposed by Pecora and Carroll [44] to systematically determine the stability of the synchronized state in a network of identical coupled oscillators. This method, the *master stability function*, has been used to study the synchronization properties of different networks [45, 46]. Deng et al. [58] have obtained, using the master stability function technique, conditions for the distribution of the connection strengths that yield average stability of the synchronized state. Galias and Ogorzalek [59] have studied the effect of adding small perturbations to the coupling strengths in relatively small arrays of coupled chaotic oscillators. Denker et. al. [60] have studied the effect of small coupling strength heterogeneity in networks of pulse-coupled oscillators. Our approach in this Chapter will be different: we consider the coupling strengths to have a relatively large spread, and will discuss phenomena that can be expected when a large number of periodic oscillators are coupled in such a network. In particular, we will see that as the coupling strength is increased, the oscillators desynchronize in a localized region. The localization results because the connection matrix has random components and the eigenvectors of this matrix are Anderson localized [61, 62]. The effect of the localized instability spreads as a wave throughout the array, eventually resulting in an ordered state. Remarkably, in the case where the oscillators are not identical the final state of the locally unstable system was found to be, for the system we considered, more ordered than in the case where the system is stable.

4.1 Localized instabilities in oscillator arrays

We consider a model system of N identical dynamical units, each one of which, when isolated, satisfies $\dot{X}_i = F(X_i)$, where $i = 1, 2, \ldots N$, and X_i is the d-dimensional state vector for unit i. (The case of nearly identical units is considered at the end of this Chapter. See also Chapter 2.) The oscillators, when coupled, are taken to satisfy (e.g., [44])

$$\dot{X}_i = F(X_i) - g \sum_{j=1}^{N} G_{ij} H(X_j), \tag{4.1}$$

where the coupling function H is independent of i and j, and the matrix G is a symmetric Laplacian matrix ($\sum_j G_{ij} = 0$) describing the network connections. The constant g determines the global strength of the coupling.

There is an exactly synchronized solution of Eqs. (4.1), $X_1 = X_2 = \cdots = X_N = s(t)$, whose time evolution is the same as the uncoupled dynamics of a single unit, $\dot{s} = F(s)$. In this Chapter we will be concerned with the case where the synchronized state is *periodic*, $s(t + T) = s(t)$. The stability of the synchronized state can be determined from the variational equations obtained by considering an infinitesimal perturbation ϵ_i from the synchronous state, $X_i(t) = s(t) + \epsilon_i(t)$,

$$\dot{\epsilon}_i = DF(s)\epsilon_i - g \sum_{j=1}^{N} G_{ij} DH(s)\epsilon_j. \tag{4.2}$$

Let $\epsilon = [\epsilon_1, \epsilon_2, \ldots, \epsilon_N]$, and define the $d \times N$ matrix $\eta = [\eta_1, \eta_2, \ldots, \eta_N]$ by $\epsilon = \eta L^T$, where L is the orthogonal matrix whose columns are the corresponding real orthonormal eigenvectors of G; $GL = L\Lambda$, $\Lambda = diag(\lambda_1, \lambda_2, \ldots, \lambda_N)$ where λ_k is the eigenvalue of G for eigenvector k. Then Eqs. (4.2) are equivalent to

$$\dot{\eta}_k = \left(DF(s) - g\lambda_k DH(s)\right) \eta_k. \tag{4.3}$$

The quantity η_k is the weight of the k^{th} eigenvector of G in the perturbation ϵ. The linear stability of each 'spatial' mode k is determined by the stability of Eq. (4.3). By introducing a scalar variable $\alpha = g\lambda_k$, the set of equations given by (4.3) can be encapsulated in the single equation,

$$\dot{\eta} = \left(DF(s) - \alpha DH(s)\right) \eta. \tag{4.4}$$

The *master stability function* $\Psi(\alpha)$ [44] associated with Eq. (4.4) is its largest Lyapunov exponent (or equivalently for our case of periodic $s(t)$, the largest real part of its Floquet exponents). This function

depends only on the coupling function H and the chaotic dynamics of an individual uncoupled element, but not on the network connectivity. The network connectivity determines the eigenvalues λ_k (independent of details of the dynamics of the chaotic units). The stability of the synchronized state of the network is determined by $\Psi_* = \sup_k \Psi(g\lambda_k)$, where $\Psi_* > 0$ indicates instability.

As an illustrative example, we consider periodic Rössler oscillators [51], obeying the equations

$$\dot{x} = -(y + z), \tag{4.5}$$

$$\dot{y} = x + 0.2y,$$

$$\dot{z} = 0.2 + z(x - 2.5).$$

In terms of our previous notation, $d = 3$, and $X = [x, y, z]^T$. The master stability function for this system is shown in Fig. 4.1. As seen in this figure, $\Psi(\alpha)$ approaches zero from negative values as $\alpha \to 0^+$. This is a general feature for systems where the individual, uncoupled units are stable limit cycle oscillators. We also see that $\Psi(\alpha)$ crosses from negative (stable) values to positive (unstable) values at a critical α value ($\alpha \approx 4.15$). The existence of such a transition is a robust feature that depends on the type of coupling and oscillator. We now consider a network of N of these oscillators nearest-neighbor coupled in a ring, such

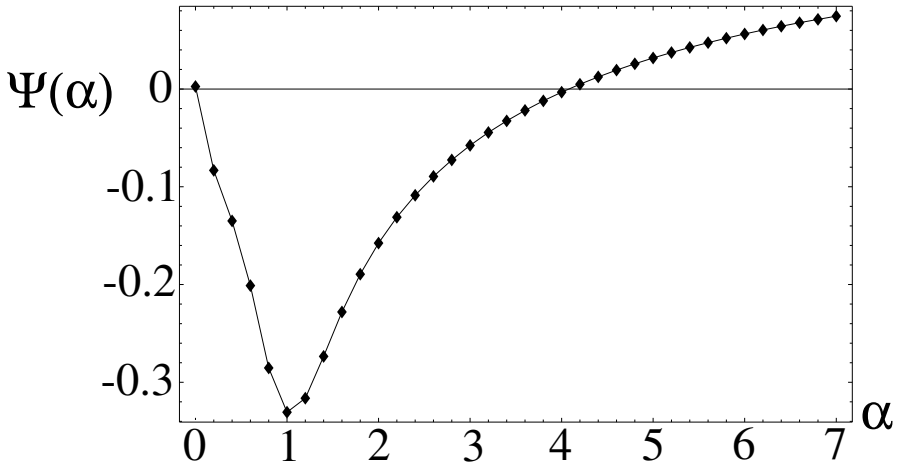

Figure 4.1: Master stability function $\Psi(\alpha)$ versus α for Eqs. (4.5).

that the strength of each individual link is random. The coupling strengths are obtained from an independent

and identically distributed random sequence $\{a_i\}_{i=1}^N$. The matrix G is then

$$G = \begin{pmatrix} b_1 & -a_1 & 0 & 0 & \cdots & 0 & -a_N \\ -a_1 & b_2 & -a_2 & 0 & \cdots & 0 & 0 \\ 0 & -a_2 & b_3 & -a_3 & \cdots & 0 & 0 \\ \vdots & \vdots & \vdots & \vdots & \vdots & \vdots & \vdots \\ -a_N & 0 & 0 & 0 & 0 & -a_{N-1} & b_N \end{pmatrix}, \tag{4.6}$$

where $b_i = (a_{i-1} + a_i)$ for $i = 1, \ldots, N$ (we take $a_0 \equiv a_N$).

The eigenvectors of the matrix G determine the possible desynchronization patterns. It is known that the eigenvectors of certain types of random matrices are exponentially localized (e.g., Anderson localization [61, 62]). In our case, the eigenvector $\{u_i\}_{i=1}^N$ with eigenvalue λ satisfies

$$t_{i+1} = a_{i+1}^{-1}(\lambda + a_i + a_{i+1} - a_i t_i^{-1}), \tag{4.7}$$

where $t_i \equiv \frac{u_i}{u_{i-1}}$. Viewing Eq. (4.7) as a random dynamical system for t_i, we find numerically that in our case,

$$\gamma = \lim_{n\to\infty} \frac{1}{n} \sum_{i=0}^{n} \log(|t_i|). \tag{4.8}$$

exists and is independent of the initial condition and noise realization. Eigenvectors of (4.6) tend to have a localized amplitude peak at some location i_0 and decay like $|u_i| \propto e^{\gamma|i-i_0|}$ away from the peak; γ^{-1} is thus the localization length. (See [62].)

We choose the a_i's to be uniformly distributed in $(0.1, 1)$ (note that any multiple of this would lead to the same eigenvectors). (Since $a_i \geq 0.1$ we avoid the possibility $a_i \ll 1$ that would effectively disconnect the network.) The effects we will describe for this network should be regarded as an example of what could be expected in more general networks with random coupling. In Fig. 4.2(a) we show the eigenvector with largest eigenvalue for a realization of the matrix G using $N = 500$. Figure 4.2(b) shows the localization length γ^{-1} as a function of λ calculated using Eq. (4.8). The eigenvectors are seen to be sharply localized for the largest eigenvalues, and become less localized as the eigenvalues decrease. As the coupling strength g is increased, the eigenvectors with largest eigenvalue become unstable. These eigenvectors have the smallest localization length [see Fig. 4.2 (b)]. We will now describe what occurs

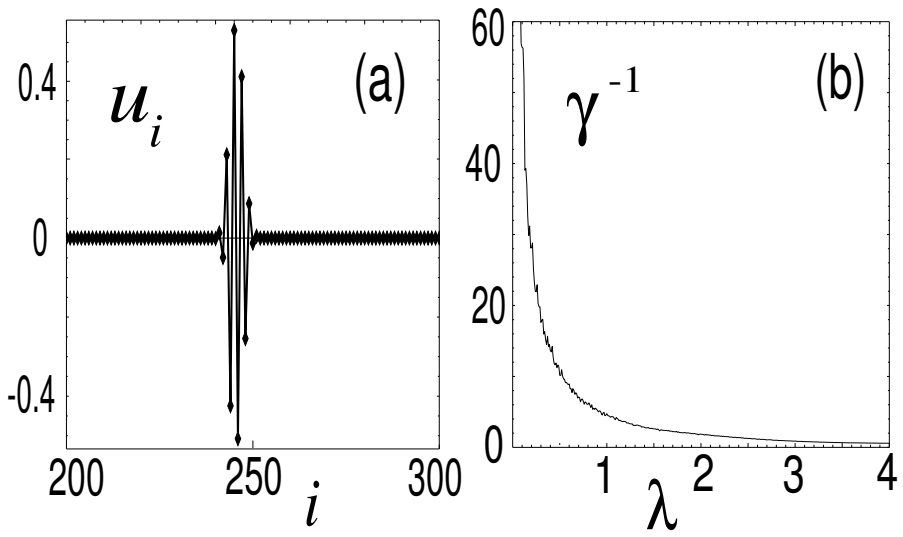

Figure 4.2: (a) Eigenvector u_i for the largest eigenvalue $\lambda = 3.61$ for a particular realization of the matrix G in (4.6) with $N = 500$. (b) Localization length γ^{-1} calculated using Eq. (4.8).

in this situation. We fixed the same realization of the matrix G used in producing Fig. 4.2(a). The four largest eigenvalues are 3.61, 3.41, 3.38, and 3.30. For $g = 1.24$ the eigenvector with largest eigenvalue is unstable, and the next two eigenvectors are barely unstable [$\alpha = 4.47$, 4.23 and 4.19 in Fig. (4.1)]. We start with initial conditions near the synchronized state and then let the system evolve according to Eqs. (4.1). In Fig. 4.3 we show snapshots of x_i as a function of the site index i for six successively increasing times. Starting from a nearly synchronized state [Fig. 4.3(a)], the oscillators desynchronize at the location [see Fig. 4.2(a)] of the localized mode [Fig. 4.3(b)]. The desynchronization spreads as a wave to farther regions of the array [Figs. 4.3(c)-(e)]. At the end, the domain of the wave covers the entire array [Fig. 4.3(f)]. This process is dominated by the most unstable mode. The other two less unstable modes can be seen as tiny defects at $i \approx 327$, 402 in the otherwise smooth wave. (The effect of these less unstable modes is most evident in Fig. 4.3(c). They also have a discernible, although small, effect in the final state [arrows in Fig. 4.3(f)].)

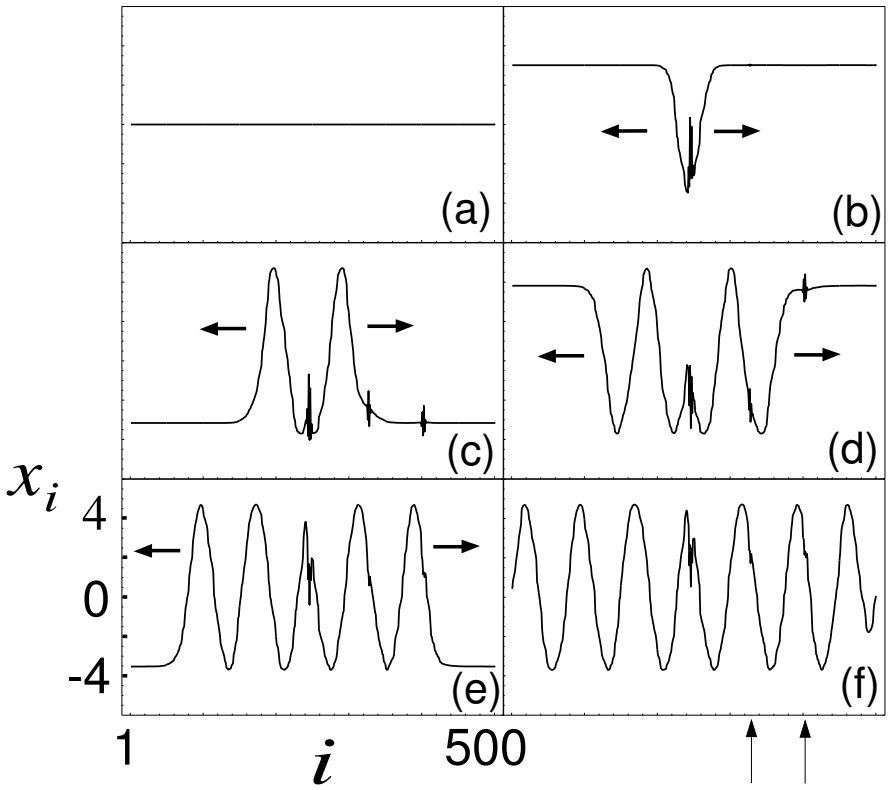

Figure 4.3: Plots of the x coordinate of oscillator i versus the site index i, at times (a) 0, (b) 1400, (c) 2800, (d) 4200, (e) 5600, and (f) 10000. All the plots have the same scale as (e).

4.2 Phase description of desynchronization waves

The final state and the process leading to it can be understood in terms of the phase of the oscillators. Define the phase $\phi(i,t) \equiv 2\pi\{n(i,t) + (t - t_-(i,t))(t_+(i,t) - t_-(i,t))^{-1}\}$, where $t_-(i,t) = \max\{s : x_i(s) = 0, \dot{x}_i > 0, s \leq t\}$, $t_+(i,t) = \min\{s : x_i(s) = 0, \dot{x}_i > 0, s > t\}$, and $n(i,t)$ is an integer chosen so that ϕ is a continuous function of t and that $\phi(i+1,t)$ is close to $\phi(i,t)$ for all i. Figure 4.4 shows two snapshots of the x coordinate and the phase as defined above as a function of i (the i origin was displaced so that what happens opposite the location of the unstable mode can be observed clearly, and for each time a constant was added to ϕ so that $\max_i \phi = 0$). As can be observed in the Figs. 4.4 (a) and (c), a region with a constant phase gradient expands on both sides of the unstable mode. In the final state [Figs. 4.4(b) and (d)] the phase has a minimum at the location of the unstable mode and increases linearly on both sides

reaching a maximum at the opposite end of the ring. This phase profile increases uniformly with time. The

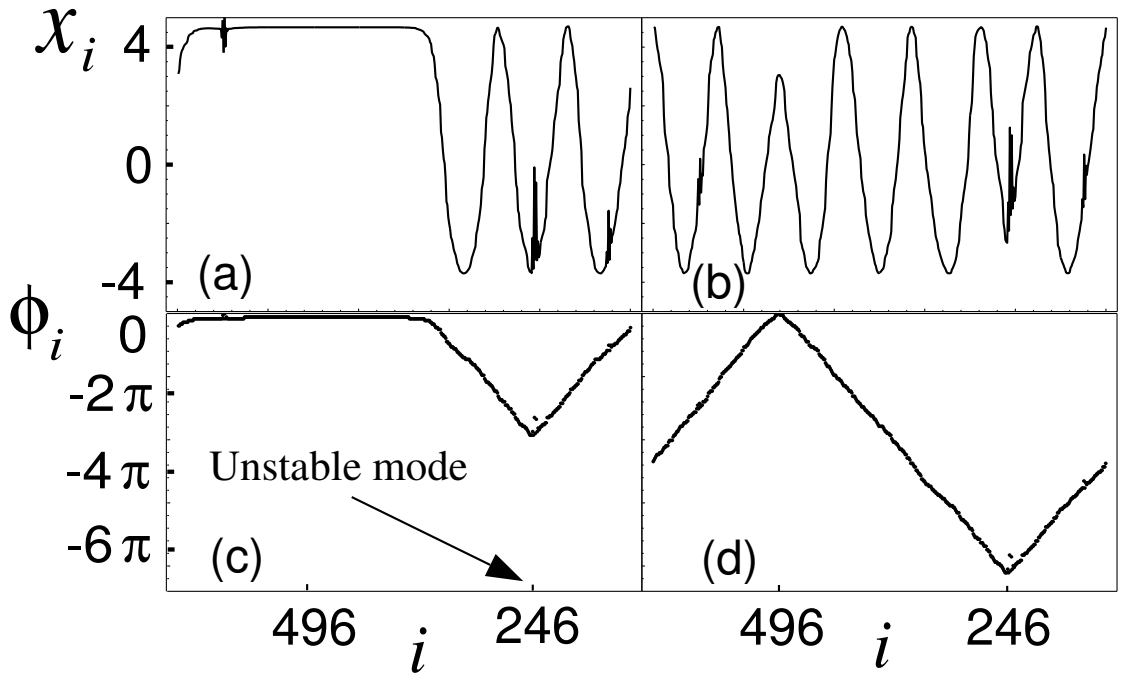

Figure 4.4: Plots (a) and (b) shows the x coordinate of oscillator i versus the site index i for times 3750 and 9660. Plots (c) and (d) show the phase of oscillator i at the same times as for (a) and (b) respectively. Compare with Eq. (4.10)

cause of this phenomenon is that, as the oscillators in the region of the unstable mode desynchronize, they go to limit cycles that have a slightly lower frequency than that of the original orbit. Oscillating at a slower pace than the others, they drag the adjacent oscillators, and these drag theirs in turn, continuing until an equilibrium is reached. An equation describing approximately the evolution of the phase of the oscillator at location ξ and time t, $\phi(\xi, t)$, in a chain of diffusively coupled oscillators is given in the continuous limit by [25]

$$\frac{\partial \phi}{\partial t} = a\frac{\partial^2 \phi}{\partial \xi^2} + b\left(\frac{\partial \phi}{\partial \xi}\right)^2 + w(\xi), \tag{4.9}$$

where $w(\xi)$ is the frequency of the oscillator at location ξ, and a and b are constants. If this frequency is sufficiently smaller (larger) in a localized region and b is negative (positive), the equation predicts the development of waves that emanate from that region. The phase profile resulting from such forcing in a

small region centered at the origin ($|\xi| < l$) can be approximated for large ξ and t as [25]

$$\phi(\xi, t) = w_0 t - \max(0, k(vt - |\xi|)), \tag{4.10}$$

where $w_0 = w(\xi)$ for $|\xi| > l$ and k and v depend on a and b and $w(\xi)$. For appropriate k and v, equation (4.10) agrees well with Figs. 4.4 (c) and (d).

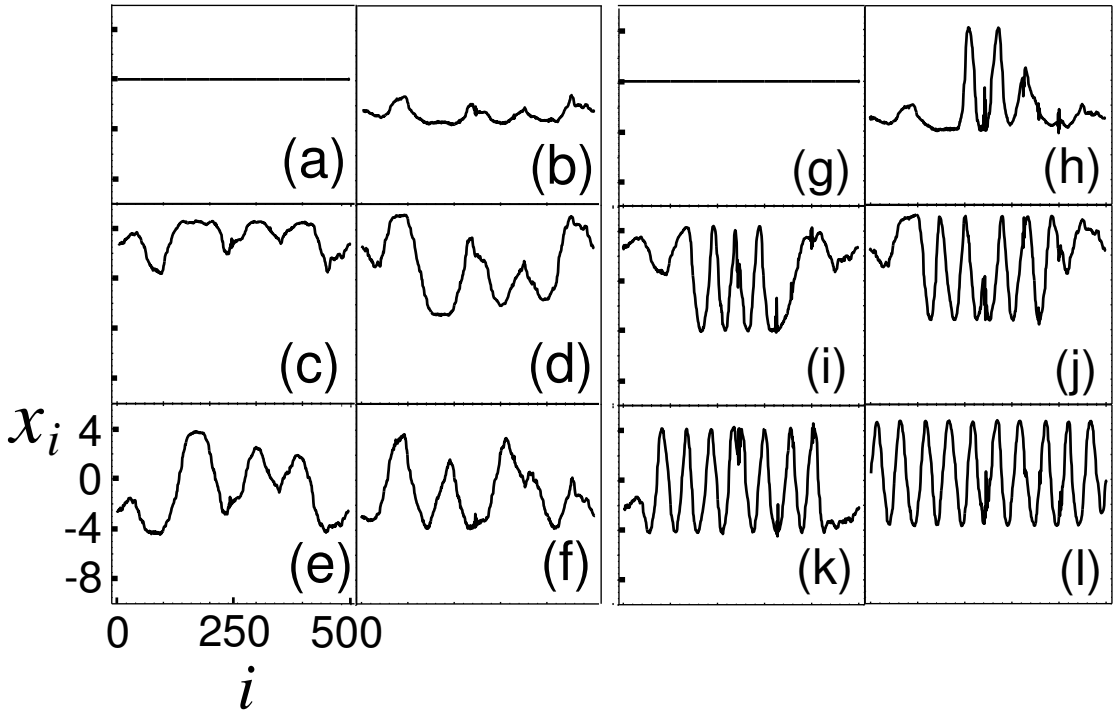

Figure 4.5: Each plot shows the x coordinate of oscillator i as a function of the site index i. The time is 0, 1400, 2800, 4200, 5600, and 9970 for plots (a) to (f) and similarly for plots (g) to (l). A parameter mismatch was introduced in the oscillators. (a)-(f): All the modes are stable. (g)-(l): The pattern is organized by an unstable mode as in Fig. 4.3(f). All the plots have the same scale as (e).

In the example presented above, the pattern created by the unstable mode can be regarded as a more disordered synchronization than that of the original identical synchronization. However, in realistic situations, an unstable mode can actually make synchronization more orderly. In real systems, small differences in the parameters or small noise are expected. Under these circumstances, the different oscillators will be subject to small perturbations. The modes with eigenvalues close to zero have a master stability function close to zero [see Fig. 4.1] and also are nearly unlocalized [see Fig. 4.2(b)]. Thus, the phase of each os-

cillator will be subject to perturbations whose projection onto the nearly unlocalized modes are only very weakly damped. The identical synchronization of the array is thus spoiled by mismatch or noise. As an illustration, we randomly perturb the parameters of the different oscillators, so that they lie within $\pm 3\%$ of the original parameters. We then solved Eqs. (4.1) with $g = 1.1$ and $g = 1.24$. For $g = 1.1$, all the modes are stable; in the case $g = 1.24$, three modes are stable as discussed above. In Figs. 4.5 (a)-(f) we show snapshots of the case $g = 1.1$, and in Figs. 4.5 (g)-(l) we show the corresponding snapshots for the case $g = 1.24$. When all of the modes are stable, the system exhibits a state in which there is erratic slow variation of the x_i with i. When there is an unstable mode, however, a more organized state is reached. If one picks two different oscillators j and k, they will satisfy asymptotically $X_j(t - \tau) = X_k(t)$, where τ is a simple function of j and k [see Fig. 4.4 (d)]. Thus the oscillators are pairwise lag synchronized [63]. In realistic large arrays of periodic oscillators, it might be convenient to have one unstable mode. Our results suggest that this mode could, despite its localized nature, induce global organization of the system (Fig. 4.5).

4.3 Discussion

In conclusion, we find that large arrays of periodic oscillators locally coupled by connections of randomly heterogeneous strength can experience a desynchronization transition characterized by the appearance of unstable Anderson localized modes. Furthermore, we find that, past the transition, the localized mode might play the key role in organizing the final global pattern of the system oscillations.

Chapter 5

The onset of synchronization in large networks of coupled oscillators

In recent years, the importance of networks in different fields has become increasingly clear [7, 8]. It has been observed that many real world networks possess topologies which introduce important effects on the processes taking place on them. One of the most interesting and important of these processes is the synchronization of coupled dynamical systems. Synchronization is found in fields ranging from physics to biology [18, 20], and in many cases involves a large network of dynamical systems. The structure of this network plays a crucial role in determining the synchronization of the coupled elements.

Kuramoto [25] proposed and exactly solved a model for the synchronization of all-to-all uniformly coupled phase oscillators. His model and solution have become a guide as to how the coupling strength and the properties of the oscillators (e.g., their natural frequencies) might affect their synchronization, and generalizations of this basic model have been studied (for a review, see [31], Chapter 12 of [20], and Chapter 6 of [32]). Some attempts to study the Kuramoto model with networks different from the all-to-all network have been made [33]. Networks in which the interaction strength depends on a distance have been studied, and it has been numerically found that a transition from incoherent to coherent behavior occurs at a critical value of the coupling strength [34]. The Kuramoto model in networks without global coupling has recently started to receive attention. It was numerically observed [35] that a transition is also present in scale free networks. Very recently, a mean field theory to determine the transition to synchronization in more general networks has been proposed [36, 37]. The mean field theory result is that the critical coupling strength k_{mf} is determined by the Kuramoto value, k_0, rescaled appropriately by the first two moments of the degree distribution of the nodes in the network: $k_{mf} = k_0\langle d\rangle/\langle d^2\rangle$, where

$$\langle d^q\rangle = \frac{1}{N}\sum_{n=1}^{N} d_n^q, \tag{5.1}$$

the degree d_n of node n is the number of connections between node n and other nodes of the network, and N is the number of nodes in the network.

In this Chapter we go beyond the mean field approximation, obtaining a better estimate of the crit-

ical coupling strength. We also describe the behavior of a suitably defined order parameter past the transition. We show how our results reduce to those of the mean field theory when an additional assumption is introduced, and present examples in different regimes. We find that in some regimes the mean field approximation does not provide an adequate description of the transition, whereas our more general estimate does. We also show how our results explain observations for networks with distance dependent interaction strength. We study finite size effects caused mainly by nodes of small degree, and find that the transition point is shifted to larger values of the coupling strength when these effects are taken into account.

This Chapter is organized as follows. In Section 5.1 we present our theory and discuss the mean field approach. In Section 5.2, we present numerical examples for different situations and test the different approximations. In Section 5.3 we discuss the case of networks with nonuniform coupling strength. In Section 5.4, we present a linear analysis of the problem. In Section 5.5 we consider finite size effects caused primarily by nodes with a small number of connections. Finally, we conclude in Section 5.6. Some calculations were relegated to Appendices A, B, and C.

5.1 Self consistent analysis

As shown by Kuramoto [25], the dynamics of weakly coupled, nearly identical limit cycle oscillators can, under certain conditions, be approximated by an equation for the phases θ_n of the form

$$\dot{\theta}_n = \omega_n + \sum_{m=1}^{N} \Omega_{nm}(\theta_m - \theta_n), \tag{5.2}$$

where ω_n is the natural frequency of the oscillator n, N is the total number of oscillators and Ω_{nm} is a periodic function depending on the original equations of motion. The all-to-all Kuramoto model assumes that $\Omega_{nm}(\theta_m - \theta_n) = (k/N)\sin(\theta_m - \theta_n)$, where k represents an overall coupling strength. In order to incorporate the presence of a heterogeneous network, we assume that $\Omega_{nm}(\theta_m - \theta_n) = kA_{nm}\sin(\theta_m - \theta_n)$, where A_{nm} are the elements of a $N \times N$ adjacency matrix A determining the connectivity of the network. Therefore, we study the system

$$\dot{\theta}_n = \omega_n + k\sum_{m=1}^{N} A_{nm}\sin(\theta_m - \theta_n). \tag{5.3}$$

For specificity, we will primarily consider the case where the A_{nm} are either 0 (nodes n and m are

not connected) or 1 (nodes n and m are connected, and all connections have equal strength). We assume that the network is undirected, so that $A_{nm} = A_{mn}$. We assume also that, for each n, the corresponding ω_n is independently chosen from a known oscillation frequency probability distribution $g(\omega)$. We assume that $g(\omega)$ is symmetric about a single local maximum (cf. Sec 5.4), which without loss of generality we can take to be at $\omega = 0$. (If the mean frequency is $\omega_0 \neq 0$, we make the change of coordinates that shifts each ω_n by ω_0 and each θ_n by $\omega_0 t$.) In this case, synchronization will occur at frequency 0, i.e., θ_n will remain approximately constant for synchronized nodes.

We define a positive real valued local order parameter r_n by

$$r_n e^{i\psi_n} \equiv \sum_{m=1}^{N} A_{nm} \langle e^{i\theta_m} \rangle_t, \tag{5.4}$$

where $\langle \dots \rangle_t$ denotes a time average. In terms of r_n, Eq. (5.3) can be rewritten as

$$\dot{\theta}_n = \omega_n - k r_n \sin(\theta_n - \psi_n) - k h_n(t), \tag{5.5}$$

where the term $h_n(t)$ takes into account time fluctuations and is given by

$h_n = Im\{e^{-i\theta_n} \sum_m A_{nm} \left(\langle e^{i\theta_m} \rangle_t - e^{i\theta_m} \right)\}$, where Im stands for the imaginary part. Since we regard h_n as a sum of d_n approximately uncorrelated terms (where d_n is the degree of node n given by $d_n = \sum_m A_{nm}$), we expect h_n to be of order $\sqrt{d_n}$. Substantially above the transition, due to the synchronization of the phases, the quantity $r_n \approx \sum_m A_{nm} \langle e^{i\theta_m} \rangle_t$ is $\mathcal{O}(d_n)$. Thus, if we assume that $d_n \gg 1$, substantially above the transition the term h_n can be neglected with respect to r_n. However, just above the transition to coherence, the number of oscillators that are phase locked is small (see below), and so the term r_n is also small. We need the number of locked oscillators to be large enough so that we can neglect h_n, but, in cases where we use perturbative methods, we also require that the number of locked oscillators be small enough that the perturbative methods are still valid. We therefore do not expect the perturbative methods to agree perfectly just at the transition point. [Indeed in the classical Kuramoto (all-to-all) model a similar reservation holds for finite networks, as there are $\mathcal{O}(N^{-1/2})$ fluctuations of $k \sum_{m=1}^{N} e^{i\theta_m}$ for k below its critical transition value.] In Sec. 5.5 we will investigate the effects of the time fluctuating term h_n in Eq. (5.5), but, for now, we neglect it.

With h_n neglected in Eq. (5.5), oscillators with $|\omega_n| \leq k r_n$ become locked, i.e., for these oscillators

θ_n settles at a value for which

$$\sin(\theta_n - \psi_n) = \omega_n/(kr_n). \tag{5.6}$$

(In general there are two such θ_n; the one closest to ψ_n is stable.) Then

$$r_n = \sum_{m=1}^{N} A_{nm}\langle e^{i(\theta_m-\psi_n)}\rangle_t \tag{5.7}$$

$$= \sum_{|\omega_m|\le kr_m} A_{nm}e^{i(\theta_m-\psi_n)} + \sum_{|\omega_m|>kr_m} A_{nm}\langle e^{i(\theta_m-\psi_n)}\rangle_t.$$

In order to proceed further, we will introduce the following assumption:

Assumption ★ *We assume the existence of solutions r_n, ψ_n that are statistically independent of ω_n.*

This is a nontrivial assumption; however, it is reasonable if most of node n's neighbors have reasonably large degree, so that they are not strongly affected by the value of ω_n. And, as we show below, such a solution can be found in a self consistent manner. Using a milder version of Assumption ★, we show in Appendix A that the sum over the unlocked oscillators in Eq. (5.7) can be neglected. Therefore, only the locked oscillators remain in the sum, and we get from Eq. (5.7) using Eq. (5.6), since r_n is by definition real,

$$r_n = Re\{\sum_{|\omega_m|\le kr_m} A_{nm}e^{i(\theta_m-\psi_m)}e^{i(\psi_m-\psi_n)}\} \tag{5.8}$$

$$= \sum_{|\omega_m|\le kr_m} A_{nm}\cos(\psi_m-\psi_n)\sqrt{1-\left(\frac{\omega_m}{kr_m}\right)^2} - \sum_{|\omega_m|\le kr_m} A_{nm}\sin(\psi_m-\psi_n)\left(\frac{\omega_m}{kr_m}\right),$$

where Re represents the real part. For the imaginary part of Eq. (5.7), we get

$$0 = \sum_{|\omega_m|\le kr_m} A_{nm}\cos(\psi_m-\psi_n)\left(\frac{\omega_m}{kr_m}\right) \tag{5.9}$$

$$+ \sum_{|\omega_m|\le kr_m} A_{nm}\sin(\psi_m-\psi_n)\sqrt{1-\left(\frac{\omega_m}{kr_m}\right)^2}.$$

Using Assumption ★, the contribution of the last term in the real part equation (5.8) can be neglected because of the symmetry of $g(\omega)$ about 0. We thus obtain the approximation

$$r_n = \sum_{|\omega_m| \leq k r_m} A_{nm} \cos(\psi_m - \psi_n) \sqrt{1 - \left(\frac{\omega_m}{k r_m}\right)^2}. \tag{5.10}$$

Since we are interested in the transition to coherence, we look for the solution of Eq. (5.10) that yields the smallest critical coupling k. The smallest critical coupling is obtained when the cosine in Eq. (5.10) is 1. (Note that both the number of terms in the sum and their size decreases as k decreases. Hence, a smaller k corresponds to a larger value of the cosine.) We therefore will look for solutions for which $\psi_n - \psi_m = 0$, i.e., ψ_n does not depend on n, and without loss of generality, we will take $\psi_n \equiv 0$. Note that this is a consistent condition in the sense that the imaginary part equation (5.9) is satisfied: the first term vanishes in the limit of a large number of connections per node due to the symmetry around 0 of $g(\omega)$, and the second due to our assumed form that ψ_n does not depend on n.

Equation (5.10) then reduces to

$$r_n = \sum_{|\omega_m| \leq k r_m} A_{nm} \sqrt{1 - \left(\frac{\omega_m}{k r_m}\right)^2}. \tag{5.11}$$

If the particular collection of frequencies ω_n is known, this equation can be solved numerically. We will refer to this approximation, based on neglecting the time fluctuations in Eq. (5.5), as the *time averaged theory* (TAT). We now define an order parameter r by

$$r = \frac{\sum_{n=1}^{N} r_n}{\sum_{n=1}^{N} d_n}, \tag{5.12}$$

where d_n is the degree of node n defined by $d_n = \sum_{m=1}^{N} A_{nm}$. Note that $r = \sum_{n=1}^{N} d_n \langle e^{i\theta_n} \rangle_t / \sum_{n=1}^{N} d_n$ coincides with the order parameter used in Refs. [36, 37].

If the number of connections per node is large, the particular collection of frequencies of the neighbors of a given node will likely be a faithful sample of the frequency distribution $g(\omega)$. Assuming this is the case, and using Assumption ★, we approximate the sum in Eq. (5.11) as

$$r_n = \sum_m A_{nm} \int_{-k r_m}^{k r_m} g(\omega) \sqrt{1 - \left(\frac{\omega}{k r_m}\right)^2} d\omega, \tag{5.13}$$

or, introducing $z \equiv \omega/(k r_m)$,

$$r_n = k \sum_m A_{nm} r_m \int_{-1}^{1} g(z k r_m) \sqrt{1 - z^2} dz \tag{5.14}$$

This equation is one of our main results. It is analogous to Eq. (13) in Ref. [36] and Eq. (6) in Ref. [37], but, as opposed to including only information of the degree distribution of the network, it depends on the adjacency matrix, which completely describes the topology of the network. Equation (5.14) determines implicitly the order parameter r as a function of the network A_{nm}, the frequency distribution $g(\omega)$, and the coupling constant k. We will refer to this approximation as the *frequency distribution approximation* (FDA). As with the TAT approximation (5.11), nonlinear matrix equation (5.14) can be solved numerically and the order parameter r computed from r_n using Eq. (5.12).

We will now study the implications of Eq. (5.14) by using approximation schemes in different regimes in order to obtain explicit expressions for the order parameter and the critical coupling strength.

5.1.1 Perturbation Theory (PT)

From the discussion above, coherent behavior is characterized by a nonzero value of r_n. We determine the critical value of k by letting $r_n \to 0^+$. The first order approximation $g(zkr_m) \approx g(0)$ in Eq. (5.14) produces

$$r_n^{(0)} = \frac{k}{k_0} \sum_m A_{nm} r_m^{(0)}, \tag{5.15}$$

where $k_0 \equiv 2/(\pi g(0))$. Since we are interested in the transition to coherence, the smallest k satisfying Eq. (5.15) is of interest. We thus identify the critical transition value of k_0/k with the largest eigenvalue λ of the adjacency matrix A, obtaining

$$k_c = \frac{k_0}{\lambda}. \tag{5.16}$$

(In the case $A_{nm} \equiv 1$ of all-to-all coupling, $\lambda = N - 1$.) Also $r_m^{(0)}$ is proportional to the mth component of the eigenvector $u = [u_1, u_2, \ldots, u_N]^T$ associated with this eigenvalue. Note that this is consistent with Assumption ★, since r_n depends only on network properties (i.e., the matrix A) and is thus independent of ω_n. Equation (5.16) is one of our main results. It determines when the transition to coherence occurs in terms of the largest eigenvalue λ of the adjacency matrix A.

In order to assess how the order parameter r given by Eq. (5.12) grows as k grows from k_c, we must take into account that $g(zkr_m)$ in Eq. (5.14) is not constant. For kr_n small (see the discussion at the end of

Sec. 5.1.2), the second order approximation yields

$$r_n = k\sum_m A_{nm} r_m \times \int_{-1}^{1} \left(g(0) + \frac{1}{2} g''(0)(zkr_m)^2 \right) \sqrt{1-z^2}\, dz. \tag{5.17}$$

Defining $\alpha \equiv -\pi g''(0) k_0/16$, we get

$$r_n = \frac{k}{k_c \lambda} \sum_m A_{nm} \left(r_m - \alpha k^2 r_m^3 \right). \tag{5.18}$$

We consider perturbations from the first order critical values as follows:

$$r_n = r_n^{(0)} + \delta r_n, \tag{5.19}$$

where $\delta r_n \ll r_n^{(0)} \ll 1$ as $k \to k_c$. Inserting this into Eq. (5.18), and canceling terms of order $r_n^{(0)}$, the leading order terms remaining are

$$\delta r_n = \frac{k}{k_c \lambda} \sum_m A_{nm} \delta r_m - \frac{\alpha k^3}{k_c \lambda} \sum_m A_{nm} (r_m^{(0)})^3 + \frac{k - k_c}{k_c \lambda} \sum_m A_{nm} r_m^{(0)}. \tag{5.20}$$

In order for Eq. (5.20) to have a solution for δr_n, it must satisfy a solubility condition. This condition can be obtained by multiplying by $r_n^{(0)}$, summing over n, using Eq. (5.15) and the assumed symmetry $A_{nm} = A_{mn}$, to obtain

$$\frac{\sum_m (r_m^{(0)})^4}{\sum_m (r_m^{(0)})^2} = \frac{k - k_c}{\alpha k^3}. \tag{5.21}$$

In terms of u, the normalized eigenvector of A associated with the eigenvalue λ, the square of the order parameter r can be expressed as

$$r^2 = \left(\frac{\eta_1}{\alpha k_0^2} \right) \left(\frac{k}{k_c} - 1 \right) \left(\frac{k}{k_c} \right)^{-3} \tag{5.22}$$

for $k/k_c > 1$, where

$$\eta_1 \equiv \frac{\langle u \rangle^2 \lambda^2}{N \langle d \rangle^2 \langle u^4 \rangle}. \tag{5.23}$$

Eqs. (5.22) and (5.23) describe the behavior of the order parameter near the transition in terms of λ and its associated eigenvector. We will refer to them as the *perturbation theory* (PT).

The presence of the term $\langle u^4 \rangle$ in Eq. (5.23) suggests that the expansion of g to second order might fail when there are a few components of the eigenvector u that are much larger than the rest. This occurs when the degree distribution is highly heterogeneous. We formulate more precisely this constraint in the discussion at the end of Sec. 5.1.2.

5.1.2 Mean field theory (MF)

In this section we describe an approximation that works in some regimes and has the advantage of greater analytical tractability. In this section we also recover some of the results in Refs. [36, 37]. Here we assume that r_n is proportional to d_n, $r_n \propto d_n$. The assumption consists in treating the average

$$\frac{r_n}{d_n} = \frac{1}{d_n} \left| \sum_{m=1}^{N} A_{nm} \langle e^{i\theta_m} \rangle_t \right|, \tag{5.24}$$

which depends on n, as if it were a constant independent of n. Following Refs. [36, 37], we call this the *mean field* (MF) approximation. It is also equivalent, near the transition, to assuming that the eigenvector associated with the largest eigenvalue λ satisfies $u_n \propto d_n$. We will discuss later the range of validity of this assumption. Note that this form for r_n is again consistent with our Assumption ★ that r_n is independent of ω_n. The ratio r_n/d_n coincides under this approximation with the order parameter r defined in Eq. (5.12).

Summing over n and substituting $r_n = r d_n$ in Eq. (5.14), we obtain

$$\sum_{m=1}^{N} d_m = k \sum_{m=1}^{N} d_m^2 \int_{-1}^{1} g(zkrd_m) \sqrt{1 - z^2} dz, \tag{5.25}$$

which coincides with Eq. (13) in Ref. [36]. As we approach the transition from above, $r \to 0^+$, the first order approximation is $g(zkrd_m) \approx g(0)$, from which we obtain

$$k \equiv k_{mf} = k_0 \frac{\langle d \rangle}{\langle d^2 \rangle}, \tag{5.26}$$

the main result of Ref. [36].

In the limit $N \to \infty$, we can replace $\langle d^q \rangle$ as defined by Eq. (5.1) by

$$\langle d^q \rangle_\infty = \int d^q p(d) dd, \tag{5.27}$$

where $p(d)$ is the probability distribution function for the degree. Note that from Eq. (5.1), $\langle d^q \rangle$ is always well-defined for finite N, but that Eq. (5.27) indicates that $\langle d^q \rangle_\infty$ diverges for power law degree distributions $p(d) \propto d^{-\gamma}$ if $\gamma \leq q + 1$. We also note that many real networks have approximate power law $p(d)$

with $\gamma < 3$ (see Ref. [7]). On the basis that $\langle d^2\rangle_\infty/\langle d\rangle_\infty = \infty$ for $2 \leq \gamma \leq 3$, Ichinomiya [36] notes that from Eq. (5.26) $k_{mf} \to 0$ as $N \to \infty$; i.e., predicts that in the limit $N \to \infty$ there is no threshold for coherent oscillations when $2 \leq \gamma \leq 3$. As will become evident, our numerical experiments, although for $N \gg 1$, are often not well-approximated by the $N \to \infty$ limit, in particular for $\gamma < 3$.

The mean field approximation can be pushed further to second order by expanding $g(zkrd_m) \approx g(0) + \frac{1}{2}g''(0)(zkrd_m)^2$ in Eq. (5.25), obtaining, provided krd_m is small,

$$1 = \frac{k}{k_{mf}} + k^3 r^2 \frac{\pi}{16} g''(0) \frac{\sum_{m=1}^{N} d_m^4}{\sum_{m=1}^{N} d_m}, \tag{5.28}$$

so that

$$r^2 = \left(\frac{\eta_2}{\alpha k_0^2}\right)\left(\frac{k}{k_{mf}} - 1\right)\left(\frac{k}{k_{mf}}\right)^{-3} \tag{5.29}$$

for $k/k_c > 1$, where

$$\eta_2 \equiv \frac{\langle d^2\rangle^3}{\langle d^4\rangle\langle d\rangle^2}. \tag{5.30}$$

In expanding g to second order, it was assumed that kd_m is small. The term $\langle d^4\rangle$ in Eq. (5.30) suggests that the conditions under which the expansion of g is appropriate are those under which $\langle d^4\rangle_\infty$ is finite. In fact, Lee shows [37] that for a power law distribution of the degrees, $p(d) \propto d^{-\gamma}$, the above expansion is appropriate for $\gamma > 5$. For $3 \leq \gamma \leq 5$, he obtains in the limit $N \to \infty$ that r scales near the transition as $r \propto \left(\frac{k}{k_{mf}} - 1\right)^{1/(\gamma-3)}$. A similar situation occurs in the perturbation theory [Eqs. (5.22) and (5.23)], which was also based on expanding g to second order. According to the previous discussion, we will only use the expression for r obtained from the perturbation theory for situations in which $\langle d^4\rangle_\infty$ is finite. The critical coupling strength in Eq. (5.16), on the other hand, does not have this restriction.

The expressions in Eqs. (5.23) and (5.30) can be shown to coincide under the approximation $u_n \propto d_n$. The treatment in Section 5.1.1 does not assume that r_n/d_n is independent of n, and we will show in Section 5.2 that there are significant cases where it gives better results for the critical coupling strength than the mean field approximation.

5.1.3 Summary of approximations and range of validity

In the previous sections, we developed different approximations to find the critical coupling constant and the behavior of the order parameter past the transition. Here we summarize the different approximations

Approximation	Abbreviation	Equation
Time averaged theory	TAT	(5.11)
Frequency distribution approximation	FDA	(5.14)
Perturbation theory	PT	(5.22,5.23)
Mean field theory	MF	(5.25)

Table 5.1: Approximations considered, their abbreviation, and their corresponding equations.

and the assumptions used in obtaining them. All the approximations mentioned above assume that the number of connections per node is very large. This allowed us, among other things, to neglect the time fluctuating term $h_n(t)$ in Eq. (5.5). We will discuss the effect of this term in Section 5.5.

The most fundamental approximation is given by Eq. (5.11). This equation can be solved numerically if the frequency of each oscillator and the adjacency matrix is known. This is the time averaged theory (TAT). Assuming that the local mean field r_n is statistically independent of the frequency ω_n, the frequency distribution approximation (FDA) given by Eq. (5.14) is obtained. This equation can also be solved numerically, but only knowledge of the probability distribution for the frequencies and the adjacency matrix is required. Obtained by expanding the FDA approximation near the transition point, the perturbation theory (PT) describes the behavior of the order parameter in terms of the largest eigenvalue of the adjacency matrix and its associated eigenvector in networks where the degree distribution is relatively homogeneous, more precisely when $\langle d^4 \rangle_\infty$ is finite. Taking r_n in the FDA approximation to be proportional to the degree, $r_n \propto d_n$, leads to the mean field theory (MF). Table 5.1 summarizes the different approximations, their abbreviations and their corresponding equations. The diagram in Fig. 5.1 indicates the assumptions leading to each approximation.

The mean field theory requires only knowledge of the frequency distribution and the degree distribution of the network, and thus it requires less information than the other approximations. However, it can produce misleading results if not used carefully. The mean field approximation has the added assumption that the eigenvector u of A associated with the largest eigenvalue λ satisfies $u_n \propto d_n$ (since,

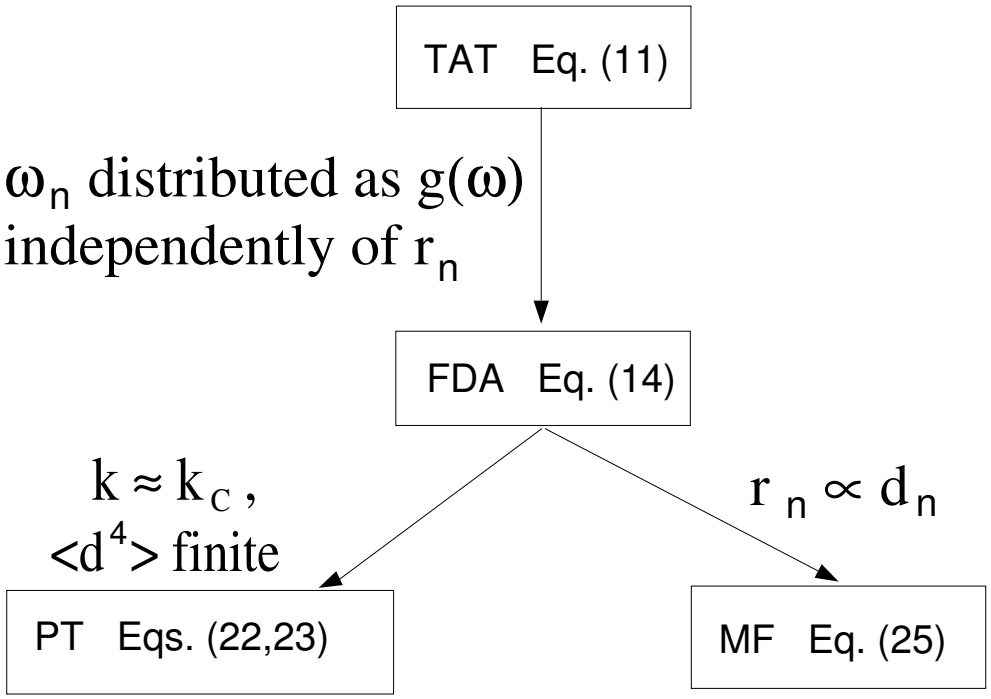

Figure 5.1: Different approximations and the assumptions leading to them. See text for details.

close to the transition, $r_n \approx u_n$). While correlations might exist [64], these two quantities are in general not proportional. Further, the mean field approximation implies that $\lambda \approx \langle d^2\rangle/\langle d\rangle$, a result that, although a good approximation in some cases, is not always true. Asymptotic forms for the largest eigenvalue in random networks with given degree distributions are discussed and a sufficient condition for $\lambda \approx \langle d^2\rangle/\langle d\rangle$ to be valid is presented in [65] as follows. Let d_{max} be the maximum expected degree of the network. If $\langle d^2\rangle/\langle d\rangle > \sqrt{d_{max}}\log N$, then $\lambda \approx \langle d^2\rangle/\langle d\rangle$ almost surely as $N \to \infty$. We note also that, if the degree distribution is tightly distributed around its mean, so that $\sqrt{\langle d^2\rangle} \sim \langle d\rangle \sim d_{max} \gg (\log N)^2$, the condition for the validity of $\lambda \approx \langle d^2\rangle/\langle d\rangle$ is satisfied. If instead $\sqrt{d_{max}} > (\langle d^2\rangle/\langle d\rangle)(\log N)^2$, then almost surely the largest eigenvalue is $\lambda \approx \sqrt{d_{max}}$ as $N \to \infty$ [65]. We will show that, indeed, to the extent that the approximation $\lambda \approx \langle d^2\rangle/\langle d\rangle$ does not hold, the results from the numerical simulation of Eq. (5.3) agree with the critical coupling strength as determined by the eigenvalue of the adjacency matrix, rather than by the quantity $\langle d^2\rangle/\langle d\rangle$.

The asymptotic regimes described in [65] are not available with the relatively small networks ($N \sim$

5000) we are restricted to study due to limited computational resources (see the end of Appendix B). Also, finite but large networks are also interesting from an applied point of view. Thus, we numerically compare both approximations in order to illustrate the possible discrepancies between them in particular cases. Figure 5.2 was obtained using (for each γ) a single random realization of a network where the degrees d_n are drawn from a power law degree distribution with power law exponent γ (with $d_n \geq d_0 = 20$) and with $N = 5000$ nodes (see Sec. 5.2 for details on how the networks are generated). We plot $\langle d^2 \rangle / \langle d \rangle$ and λ as a function of γ. For the parameters used in the plot, $\langle d^2 \rangle / \langle d \rangle$ coincides with the largest eigenvalue λ for

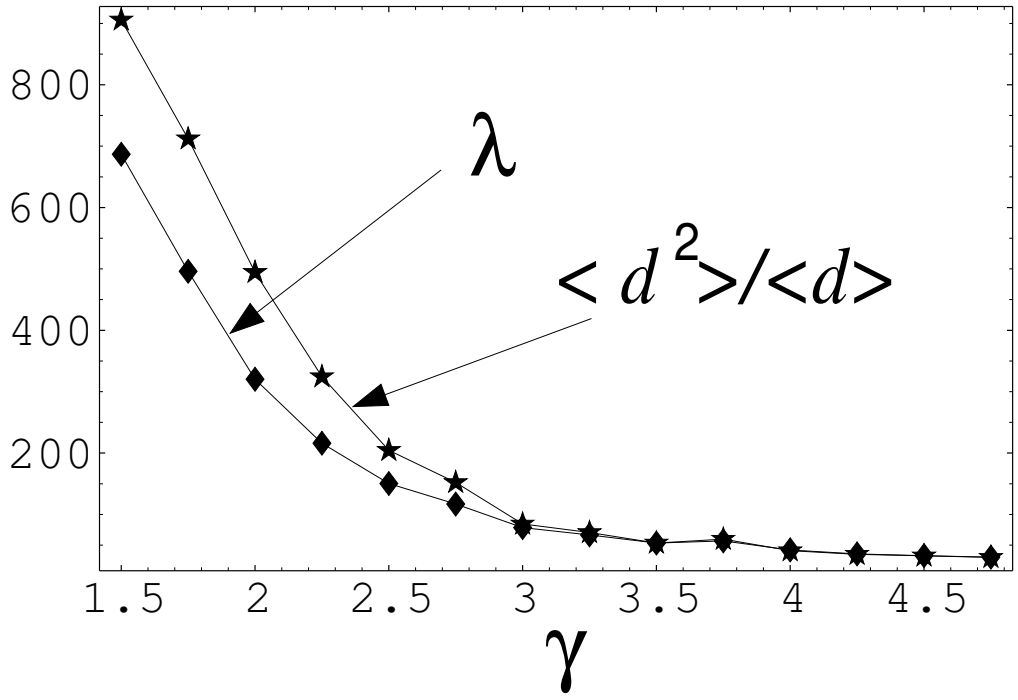

Figure 5.2: Largest eigenvalue λ (diamonds) and $\langle d^2 \rangle / \langle d \rangle$ (stars) as a function of γ for $N = 5000$ and $d_0 = 20$.

values of γ greater than 3. This suggests that the mean field result for the critical coupling strength k_{mf} is valid for $N = 5000$ and $\gamma > 3$. This is consistent with our numerical experiments in Sec. 5.2. We show in Appendix B, however, that the mean field approximation $\langle d^2 \rangle / \langle d \rangle$ underestimates λ for sufficiently large N (too large for us to simulate). In fact, as $N \to \infty$, λ diverges while $\langle d^2 \rangle / \langle d \rangle$ remains finite. Thus, the critical coupling constant obtained from our theory approaches zero as $N \to \infty$, while the one obtained from the mean field theory remains constant. This suggests that the few nodes with high degree are able, for

large enough N, to synchronize the network, and that these nodes are not taken into account by the mean field theory.

For $\gamma < 3$, we observe from Fig. 5.2 that λ is less than $\langle d^2 \rangle / \langle d \rangle$ when $N = 5000$. Thus, in this range, the mean field theory predicts a transition for a coupling constant that is *smaller* than that predicted by the perturbative approach. In the next section we will show, for a numerical example in this regime, that the transition occurs for a larger coupling than that predicted by the mean field theory.

5.2 Examples

In order to test the results in Sec. 5.1, we choose a distribution for the natural frequencies given by $g(\omega) = (3/4)(1 - \omega^2)$ for $-1 < \omega < 1$ and $g(\omega) = 0$ otherwise. In order to generate the network, we specify a degree distribution and we use the "configuration" model (e.g., Sec. 4.2.1 of Ref. [7] and references therein) to generate a random network realization with the specified degree distribution: (i) we first generate a *degree sequence* by assigning a degree d_n to each node n according to the given distribution; (ii) imagining that each node n is given d_n spokes sticking out of it, we choose pairs of spoke ends at random, and connect them.

We consider a fixed number of nodes, $N = 2000$, and the following networks with uniform coupling strength (i.e., $A_{nm} = 1$ or 0) (i) the degrees are uniformly distributed between 50 and 149, and (ii) the probability of having a degree d is given by $p(d) \propto d^{-\gamma}$ if $50 \leq d \leq 2000$ and $p(d) = 0$ otherwise, where γ is taken to be 2, 2.5, 3 and 4. [Our choice $p(d) = 0$ for $d < 50$ insures that there are no nodes of small degree, and suggests that our approximation of neglecting the noise-like, fluctuating quantity h_n in Eq. (5.5) is valid. We return to this issue in Section 5.5.]

The initial conditions for Eq. (5.3) are chosen randomly in the interval $[0, 2\pi]$ and Eq. (5.3) is integrated forward in time until a stationary state is reached (stationary state here means stationary in a statistical sense, i.e. the solution might be time dependent but its statistical properties remain constant in time). From the values of $\theta_n(t)$ obtained for a given k, the order parameter r is estimated as $r \approx \left| \sum_{m=1}^{N} d_m \langle e^{i\theta_m} \rangle_t / \sum_{m=1}^{N} d_m \right|$, where the time average is taken after the system reaches the stationary state. (Close to the transition, the time needed to reach the stationary state is very long, so that it is difficult

to estimate the real value of r. This problem also exists in the classical Kuramoto all-to-all model.) The value of k is then increased and the system is allowed to relax to a stationary state, and the process is repeated for increasing values of k.

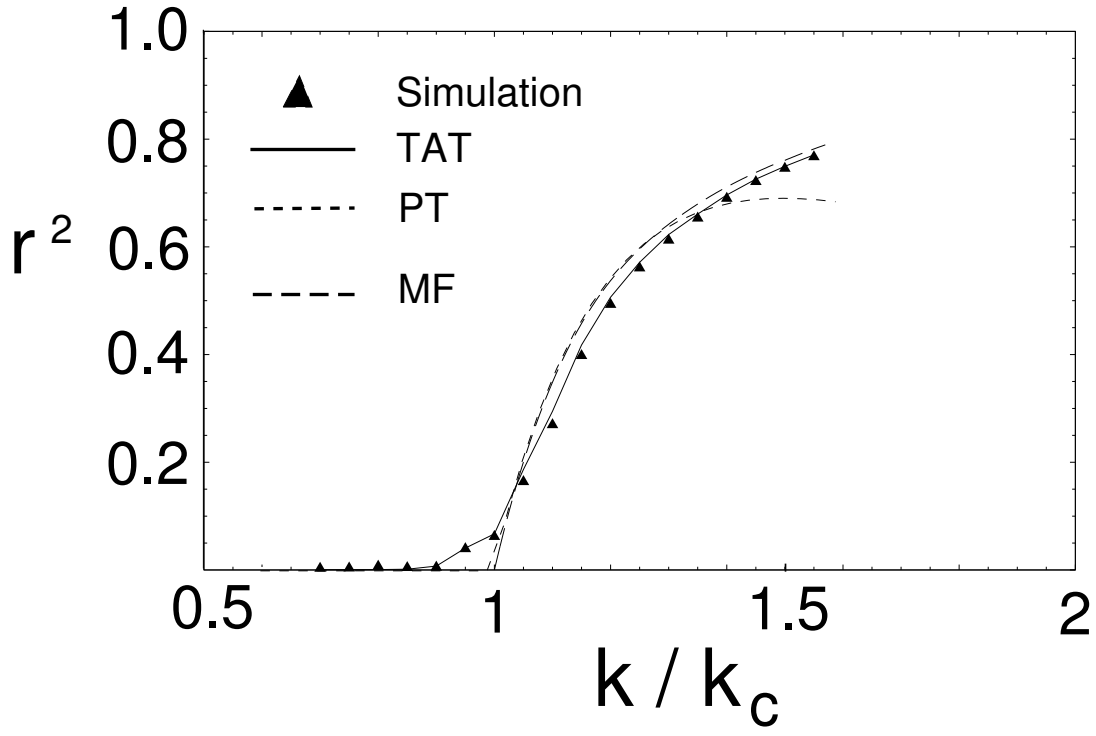

Figure 5.3: Order parameter r^2 obtained from numerical solution of Eq. (5.3) (triangles), time averaged theory (solid line), mean field theory (long-dashed line), and perturbation theory (short-dashed line) as a function of k/k_c for network (i), with the degree of the nodes uniformly distributed in $\{50, \ldots, 149\}$. All curves are obtained using the same single random network realization.

In Fig. 5.3 we show the results for the network with a uniform degree distribution as described above [network (i)]. We plot r^2 from numerical solution the full system in Eq. (5.3) (triangles), the theoretical prediction from the time averaged theory (solid line), the prediction from the mean field theory (long-dashed line), and from the perturbation theory (short-dashed line) (see Table 5.1) as a function of k/k_c, where k_c is given by Eq. (5.16). The frequency distribution approximation agrees with the time averaged theory, so we do not include it in the plot. In this case, all the theoretical predictions provide good approximations to the observed numerical results. The time averaged theory reproduces remarkably well the numerical

observations. Even the irregular behavior near the transition is taken into account by the time averaged theory. The mean field theory is in this case a good approximation, providing a fair description of the order parameter past the transition. The perturbation theory is valid in this case up to $k/k_c \approx 1.3$.

The results for the networks with power law degree distributions [networks (ii)] are shown in Figs. 5.4 (a), (b), (c) and (d) for $\gamma = 2$, 2.5, 3, and 4, respectively. The order parameter r^2 from numerical solution of the full system in Eq. (5.3) (triangles), the time averaged theory (solid line), the frequency distribution approximation (stars), and the mean field theory (long-dashed line) are plotted as a function of k/k_c. We do not show the perturbation theory since in all these cases $\gamma < 5$ and so we do not expect the perturbative theory to be valid as $N \to \infty$.

The time averaged theory agrees best with the numerical simulations in all cases. The frequency distribution approximation also agrees well in all cases; though it predicts a sharper transition than actually occurs. The mean field approximation agrees closely with the frequency distribution approximation for $\gamma = 4$ and, away from the transition, for $\gamma = 3$. However, for $\gamma = 2$ and $\gamma = 2.5$, it deviates greatly from the other approximations and from the numerical simulation. The critical coupling strengths predicted by the mean field theory and by the perturbation theory are very close for $\gamma = 4$, but the mean field theory predicts a transition at about 10% smaller coupling for $\gamma = 3$, about 20% smaller for $\gamma = 2.5$, and about 40% smaller for $\gamma = 2$. Since the transition in the numerical simulation is not so well-defined, both approximations are reasonable for $\gamma = 3$, but for $\gamma = 2$ and $\gamma = 2.5$ the critical coupling strength predicted by the mean field approximation is clearly too small.

In the past years, it has been discovered that many real world networks have degree distributions which are power laws with exponents between 2 and 3.5 [7, 8, 66]. In order to accurately predict the critical coupling strength across this range of exponents, the critical coupling constant given by $k_c = k_0/\lambda$ determined by the largest eigenvalue of the adjacency matrix should be used. The behavior of the order parameter can be estimated using the time averaged theory or the frequency distribution approximation. These two approximations were found to be consistently accurate for the range of exponents and values of the coupling constant studied. For the value of N used, the mean field theory works well in predicting the critical coupling strength and the behavior of the order parameter if one is interested in values of γ larger

than 3.

Tables 5.2 and 5.3 present the results of comparing the theoretical predictions with the numerical integration of Eq. (5.3) for different networks. Table 5.2 compares the observed critical coupling strength with the theoretical estimate. If both are close, the entry is "G", and otherwise "NG". Table 5.3 compares the predicted behavior of the order parameter past the transition with the observed one. If the corresponding entry in Table 5.2 is "NG", no comparison is attempted. The entries are the range of k/k_c over which the corresponding theoretical prediction agrees with the numerical simulation.

5.3 Nonuniform coupling strength

So far, our examples have assumed that the coupling strength is uniform (i.e., all the entries of the adjacency matrix A have been taken to be 0 or 1). However, considering that the degree of a node is defined as $d_n \equiv \sum_m A_{nm}$, our results carry through to the more general case of non uniform coupling. As an example of this situation, we apply our results to the case treated in Refs. [34] of a distance dependent interaction strength. Assume that the nodes n are equidistantly located on a circle and the matrix elements are given by

$$A_{nm} = f(|n - m|), \tag{5.31}$$

where $|n - m|$ represents distance modulo N (e.g. $|1 - N| = 1$), $f(0) = 0$, and $f \geq 0$. Then each row of A has the same sum $\lambda = \sum_m A_{nm}$, and $[1, 1, \ldots, 1]^T$ is an eigenvector with eigenvalue λ. By the Gershgorin circle theorem [67] (each eigenvalue σ of A satisfies, for some n, $|\sigma - A_{nn}| \leq \sum_{m \neq n} |A_{nm}|$), this is the largest eigenvalue (since $A_{nn} = 0$), and thus determines the transition to synchrony as described in the previous section. This scaling factor has been proposed before, by analogy to spin systems, to determine the transition to coherence in the case of a power law decaying interaction strength $f(x) = x^{-\gamma}$ [34].

5.4 Linear stability approach

Partly as a precursor to the next section (Sec. 5.5), in this section we discuss another approach that has the advantage of providing information on the dynamics of the system. We study the linear stability of the incoherent state by a method similar to that used in Ref. [28]. We assume that in the incoherent state the

Degree distribution	TAT	FDA	MF	PT
$p(d)$ uniform in $\{50, \ldots, 149\}$	G	G	G	G
$p(d) \propto d^{-\gamma}$, $\gamma = 2$	G	G	NG	-
$p(d) \propto d^{-\gamma}$, $\gamma = 2.5$	G	G	NG	-
$p(d) \propto d^{-\gamma}$, $\gamma = 3$	G	G	G	-
$p(d) \propto d^{-\gamma}$, $\gamma = 4$	G	G	G	-

Table 5.2: Comparison of the predicted critical coupling strength versus the observed one for the different approximations (columns) and different networks (rows). If the critical coupling strength is predicted by a given approximation for a certain network, the corresponding entry is marked "G". Otherwise, "NG" is entered. A "-" is entered when the perturbation theory is inapplicable ($\gamma < 5$), see Sec. 5.1.2.

Degree distribution	TAT	FDA	MF	PT
$p(d)$ uniform in $\{50, \ldots, 149\}$	$0.5+$	$0.5+$	$0.5+$	0.3
$p(d) \propto d^{-\gamma}$, $\gamma = 2$	$0.7+$	$0.7+$	-	-
$p(d) \propto d^{-\gamma}$, $\gamma = 2.5$	$0.5+$	$0.5+$	-	-
$p(d) \propto d^{-\gamma}$, $\gamma = 3$	$0.7+$	$0.7+$	$0.7+$	-
$p(d) \propto d^{-\gamma}$, $\gamma = 4$	$0.7+$	$0.7+$	$0.7+$	-

Table 5.3: Comparison of the predicted behavior of the order parameter versus the observed one for the different approximations (columns) and different networks (rows). If the behavior is correctly predicted by a given approximation for a certain network, the corresponding entry contains the range of k/k_c after $k/k_c = 1$ for which the approximation works well. A "$+$" indicates that the agreement possibly persists for larger values of k. When "NG" appears in the corresponding entry in table 5.2, no comparison is attempted and a "-" is entered. A "-" is also entered when the perturbation theory is inapplicable ($\gamma < 5$), see Sec. 5.1.2.

solution to Eq. (5.3) is given approximately by

$$\theta_n^0 = \omega_n t + \phi_n, \tag{5.32}$$

where ϕ_n is a random initial condition. We introduce infinitesimal perturbations to this state by

$$\theta_n = \theta_n^0 + \delta_n. \tag{5.33}$$

In Appendix C, we assume that the perturbations grow as a function of time as e^{st}, and obtain the eigenvalue equation

$$b_n = \frac{k}{2} \sum_{m=1}^{N} \frac{A_{nm} b_m}{s - i\omega_m}. \tag{5.34}$$

We look for solutions b_n of this equation that are independent of the frequencies ω_n (similar to Assumption ★). Under this assumption, replacing $(s - i\omega_n)^{-1}$ in Eq. (5.34) with its expected value, we get

$$b_n = \frac{k}{2} \left\langle \frac{1}{s - i\omega} \right\rangle \sum_{m=1}^{N} A_{nm} b_m, \tag{5.35}$$

where

$$\left\langle \frac{1}{s - i\omega} \right\rangle = \int_{-\infty}^{\infty} \frac{g(\omega) d\omega}{s - i\omega} \tag{5.36}$$

and the integration contour is defined in the causal sense [i.e., for $Re(s) > 0$ it is along the real axis, and for $Re(s) \leq 0$ it passes above the pole $\omega = -is$]. We thus obtain the dispersion relation

$$1 = \frac{k\lambda}{2} \int \frac{g(\omega) d\omega}{s - i\omega}, \tag{5.37}$$

where, as in Sec. 5.1, λ is the largest eigenvalue of the adjacency matrix A. Except for the presence of the eigenvalue λ, this is the known dispersion relation for the stability of the incoherent state of the Kuramoto model [31]. Under our assumption that $g(\omega)$ is even and decreases monotonically away from 0 (Sec. 5.1), an unstable [$Re(s) > 0$] solution of Eq. (5.37) is real [68] (note that, since A is symmetric, λ is real). In order to find the critical coupling, we let $s \to 0^+$, $(s - i\omega)^{-1} \to iP(1/\omega) + \pi\delta(\omega)$. Since $g(\omega)$ is symmetric, $\left\langle (s - i\omega)^{-1} \right\rangle \to \pi g(0)$. According to Eq. (5.35), the critical coupling is then given by

$$k_c = \frac{k_0}{\lambda}, \tag{5.38}$$

in agreement with the nonlinear approach. [We note, however, that, if $g(\omega)$ has multiple maxima, then the first instability can occur at $Im(s) \neq 0$ at a value of k below that given by Eq. (5.38). This is why we have assumed that $g(\omega)$ decreases monotonically away from $\omega = 0$.]

5.5 Effect of fluctuations

So far we have neglected the effect of the small fluctuations due to the finite number of connections per node. In our examples, we have presented networks that do not have nodes with small degree. However, in many networks there is a large fraction of the nodes with small degree; in all our examples in Sec. 5.2 there were no nodes with degree less than 50 [$p(d) = 0$ for $d < 50$]. For example, scale free networks generated using the Barabási-Albert method [8] sometimes have parameters so that $\langle d \rangle = 6$.

In developing our theory, we neglected the time variations in Eq. (5.5), and worked thereafter with the average value of the phase of the locked oscillators. In order to gain insight into the effect of these fluctuations, we will treat the time fluctuations as a noise term.

The theory we present is heuristic and may be thought of as an expansion giving a small lowest order correction to the linear stability approach of Sec. 5.4 for large but finite $\langle d \rangle$. On the other hand, later in this section, we will apply this theory to numerical examples where the finite size effect is not small, and we will find that the theory is still useful in that it correctly indicates the trend of the numerical observations.

Like in Sec. 5.4, we consider perturbations to the incoherent state described by Eq. (5.32). As an approximation, we regard the coupling term in Eq. (5.3), $f_n(t) \equiv k \sum_{m=1}^{N} A_{nm} \sin(\theta_m - \theta_n)$, as a noise term. In addition to growing linearly with time, the phase of the oscillator n will diffuse under the influence of this noise. We assume that $\theta_n(t) = \phi_n + \omega_n t + W_n(t)$, where $W_n(t)$ is a random walk such that $\langle W_n(t) \rangle = 0$ and $\langle W_m(t) W_n(t) \rangle = 2 D_{nm} t$, and ϕ_n is an initial condition, which we assume to be randomly drawn from $[0, 2\pi)$. (In this section, by $\langle \dots \rangle$ we mean an expected value, i.e. and ensemble average, rather than an average over t or n.)

By using the linear approach of Section 5.4, the diffusion coefficients D_{nm} will give us information on how the critical coupling strength differs from Eq. (5.38). The diffusion coefficients D_{nm} are given by

$$\begin{aligned} D_{nm} &= \int_0^\infty \langle f_n(t + \tau/2) f_m(t - \tau/2) \rangle d\tau \qquad (5.39) \\ &= \int_0^\infty \sum_{j,k} A_{nj} \langle \sin(\theta_j^+ - \theta_n^+) A_{mk} \sin(\theta_k^- - \theta_m^-) \rangle d\tau, \end{aligned}$$

where $+$ (respectively $-$) indicates evaluation at $t + \tau/2$ (respectively $t - \tau/2$). Consider first the case $n \neq m$. The contribution of the terms with $\{j, n\} \neq \{k, m\}$ vanishes after the integration, and we obtain,

using the symmetry of A,

$$D_{nm} = \frac{k^2}{2} A_{nm}^2 \langle \sin(\theta_m^+ - \theta_n^+) \sin(\theta_n^- - \theta_m^-) \rangle. \tag{5.41}$$

We now introduce our aforementioned assumption that $\theta_n(t) - \omega_n t$ is a random walk plus a random initial condition, $\theta_n(t) = \phi_n + \omega_n t + W_n(t)$. Using the identity $\sin(x)\sin(y) = [\cos(x-y) - \cos(x+y)]/2$ and averaging over the initial phases ϕ_n we get

$$D_{nm} = -\frac{k^2}{2} \int_0^\infty A_{nm}^2 \langle \cos(\Delta W_m - \Delta W_n + \omega_{mn}\tau) \rangle d\tau, \tag{5.42}$$

where $\Delta W_n \equiv W_n^+ - W_n^-$ and $\omega_{mn} \equiv \omega_m - \omega_n$. We now use the fact that for a Gaussian random variable x with variance σ^2 we have $\langle \cos(x) \rangle = Re\langle e^{ix} \rangle = Re(e^{i\langle x \rangle - \sigma^2/2})$. In our case, $\langle x \rangle = \omega_{mn}\tau$ and $\sigma^2 = \langle (\Delta W_m - \Delta W_n)^2 \rangle = 2(D_n + D_m - 2D_{nm})\tau$, where $D_n \equiv D_{nn}$. After using this to compute the expected value, and performing the integration, we obtain for $n \neq m$

$$D_{nm} = -\frac{k^2}{2} A_{nm}^2 \frac{D_n + D_m - 2D_{nm}}{(D_n + D_m - 2D_{nm})^2 + \omega_{mn}^2}. \tag{5.43}$$

If $n = m$, the calculation proceeds along the same lines, but the nonvanishing terms in Eq. (5.39) are those for which $k = j$. Together with Eq. (5.43), this results in

$$D_n = -\sum_{m \neq n} D_{nm}. \tag{5.44}$$

In principle, Eqs. (5.43) and (5.44) can be solved for D_n as a function of k if the frequencies and the adjacency matrix are known.

In order to relate the diffusion coefficients to the critical coupling constant, we resort to the linear analysis of Sec. 5.4. When noise is introduced in the linear approach, Equation (5.34) for the growth rate s generalizes, as shown at the end of Appendix C, to

$$b_n = \frac{k}{2} \sum_{m=1}^{N} \frac{A_{nm} b_m}{s + D_m - i\omega_m}. \tag{5.45}$$

Since $Re(s) > 0$ corresponds to instability of the incoherent state, it is expected that the effect of the noise as reflected by positive D_m is to shift the transition point so that the critical coupling constant is larger.

In order to solve for the growth rate s for a given value of k, we rewrite Eq. (5.45) as

$$b = \frac{k}{2} D(s) A b, \tag{5.46}$$

where b is the vector with components $\{b_n\}$, $D(s)$ is the diagonal matrix $D(s) \equiv diag\{(s+D_m-i\omega_m)^{-1}\}$, and A is the adjacency matrix. The characteristic equation is

$$\det\left(\frac{k}{2}D(s)A - I\right) = 0, \tag{5.47}$$

where I is the $N \times N$ identity matrix. This implies

$$\det\left(\frac{k}{2}A - D(s)^{-1}\right) = 0, \tag{5.48}$$

or

$$\det\left(\frac{k}{2}A - diag\{D_m - i\omega_m\} - sI\right) = 0, \tag{5.49}$$

that is, the growth rate s is an eigenvalue of the matrix $M(k) \equiv (k/2)A - diag\{D_m - i\omega_m\}$.

For a given value of k, Eqs. (5.43) and (5.44) can be solved iteratively. We have found that, by starting from an initial guess for the values of D_{nm} and repeatedly evaluating the right hand side of Eq. (5.43) in order to get the next approximation to the values of D_{nm}, convergence is achieved to a solution that is independent of the initial guess if the condition $D_n > 0$ is imposed. When the values of D_{nm} have been found for a given value of k, the relevant growth rate is calculated as the largest real part of the eigenvalues of the matrix $M(k)$ defined above.

As an example, we consider three networks with the degree of all nodes d given by $d = 100$ in the first, $d = 50$ in the second and $d = 20$ in the third one. In order to solve numerically the coupled equations, we work with a small number of nodes, $N = 500$. In Fig. 5.5 we show the results for a realization of the three networks. The order parameter r^2 obtained from numerical solution of Eq. (5.3) (solid lines) and the growth rate obtained from Eqs. (5.43), (5.44) and (5.49) (dashed lines) are plotted as a function of k/k_c. The arrows indicate which network corresponds to the given curve. We observe that, as the connections per node are decreased, the transition point shifts to larger values of the coupling constant. This trend is reproduced by the growth rate curves, which are displaced to the right for smaller values of the degree.

We emphasize that the theory we described above is applicable to networks for which $\langle d \rangle$ is large but finite. However, in Fig. 5.5 we applied the theory to cases in which $\langle d \rangle$ is not very large. Although we do not expect the theory to be valid in this case, we find that it correctly describes the trend present in the

numerical observations, i.e., a shifting of the transition to coherence to larger values of the critical coupling as nodes of small degree become important.

5.6 Discussion

A transition to coherence in large networks of coupled oscillators should be expected at a critical value of the coupling strength which is determined by the largest eigenvalue of the adjacency matrix of the network and its associated eigenvector. In the all-to-all case, the largest eigenvalue is $N-1 \approx N$ and thus the Kuramoto result $k_c = k_0/N$ is recovered. The largest eigenvalue of the adjacency matrix of a network is of both theoretical and practical importance, and thus its properties have been studied in some detail [64, 65, 69]. We remark that our analysis allows the case of nonuniform interaction strengths by introducing continuous values in the entries of the adjacency matrix A.

We developed different approximations in order to describe the transition to coherence in terms of an appropriately defined order parameter which generalizes the parameter used in the classical Kuramoto model [36]. See Table 5.1 and Figure 5.1 for a summary of the approximations and assumptions. The time averaged theory (TAT) provided the most accurate description of the behavior of the order parameter, and assumes knowledge of the adjacency matrix A_{nm} and the individual frequencies ω_n. The frequency distribution approximation (FDA) also provides a good approximation but does not require knowledge of the individual frequencies. These approximations yield equations that have to be solved numerically. The time required to numerically solve these equations is, however, much less than that required to numerically integrate the original differential equations. The perturbation theory (PT) yields analytic expressions for the order parameter when close to the transition in terms of the largest eigenvalue of the adjacency matrix and its associated eigenvector, but is limited to networks with a relatively homogeneous degree distribution. The mean field theory (MF) [36] is obtained by introducing the additional assumption that the components of the eigenvector associated with the largest eigenvalue are proportional to the degree of the corresponding node. This does not necessarily have to be the case when close to the transition, and because of this extra assumption, we expect the other approximations to more generally accurately describe the transition than the mean field theory. Figs. 5.4(a) and (b) show that for the particular case of scale free networks with

$N = 2000$, $\gamma = 2$ and $\gamma = 2.5$ this is the case. In general, we observed that for low values of the exponent γ (see Fig. 5.4) the mean field approximation and the perturbative approximation yield different critical coupling strengths. The mean field theory has the advantage that analytic expressions can be computed without the need of solving the eigenvalue problem for the adjacency matrix, and could be useful when only limited information is available about the network. However, in general, our results suggest that one of the other approximations mentioned above should be used.

We remark that even though the time averaged theory, the frequency distribution approximation and the perturbation theory require in principle knowledge of the full matrix A, knowledge of the degree distribution may be enough in some cases. As in our examples, an adjacency matrix A can be generated randomly with a given degree distribution. Our results indicate that even this limited reconstruction of the original network might improve the mean field results (see Sec. 5.2).

Our assumptions restrict the class of networks for which the results apply. We assumed that sufficiently near the onset of synchronization each node is coupled to many *locked* oscillators. In practice this implies that most nodes should have a high degree. This is an important restriction for our theory. In Sec. 5.2 we used networks with a minimum degree of 50. As mentioned before, we observed that in networks with small average degree (about 20), the observed critical coupling was larger than the one predicted by our theory. By including the previously neglected time fluctuations, we developed a heuristic theory in Sec. 5.5 which correctly predicts the trend observed in the numerical simulations. As the nodes with small degree become important, both our theory and the numerical observations indicate that the transition to synchrony occurs at larger values of the coupling strength.

In conclusion, we have developed a theory predicting the critical coupling for the transition from incoherence to coherence in large networks of coupled oscillators. We found that for a large class of networks, a transition to coherence should be expected at a critical value of the coupling strength which is determined by the largest eigenvalue of the adjacency matrix of the network. We developed and compared various approximations to the order parameter past the transition, and studied the effect of the fluctuations caused by finite size effects.

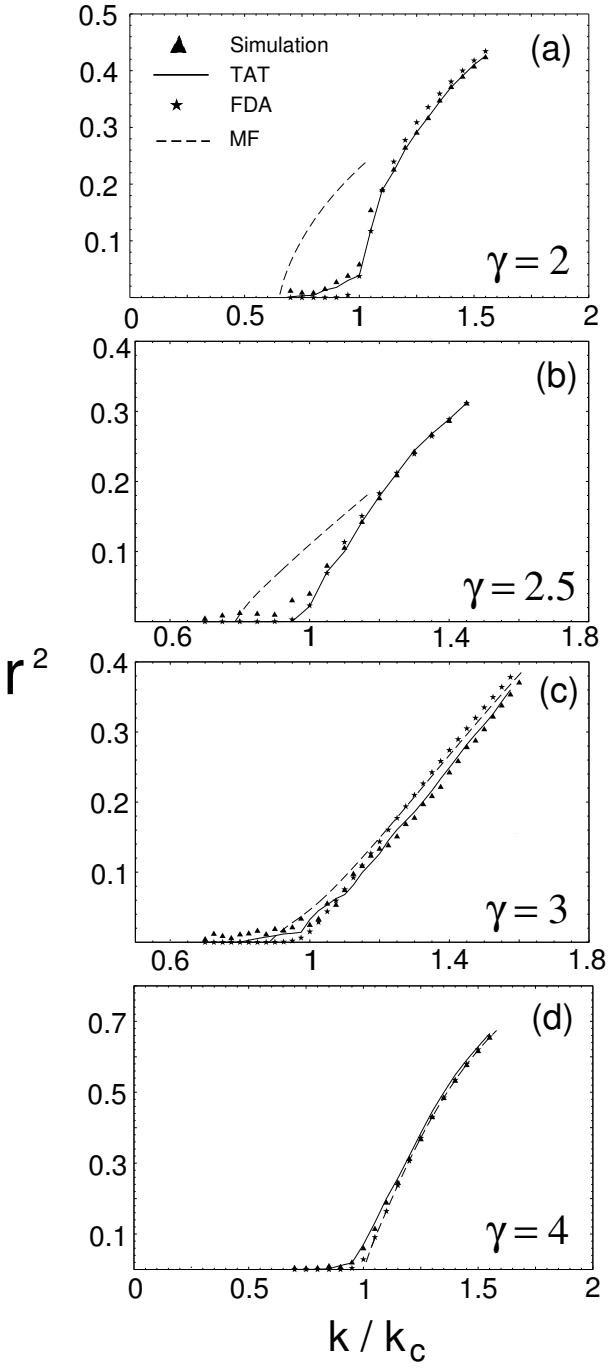

Figure 5.4: Order parameter r^2 obtained from numerical solution of Eq. (5.3) (triangles), time averaged theory (solid line), frequency distribution approximation (stars), and mean field theory (long-dashed line) as a function of k/k_c for degree distributions given by $p(d) \propto d^{-\gamma}$ if $50 \leq d \leq 2000$ and $p(d) = 0$ otherwise, with (a) $\gamma = 2$, (b) $\gamma = 2.5$, (c) $\gamma = 3$, and (d) $\gamma = 4$. All curves in each figure are obtained using the same single random network realization.

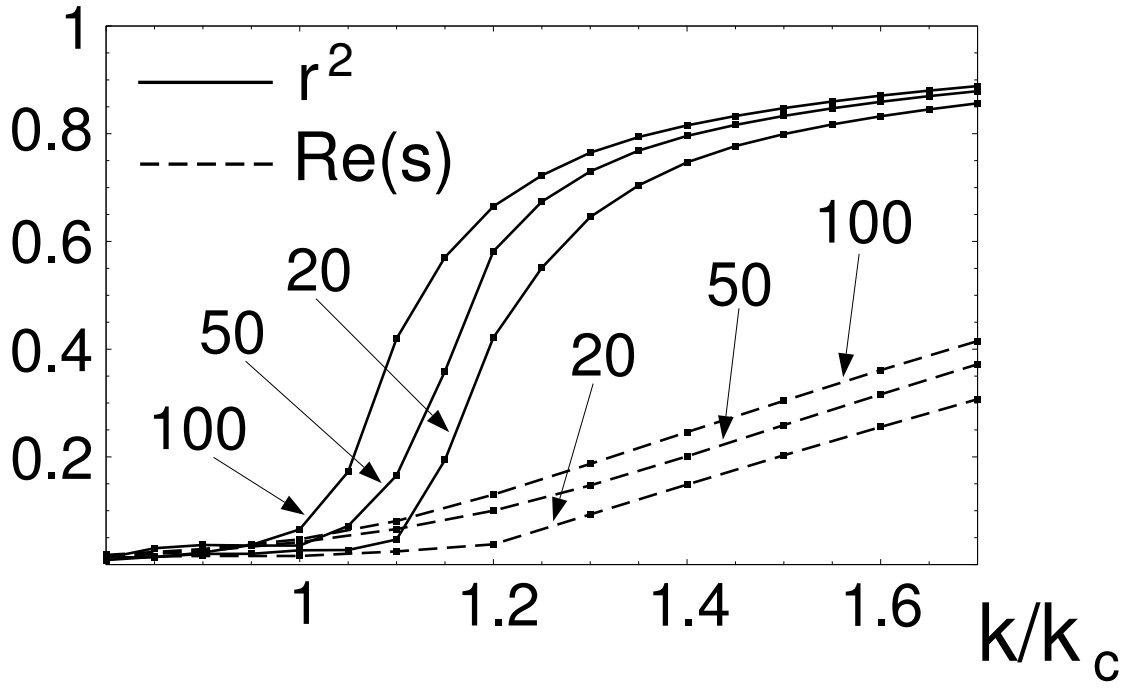

Figure 5.5: Order parameter r^2 obtained from numerical solution of Eq. (5.3) (solid lines) and growth rate $Re(s)$ (dashed lines) for a network with the degree of all nodes $d = 20$, $d = 50$ and $d = 100$ as a function of k/k_c. The arrows indicate which network corresponds to the given curve.

Appendix A

Analysis of the contribution of the non locked oscillators to the mean field

In this Appendix we show that, using Assumption ★, we can neglect the sum over the unlocked oscillators in Eq. (5.7),

$$\sum_{|\omega_m|>kr_m}^{N} A_{nm}\langle e^{i\theta_m}\rangle_t. \tag{A.1}$$

We will follow to some extent Chapter 12 of Ref. [20]. The time average is given by

$$\langle e^{i\theta_m}\rangle_t = \int_{-\pi}^{\pi} e^{i\theta} p_m(\theta) d\theta. \tag{A.2}$$

where $p_m(\theta)d\theta$ is, given the connections of node m and its natural frequency ω_m, the probability that its phase θ_m lies in the interval $[\theta, \theta + d\theta)$. It satisfies $p_m(\theta) \propto 1/\left|\dot{\theta}\right|$. Including the normalization we have, neglecting the term h_m in Eq. (5.5),

$$p_m(\theta) = \frac{\sqrt{\omega_m^2 - k^2 r_m^2}}{2\pi\left|\omega_m - kr_m \sin(\theta - \psi_m)\right|}. \tag{A.3}$$

The sum in Eq. (A.1) can be written as

$$\sum_{|\omega_m|>kr_m}^{N} A_{nm}\langle e^{i\theta_m}\rangle_t = \sum_{|\omega_m|>kr_m}^{N} A_{nm}\sqrt{\omega_m^2 - kr_m^2}\, sign(\omega_m)\frac{1}{2\pi}\int_{-\pi}^{\pi} \frac{e^{i\theta}(\omega_m + kr_m\sin(\theta-\psi_m))d\theta}{\omega_m^2 - k^2 r_m^2 \sin^2(\theta-\psi_m)}. \tag{A.4}$$

The integral of the first term vanishes since the 2π-periodic integrand changes sign under the transformation $\theta \to \theta + \pi$. We are left with

$$\sum_{|\omega_m|>kr_m}^{N} A_{nm}\langle e^{i\theta_m}\rangle_t = \sum_{|\omega_m|>kr_m}^{N} A_{nm}\sqrt{\omega_m^2 - kr_m^2}\, kr_m\, sign(\omega_m)\frac{1}{2\pi}\int_{-\pi}^{\pi} \frac{e^{i\theta}\sin(\theta-\psi_m)d\theta}{\omega_m^2 - k^2 r_m^2 \sin^2(\theta-\psi_m)}. \tag{A.5}$$

In this sum, $sign(\omega_m)$ is independent of ω_m^2 and, using Assumption ★, it is independent of r_n and ψ_n as well. If there are many terms in the sum, it will be then of order $\sqrt{d_n}$ due to the symmetry of the frequency distribution, and thus will be small compared with the sum over the locked oscillators, which is of order d_n [see Eq. (5.11)]. Note that we did not use here the full strength of Assumption ★, since we only required the sign of ω_m to be independent of r_m and ψ_m.

Appendix B

Failure of the mean field approximation as $N \to \infty$

Here we show that for sufficiently large N and a power law degree distribution of the degrees, $p(d) \propto d^{-\gamma}$, the mean field approximation $\langle d^2\rangle/\langle d\rangle$ underestimates λ for $\gamma > 3$. We base our argument in the results of Ref. [65]: if for a random graph $\sqrt{d_{max}} > \langle d^2\rangle/\langle d\rangle(\log N)^2$, then $\lambda \sim \sqrt{d_{max}}$ almost surely as $N \to \infty$, where d_{max} is the largest expected degree.

In the case under consideration ($\gamma > 3$), $\langle d^2\rangle/\langle d\rangle$ converges to the finite value $\langle d^2\rangle_\infty/\langle d\rangle_\infty$ [$\langle\dots\rangle_\infty$ is defined by Eq. (5.27)], while d_{max} diverges as $N^{1/(\gamma-1)}$ [7]. Thus, for large enough N, the conditions for $\lambda \sim \sqrt{d_{max}}$ will be satisfied, since $N^{1/(\gamma-1)}/(\log N)^4 \to \infty$ as $N \to \infty$. While $\lambda \sim \sqrt{d_{max}} \to \infty$ as $N \to \infty$, the mean field approximation $\langle d^2\rangle/\langle d\rangle$ remains finite.

We can estimate an upper bound on how large N needs to be for this discrepancy to be observed. For large N, $\langle d^2\rangle/\langle d\rangle \sim d_0$, where d_0 is the minimum degree [$p(d) = 0$ for $d < d_0$]. The maximum degree is approximately given by $d_{max} \sim d_0 N^{1/(\gamma-1)}$ [7]. Inserting these estimates in the condition $\sqrt{d_{max}} \sim \langle d^2\rangle/\langle d\rangle(\log N)^2$ we obtain

$$N \sim d_0^{\gamma-1}(\log N)^{4(\gamma-1)}. \tag{B.1}$$

As an example, for $\gamma = 4$ and $d_0 = 20$, the upper bound is approximately $N \sim 10^{25}$, a far larger system than we can simulate.

Appendix C

Linear stability of the incoherent state

In this Appendix we study the linear stability of the incoherent state by a method similar to that presented in Ref. [28]. As described in Section 5.4, we assume that in the incoherent state the solution to Eq. (5.3) is given approximately by

$$\theta_n^0(t) \approx \omega_n t + \phi_n, \tag{C.1}$$

where ϕ_n is an initial condition. We introduce infinitesimal perturbations to this state by

$$\theta_n = \theta_n^0 + \delta_n. \tag{C.2}$$

Linearizing Eq. (5.3), we get

$$\dot{\delta}_n = k \sum_{m=1}^{N} A_{nm} \cos(\theta_m^0 - \theta_n^0)\delta_m + \mu_n - \nu_n \delta_n, \tag{C.3}$$

where $\mu_n = k\sum_{m=1}^{N} A_{nm}\sin(\theta_m^0 - \theta_n^0)$ and $\nu_n = k\sum_{m=1}^{N} A_{nm}\cos(\theta_m^0 - \theta_n^0)$. As before, we assume that the number of links to node n is so large that, due to the incoherence, we may neglect the terms μ_n and ν_n. With this simplification, Eq. (C.3) can be recast as an integral equation as follows:

$$\delta_n(t) = k\int_{-\infty}^{t} dt' \sum_{m=1}^{N} A_{nm}\delta_m(t')\cos[\theta_m^0(t') - \theta_n^0(t')] \tag{C.4}$$

$$= \frac{k}{2}\int_{-\infty}^{t} dt' e^{-i\theta_n^0(t')}\left(\sum_{m=1}^{N} A_{nm}e^{i\theta_m^0(t')}\delta_m(t') + \sum_{m=1}^{N} A_{nm}e^{i[2\theta_n^0(t') - \theta_m^0(t')]}\delta_m(t')\right).$$

Multiplying by $A_{jn}e^{i\theta_n^0(t)}$, summing over n and defining $B_n(t) \equiv \sum_{m=1}^{N} A_{nm}\delta_m(t)e^{i\theta_m^0(t)}$, we get

$$B_j(t) = \frac{k}{2}\int_{-\infty}^{t} dt' \sum_{n=1}^{N} A_{jn}e^{i[\theta_n^0(t) - \theta_n^0(t')]}\left(B_n(t') + e^{2i\theta_n^0(t')}B_n^*(t')\right). \tag{C.5}$$

We assume that the quantities B_n grow exponentially with time as $B_n(t) = b_n e^{st}$, where $Re(s) > 0$. Inserting this ansatz in Eq. (C.5), and performing the integration we get

$$b_j = \frac{k}{2}\sum_{n=1}^{N}\frac{A_{jn}b_n}{s - i\omega_n} + \frac{k}{2}e^{2iIm(s)t}\sum_{n=1}^{N}\frac{A_{jn}b_n^* e^{2i\theta_n^0(t)}}{s^* + i\omega_n}. \tag{C.6}$$

The second sum is very small due to the incoherence of the θ_n^0's. So, changing indices, we are left with the eigenvalue equation

$$b_n = \frac{k}{2} \sum_{m=1}^{N} \frac{A_{nm} b_m}{s - i\omega_m}, \tag{C.7}$$

as claimed in Section 5.4.

If, as proposed in Section 5.5, there are fluctuations in the values of $\theta_n^0(t)$ such that $\theta_n^0(t) = \omega_n t + \phi_n + W_n(t)$, where $W_n(t)$ is a random walk such that $\langle W_n(t) \rangle = 0$ and $\langle W_n(t)^2 \rangle = 2D_n t$, we take the expected value of Eq. (C.5). We use the fact that for a Gaussian random variable x with variance σ^2 we have $\langle e^{ix} \rangle = e^{i\langle x \rangle - \sigma^2/2}$. In this case, $x = \omega_m(t' - t)$ and $\sigma^2 = 2D_m(t - t')$. We obtain after performing the integration

$$b_n = \frac{k}{2} \sum_{m=1}^{N} \frac{A_{mn} b_m}{s + D_m - i\omega_m}. \tag{C.8}$$

BIBLIOGRAPHY

[1] M. Faloutsos, P. Faloutsos, and C. Faloutsos, Computer Communications Rev., **29**, 251 (1999).

[2] A.-L. Barabási, R. Albert, and H. Jeong, Phys. A. **281**, 69 (2000).

[3] L.A.N. Amaral, A. Scala, M. Barthélemy, and H.E. Stanley, Proc. Natl. Acad. Sci. USA, **97** 11149 (2000).

[4] H. Jeong, S. Mason, A.-L. Barabási, and Z.N. Oltvai, Nature **411**, 41 (2001).

[5] S. Wasserman and K. Faust, *Social network analysis*, (Cambridge University Press, Cambridge, 1994).

[6] A.-L. Barabási, and R. Albert, Science **286**, 509 (1999).

[7] M.E.J. Newman, SIAM Review **45**, 167 (2003).

[8] A.-L. Barabási, and R. Albert, Rev. Mod. Phys. **74**, 47 (2002).

[9] A.-L. Barabási, *Linked: the new science of networks* (Perseus, Cambridge, MA, 2002).

[10] R. Roy and K.S. Thornburg, Phys. Rev. Lett. **72**, 2009 (1994).

[11] J. García-Ojalvo, J. Casademont, C.R. Mirasso, M.C. Torrent, and J.M. Sancho, Int. J. Bifur. Chaos **9**, 2225 (1999).

[12] A. Uchida, S. Kinugawa, T. Matsuura, and S. Yoshimori, Phys. Rev. E **67**, 026220 (2003).

[13] L.M. Pecora and T.L. Carroll, Phys. Rev. Lett. **64**, 821 (1990).

[14] W. Wang, I.Z. Kiss, and J.L. Hudson, Chaos **10**, 248 (2000).

[15] R.C. Elson, A.I. Selverston, R. Huerta, N.F. Rulkov, M.I. Rabinovich, and H.D.I. Abarbanel, Phys. Rev. Lett. **81**, 5692 (1998).

[16] J. Jalife, J. Physiol. **356**, 221 (1984).

[17] R.E. Mirollo and S.H. Strogatz, SIAM J. Appl. Math. **50**, 1645 (1990).

[18] E. Mosekilde, Y. Maistrenko, and D. Postnov, *Chaotic Synchronization: Applications to Living Systems* (World Scientific, Singapore, 2002).

[19] J. Buck, Q. Rev. Biol. **63**, 265 (1988).

[20] A. Pikovsky, M.G. Rosenblum, and J. Kurths, *Synchronization: A universal concept in nonlinear sciences*, (Cambridge University Press, Cambridge, 2001).

[21] S. H. Strogatz, *Sync*, (Hyperion, New York, 2003).

[22] P. Ashwin, J. Buescu, and I. Stewart, Phys. Lett. A **193**, 126 (1994).

[23] S.C. Venkataramani, B.R. Hunt, and E Ott, Phys. Rev. E **54**, 1346 (2003).

[24] A.V. Zimin, B.R. Hunt, and E. Ott, Phys. Rev. E **67**, 016204 (2003).

[25] Y. Kuramoto, *Chemical Oscillations, Waves, and Turbulence*, (Springer-Verlag, Berlin, 1984).

[26] H. Sakagucci, Progr. Theoret. Phys. **79**, 39 (1988).

[27] A. Pikovsky and S. Ruffo, Phys. Rev E **59**, 1633 (1999).

[28] H. Daido, J. Stat. Phys. **60**, 753 (1990).

[29] H. Daido, Phys. Rev. Lett. **73**, 760 (1994).

[30] M.K.S. Yeung and S.H. Strogatz, Phys. Rev. Lett. **82**, 648 (1999).

[31] S. H. Strogatz, Physica D **143**, 1 (2000).

[32] Edward Ott, *Chaos in dynamical systems*, (Cambridge University Press, Cambridge, 2002).

[33] A. Jadbabaie, N. Motee, and M. Barahona. Proceedings of the American Control Conference (ACC 2004).

[34] J. L. Rogers and L. T. Wille, Phys. Rev. E **54**, R2193 (1996); M. S. O. Massunaga and M. Bahiana, Physica D **168-169**, 136, (2002); M. Maródi, F. d'Ovidio, and T. Vicsek, Phys. Rev E **66**, 011109 (2002).

[35] Y. Moreno and A. E. Pacheco, arXiv:cond-mat/0401266.

[36] T. Ichinomiya, Phys. Rev. E **70**, 026116 (2004).

[37] D.-S. Lee, arXiv:cond-mat/0410635.

[38] L.M. Pecora, T.L. Carroll, G.A. Johnson, D.J. Mar, and J.F. Heagy, Chaos **7**, 520 (1997).

[39] K.M. Cuomo and A.V. Oppenheim, Phys. Rev. Lett. **71**, 65 (1993).

[40] M. E. J. Newman and J. Park, Phys. Rev. E **68**, 036122 (2003).

[41] M.G. Rosenblum, A.S. Pikovsky, and J. Kurths, Phys. Rev. Lett. **76**, 1804 (1996).

[42] N.F. Rulkov, M.M. Sushchik, L.S. Tsimring, and H.D.I. Abarbanel, Phys. Rev. E **51**, 980 (1995).

[43] M.G. Rosenblum, A.S. Pikovsky, and J. Kurths, Phys. Rev. Lett. **78**, 4193 (1997).

[44] L.M. Pecora and T.L. Carroll, Phys. Rev. Lett. **80**, 2109 (1998).

[45] M. Barahona and L.M. Pecora, Phys. Rev. Lett. **89**, 054101 (2002).

[46] T. Nishikawa, A. E. Motter, Y.-C. Lai, and F. C. Hoppensteadt, Phys. Rev. Lett. **91**, 014101 (2003).

[47] D.J. Watts and S.H. Strogatz, Nature, **393**, 440 (1998).

[48] N.F. Rulkov and M.M. Sushchik, Int. J. Bifur. Chaos **7**, 625 (1997).

[49] J.F. Heagy, T.L. Carroll, and L.M. Pecora, Phys. Rev. E **52**, R1253 (1995).

[50] J.F. Heagy, L.M. Pecora, and T.L. Carroll, Phys. Rev. Lett. **74**, 4185 (1995).

[51] O.E. Rössler, Phys. Lett. A **57**, 397 (1976).

[52] X. Liu, G. Strang, and S. Ott, Siam J. Discrete Math. **16**, 479 (2003).

[53] U. Parlitz, Phys. Rev. Lett. **76**, 1232 (1996).

[54] A. Maybhate and R. E. Amritkar, Phys. Rev. E **61**, 6461 (2000).

[55] H. Sakaguchi, Phys. Rev. E **65**, 027201 (2002).

[56] C. Tao, Y. Zhang, G. Du, and J.J. Jiang, Phys. Rev. E **69**, 036204 (2004).

[57] J.G. Restrepo, E. Ott, and B.R. Hunt, **69**, 066215 (2004).

[58] Y. Deng, M. Ding, and J. Feng, J. Phys. A: Math. Gen. **37**, 2163 (2004).

[59] Z. Galias and M.J. Ogorzalek, Int. Journal of Neural Systems, **13**, 397, (2003).

[60] M. Denker, M. Timme, M. Diesmann, F. Wolf, and T. Geisel, Phys. Rev. Lett. **92**, 074103 (2004).

[61] P.W. Anderson, Phys. Rev. **109**, 1492 (1958).

[62] I.M. Lifshits, S.A. Gredeskul, and L.A. Pastur, *Introduction to the Theory of Disordered Systems*, (Wiley, New York, 1988).

[63] M.G. Rosenblum, A.S. Pikovsky, and J. Kurths, Phys. Rev. Lett. **78**, 4193 (1997).

[64] K.-I. Goh, B. Kahng, and D. Kim, Phys. Rev. E **64**, 051903 (2001).

[65] F. Chung, L. Lu and V. Vu, Proc. Natl. Acad. Sci., **100**, 6313 (2003).

[66] V. M. Eguíluz, D. R. Chialvo, G. A. Cecchi, M. Baliki, and A. V. Apkarian, Phys. Rev. Letters **94**, 018102 (2005). This reference obtains $\gamma \approx 2.1$ from a network constructed from experimental measurements of brain activity.

[67] R. A. Brualdi, and S. Mellendorf, Amer. Math. Monthly **101**, 975 (1994).

[68] R. E. Mirollo and S.H. Strogatz, J. Stat. Phys. **60**, 245 (1990).

[69] D. M. Cvetković, M. Dobb, and H. Sachs, *Spectra of Graphs, Theory and Application*, (Academic Press, New York, 1979).